

**Final Report of RPSEA Project 12122-91:
4D Integrated Study Using Geology, Geophysics, Reservoir Modeling
& Rock Mechanics to Develop Assessment Models for Potential In-
duced Seismicity Risk**

Principal Investigator: Jeremy Boak, Oklahoma Geological Survey, University of Oklahoma

Investigators: G. R. Keller, ret., Oklahoma Geological Survey, University of Oklahoma
Austin Holland, United States Geological Survey, University of Oklahoma
Jefferson Chang, Oklahoma Geological Survey, University of Oklahoma
Stephen Holloway, Oklahoma Geological Survey, University of Oklahoma
Chen Chen, Oklahoma Geological Survey, University of Oklahoma
Noorulan Ghose, Oklahoma Geological Survey, University of Oklahoma
Fernando Ferrer Vargas, Oklahoma Geological Survey, University of
Oklahoma
Andrew Thiel, Oklahoma Geological Survey, University of Oklahoma
Steven Marsh, Oklahoma Geological Survey, University of Oklahoma
Deepak Devegowda, Mewbourne School, University of Oklahoma
Ahmad Ghassemi, Mewbourne School, University of Oklahoma

Table of Contents

Executive Summary	ES-1
1. Patterns of Induced Seismicity in Central and Northwest Oklahoma	1
2. Oklahoma Earthquake Summary Report 2015-16	8
3. Gravity Data Collection	22
4. Seismic Tomography of North Central Oklahoma	27
5. Gravimetric Determination of Basement Geologic Structure	41
6. Interpretation of Low Frequency Pressure Measurements in Injection and Production Wells	57
7. Modeling Pore Pressure Variations and Potential for Induced Seismicity Adjacent to Water Disposal Wells	67
8. Integrated Rock Mechanics Studies	85
9. Technology Transfer Activities	95

Executive Summary

The goal of this Project was to evaluate what properties may be most helpful in rigorously identifying both induced seismicity and the potential for induced seismicity, based on modeling and physical measurements in the target area in Central Oklahoma.

The study area is located in the zone of increased seismicity of central Oklahoma to address scientific questions with respect to the geologic conditions, monitoring and predictive modeling necessary to evaluate potential causes of the increased seismicity. The team built, tested and updated a volumetric (3D) geologic interpretation, based on information from existing well and well-log databases, rock-mechanics, rock properties, and seismic imaging. The 3D geologic interpretation was tested against existing and newly acquired gravity data, as well as ongoing seismic monitoring within the study area. The ongoing seismicity added to the 3D velocity structure within the 3D geologic interpretation volume. At the same time, the gravity modeling added to the 3D density distribution within the same interpretation volume. Using the geologic interpretation along with production and water disposal information, reservoir and rock mechanics modeling were undertaken to examine the changes through time associated with oil and gas production adding additional information dimensions (4D) to the study.

This report is divided into eight chapters describing results for technical aspects of the project and a listing of Technology Transfer activities during the term of the project. Each Chapter is preceded by the RPSEA Task description for the task (except Chapter 1, which is an introduction to the evolution of seismic activity that is the subject of this project). A separate package, comprising two Open File Reports, presents the results of compilation of fault data from literature and oil and gas company files that was funded in part by this project.

Chapter 1 is a discussion of the trends in seismicity and the regulatory response to that activity. It points out the significant increase in earthquake frequency during the first year of the project, and the flattening and decline of the frequency since mid-2015. Both trends reflect the variation of injection volumes in the Arbuckle Group sedimentary rocks that is considered the critical driver of seismicity. It also points out the significance of the decrease in oil price and the actions of the Oklahoma Corporation Commission in regard to those changes.

Oklahoma experienced an average of 1.6 earthquakes of Magnitude 3 or greater (M3.0+) from the 1980s through 2008. Since that time, seismicity has increased to 903 M3.0+ earthquakes in 2015. Earthquake frequency has declined in 2016; however, Oklahoma experienced its largest earthquake, a M5.8 event in September, near Pawnee. Combined with the M5.1 event in northwest Oklahoma in February, and an M5.0 earthquake near Cushing in November, these events ensure more seismic energy will be released in 2016 than in any year in the state's history. More than 95% of these earthquakes occur over only ~17% of the area of Oklahoma. Seismic activity occurred in two main regions, a Central zone to the east of the major Nemaha Fault, comprising parts of nine counties mostly north of Oklahoma City and West of Tulsa, and a Northwestern zone west of the fault, comprising parts of six counties.

The pattern of increased earthquake activity is generally attributed to increased injection of saline formation water co-produced along with oil and gas in salt water disposal wells. Most of the injection was into the commonly underpressured and relatively permeable Arbuckle Group, which lies directly on top of Precambrian crystalline basement (for example, Walsh and Zoback, 2015). Pressure communication from the Arbuckle to faults in the basement is interpreted to have reduced effective normal stress on the faults. This stress reduction allows faults aligned favorably with respect to the stress field in Oklahoma ($S_{HMax} = N 85^\circ E$) to move.

Chapter 2 describes in more detail the earthquake patterns and the state of the seismic network that records the earthquake data, including the improvements carried out with the support of the RPSEA and matching funds. The Oklahoma Geological Survey (OGS) located 6,668 earthquakes in 2015, in 34 counties in Oklahoma, and 3,922 in 2016 in 30 counties (through November 22); the number for 2015 is the greatest number of earthquakes that have occurred in a single year in Oklahoma's recorded seismic history, whereas the rate in 2016 reflects a significant decline in earthquake frequency. Of the earthquakes reported in 2015, 1533 were of magnitude 2.8 or greater (M2.8+), 903 were M3.0+, and 27 were of M4.0+. Of the earthquakes reported by November 30, 2016, 976 were M2.8+, 596 were M3.0+, and 14 were of M4.0+. Seismicity was concentrated in central and north-central Oklahoma with almost 96% of the earthquakes each year located in twelve counties (Alfalfa, Garfield, Grant, Lincoln, Logan, Major, Noble, Oklahoma, Pawnee, Payne, Woods and Woodward).

The OGS catalog is reasonably complete to a minimum magnitude of 2.0 during much of the time that the OGS has operated a seismic monitoring network - 1977 to about 2013. However, with the increased rate of earthquakes in 2014 and 2015, analysis to that level of detection was not possible and our efforts focused on completeness for a minimum magnitude of 2.5. The seismicity rate for Oklahoma continued to increase in early 2015. A plot of daily rates of earthquakes above M2.8 shows a peak in the 180-day moving average above 4.5/day in June of 2015. After that time, the rate declined until early 2016, then rose until April, then declined rapidly to less than 2.4/day. The 30-day moving average shows the episodic nature of the seismicity, whereas the 180-day moving average displays the longer-term trend.

In the first few months of 2014, the OGS added four temporary stations, and one permanent station in response to several earthquake swarms within central and north-central Oklahoma. Instrumentation for three of these temporary stations are generously on loan from the USGS. We received instrumentation for the Oklahoma Risk and Hazard (OKRaH) network in August 2014 and installed 12 temporary stations in central and north-central Oklahoma. These instruments were borrowed from the IRIS Portable Array Seismic Studies of the Continental Lithosphere (PASSCAL), instrument center. Twelve additional stations, acquired using matching funds for the RPSEA Project from the Oklahoma Corporation Commission, were installed during 2015 and 2016.

Chapter 3 describes the gravity measurements made in support of better understanding of the character of the basement rocks of Oklahoma (where most of the earthquakes are located). We collected gravity observations at 3,092 locations in north central Oklahoma over 160 field days from June 2014 to July 2016. Gravity observations were made along

public roadways, generally along section-line roads. Stations were located with 2-mile spacing as a compromise between coverage and density both to fill existing gravity coverage gaps and to collect a grid of higher spatial density station spacing. A total of 9,020 unique gravity readings were reduced, resulting in 3,092 gravity stations with accompanying post-processed GPS coordinates.

Chapter 4 describes a seismic tomography study conducted in the region by Chen Chen as his Doctoral dissertation. It provides an updated seismic velocity model for the deep crust and upper mantle beneath Oklahoma. This study results in enhancements to our ability to relocate earthquakes more precisely, which is important, given that perhaps 50% of earthquakes in Oklahoma occur on faults that have not been previously identified. Chen derived two velocity models using north-central Oklahoma earthquakes. He created each velocity model with >8000 earthquakes of magnitude 2.0 or greater (M2+), and >100,000 P- and S-wave picks from seismic records.

To better understand the structures in the crystalline basement, velocity models, gravity, and magnetic data were used to examine the geological correlation. On a large scale, the velocity model correlates to gravity anomalies because dense rocks generally have high velocities, and vice versa. The velocity models reveal strong lateral heterogeneities within the Precambrian crystalline basement, which indicates complex structures in the upper portion of the crust in the study area.

Most of the earthquakes in central Oklahoma are clustered and presented northeast-southwest (NE-SW) or northwest-southeast (NW-SE) trending orientation that is consistent with the ~East-West maximum horizontal stress state within the region. With the 3D velocity model, the cataloged earthquakes were relocated. The high-accuracy earthquake locations improved the resolution of fault locations by producing sharper patterns of seismicity. Furthermore, the improved earthquake locations can potentially better explain the relationship between injection wells and induced seismicity. In addition, the improvement of the earthquake locations can help identify primary fault planes from focal mechanisms, crustal deformation, and others.

As an example, the study points to a suite of earthquakes in the Cushing area in 2014 that had previously been relocated by the U. S. Geological Survey along a WNW-ESE trending alignment, suggesting a previously unidentified fault optimally oriented for slip. Using the new velocity model, these earthquakes were re-evaluated, and appear to lie on a NE-SW trend. Resolution of this difference will be critical if we are to understand patterns of seismicity on deeply buried faults.

Chapter 5 describes a gravimetric model for portions of Oklahoma and Kansas (with small portions of Arkansas and Missouri) that represents integration of all the data we have assembled. The larger regional model is required to adequately represent the gravity field in the project area. The geologic character of the upper crystalline basement can be estimated and tested using a geologically and statistically constrained density inversion of three dimensional (3D) free-air gravity data and a geologically consistent 3D density distribution of known and expected geologic features above and below the upper crystalline basement. Using published formation isopach models, a 3D geologic model is built that is consistent with known and expected geologic characteristics. As more geologic

information becomes available, the expected geologic formation model can be improved to reflect these data while maintaining consistency with both the regional and local geologic model. The Residual Free Air Gravity Anomaly resulting from the model illustrates the complexity of the basement geology between the Mid-Continent Rift, (MCR) in Kansas, and the Southern Oklahoma Aulacogen, (SOA). Associated with these two major tectonic features are parallel geologic structures like the Nemaha Uplift and Amarillo Uplift and the Anadarko basin. Also, there are additional associated structures throughout Oklahoma like the Wilzetta Fault zone and related smaller conjugate fault zones.

Although Oklahoma suffers from very sparse sampling for gravity and magnetic fields, there are recognizable boundaries that appear to correspond well to faults, both mapped and blind. There are also fault and seismic features that do not appear to show in the potential field maps. Additional data, augmented by seismic reflection data from oil and gas companies, could significantly improve our understanding of the basement structure and the potential connection to the overlying Arbuckle Group sedimentary rock. Studies under way supported by the Governor of Oklahoma may produce such integration.

Chapter 6 presents the mathematical basis for characterization of reservoirs like the Arbuckle Group sedimentary rock, and for pressure response analysis to identify highly conductive fluid migration pathways in the subsurface from injection well pumping tests. In this work, we document a low frequency asymptotic approach to interpret these pumping tests. The workflow described here depends on constructing an appropriate initial subsurface simulation model and adjusting the values of the uncertain model variables so that the model performance is in reasonable agreement with actual measurements.

The approach also calculates sensitivities of results to variations in input parameters by two methods. The first is a semi-analytical approach, from the low frequency asymptotic approach. The second is a numerical sensitivity calculation derived by perturbing each gridcell permeability value by a small value and solving the full field simulation to obtain changes in the predicted bottomhole pressure at the observation well. The approach described in this chapter allows for a high-resolution reconstruction of conductive pathways in the subsurface for fluid migration. Consequently, in the absence of other geophysical measurements or geologic interpretation, it provides a sound approach to addressing concerns over the migration of injected water and its role in induced seismicity.

Chapter 7 provides an application of this method to the problem of induced seismicity. The objective of this study is to deduce a temporal and spatial correlation between salt-water injection and earthquake frequency using numerical models. It attempts to address some key concerns, including:

- Is there a critical injection rate below which seismicity may be managed?
- What is the optimal distance for injection wells from a fault?
- Does the fault transmissibility play a role in governing induced seismicity?

The model grid employed to understand pore pressure variations in response to fluid injection in the Oklahoma City Field covers a volume 35 by 35 by 6 km, with an injection well in the center of the model, and containing four faults at varying distances from the wellbore. Fault properties (such as transmissibility contrast with the country rock) and injection rates, are varied in different simulations run for ten years. Resulting changes in

stress on different faults are calculated, using rock properties for Arbuckle Group sedimentary rocks and regional stresses representative of central Oklahoma.

The simulation results indicate that a maximum change in the pressure of close to 12 psia is observed at a depth of 5.4 km from the surface adjacent to the fault that is 500m away from the injection well. Such a pressure increase in a fault at this depth may be sufficient to trigger movement on critically stressed faults appropriately oriented to the regional stress field.

Chapter 8 presents results of an integrated rock mechanics study. Almost all studies on the increased seismicity in central Oklahoma have focused on pore pressure effects without explicit consideration of large-scale rock mass deformation. In this study, we have developed a large-scale geomechanical conceptual model for a fault system and assess its response to salt water injection. This portion of the RPSEA Project aimed to understand the effect of water injection on pore pressure increase and its consequences within the Wilzetta fault zone near Prague, Oklahoma. The study area selected for modeling salt water injection, encompassed approximately 460 square kilometers (approximately 22 × 23 km). The model consisted of seven layers; three of them are the target of injection (the Hunton group, the Simpson group, the Arbuckle group) and the bottom layer (the basement) is the location of most earthquakes. The model included two major faults; the Wilzetta fault (WFZ) and the Meeker-Prague fault (MPF). Zones surrounding the faults were refined to more accurately reflect the fault zone.

We simulated the hydraulic overpressures and potential for induced seismicity during hydraulic injection. After letting the system reach equilibrium, injection was commenced and continued for 19 years (1993 to 2011) using reported data (injection rate and well pressure). We monitored change of stress condition and redistribution of the pore pressure in the domain, and displacement along the faults to evaluate the possibility of induced seismicity. Model results suggest that injection can change the initial pore pressure by a significant amount (6 MPa) along the fault (for the assumed boundary conditions), which reduces the effective stress, and result in induced displacements in the X and Y directions after 14 years. The induced displacements suggest the potential for earthquakes.

The study also carried out tests of relevant rock types, and constructed failure envelopes for these rocks. Although full integration of the properties was not completed, the results to date suggest that reasonable parameter values in well-constructed models can provide valuable understanding of the process of injection-induced seismicity.

Chapter 9 tabulates the Technology Transfer activities conducted during the life of the project. Given the feedback from the **Workshop: Seismicity in Oklahoma**, held September 7-8, 2016 at the Moore-Norman Technology Center in Norman OK, this was the most productive of these activities. Researchers from across the U. S. with an interest in induced seismicity, especially in Oklahoma and adjacent states, came together for two days and discussed diverse aspects of the issue. The project received favorable comments comparing the workshop to an earlier one conducted by the Society of Exploration Geophysicists and the Society of Petroleum Engineers in Fort Worth in early 2016. A previous **National Seismic Hazard Workshop on Induced Seismicity** in November, 2014, hosted jointly

with the USGS, also brought a wide variety of technical personnel together to discuss a variety of topics on understanding induced seismicity with a focus on general risk from induced earthquakes. The project result in 11 publications, 19 professional presentations with published abstracts, 40 presentations for a wide variety of organizations mostly in Oklahoma. Project investigators attended numerous meetings of a Working Group of the Oklahoma Independent Petroleum Association, and interacted with industry groups on at least five occasions. Staff also met with State government staff at the Governor's Coordinating Council on Seismicity, the Secretary of Energy and Environment Director's meetings, presented at the Governor's Energy Conference, and presented to Interim study groups of the Oklahoma legislature. They also met on several occasions with U. S. Geological Survey staff, and visited the National Earthquake Information Center. The Principal Investigator also presented project results at two RPSEA sponsored meetings.

1. Patterns of Induced Seismicity in Central and Northwest Oklahoma

Jeremy Boak, Director, Oklahoma Geological Survey, Mewbourne College of Earth and Energy, University of Oklahoma, Norman OK 73019

Summary

Oklahoma experienced an average of 1.6 earthquakes of Magnitude 3 or greater (M3.0+) from the 1980s through 2008. Since that time, seismicity has increased to 903 M3.0+ earthquakes in 2015. Earthquake frequency has declined in 2016; however, Oklahoma experienced its largest earthquake, a M5.8 event in September, near Pawnee. Combined with the M5.1 event in northwest Oklahoma in February, and an M5.0 earthquake near Cushing in November, these events ensure more seismic energy will be released in 2016 than in any year in the state's history. More than 95% of these earthquakes occur over only ~17% of the area of Oklahoma (Figure 1.1). Seismic activity occurred in two main regions, a Central zone to the east of the major Nemaha Fault, comprising parts of nine counties mostly north of Oklahoma City and West of Tulsa, and a Northwestern zone west of the fault, comprising parts of six counties.

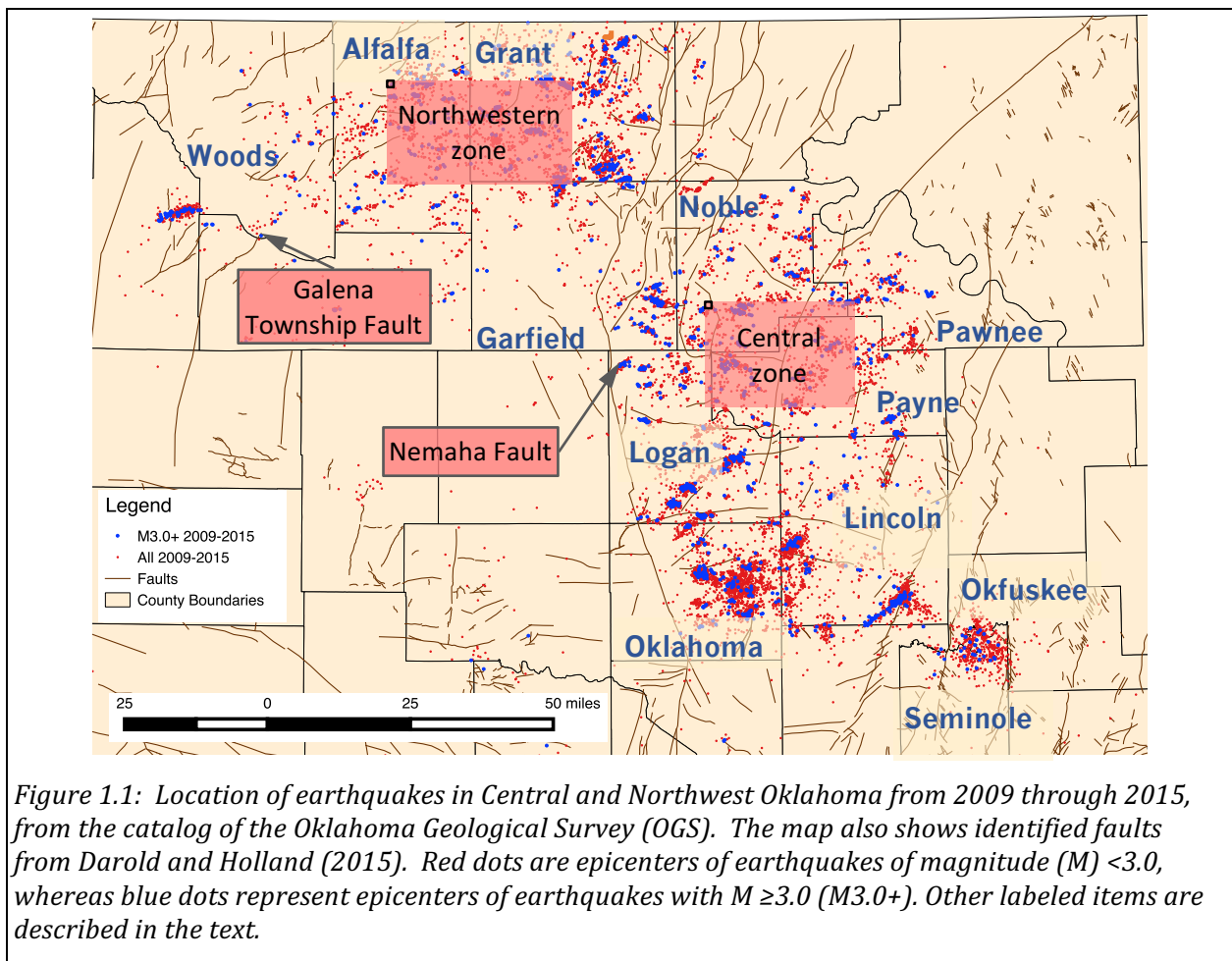


Figure 1.1: Location of earthquakes in Central and Northwest Oklahoma from 2009 through 2015, from the catalog of the Oklahoma Geological Survey (OGS). The map also shows identified faults from Darold and Holland (2015). Red dots are epicenters of earthquakes of magnitude (M) < 3.0, whereas blue dots represent epicenters of earthquakes with M ≥ 3.0 (M3.0+). Other labeled items are described in the text.

The pattern of increased earthquake activity is generally attributed to increased injection of saline formation water co-produced along with oil and gas in salt water disposal wells. Most of the injection was into the commonly underpressured and relatively permeable Arbuckle Group, which lies directly on top of Precambrian crystalline basement (for example, Walsh and Zoback, 2015). Pressure communication from the Arbuckle to faults in the basement is interpreted to have reduced effective normal stress on the faults. This stress reduction allows faults aligned favorably with respect to the stress field in Oklahoma ($S_{HMax} = N 85^\circ E$) to move. This paper discusses the evolution of this seismicity, the regulatory actions taken to reduce seismicity by reducing deep injection, and the importance of declining oil price in reducing injected volumes in advance of full implementation of these regulatory directives.

Brief History of Induced Seismicity in Oklahoma

The pattern of rising earthquake frequency is shown in Figure 1.2, which covers the period from 2011 through early November 2016. It shows the daily frequency of M2.8+ earthquakes averaged monthly. A six-month moving average of these values is also plotted. Activity had increased beginning in 2009, from an annual average of 2.9 M2.8+ earthquakes to 24 in 2009, to 60 in 2010, and to 110 in 2011. The sharp increase was associated largely with the M5.7 Prague earthquake in November 2011, which damaged numerous homes,

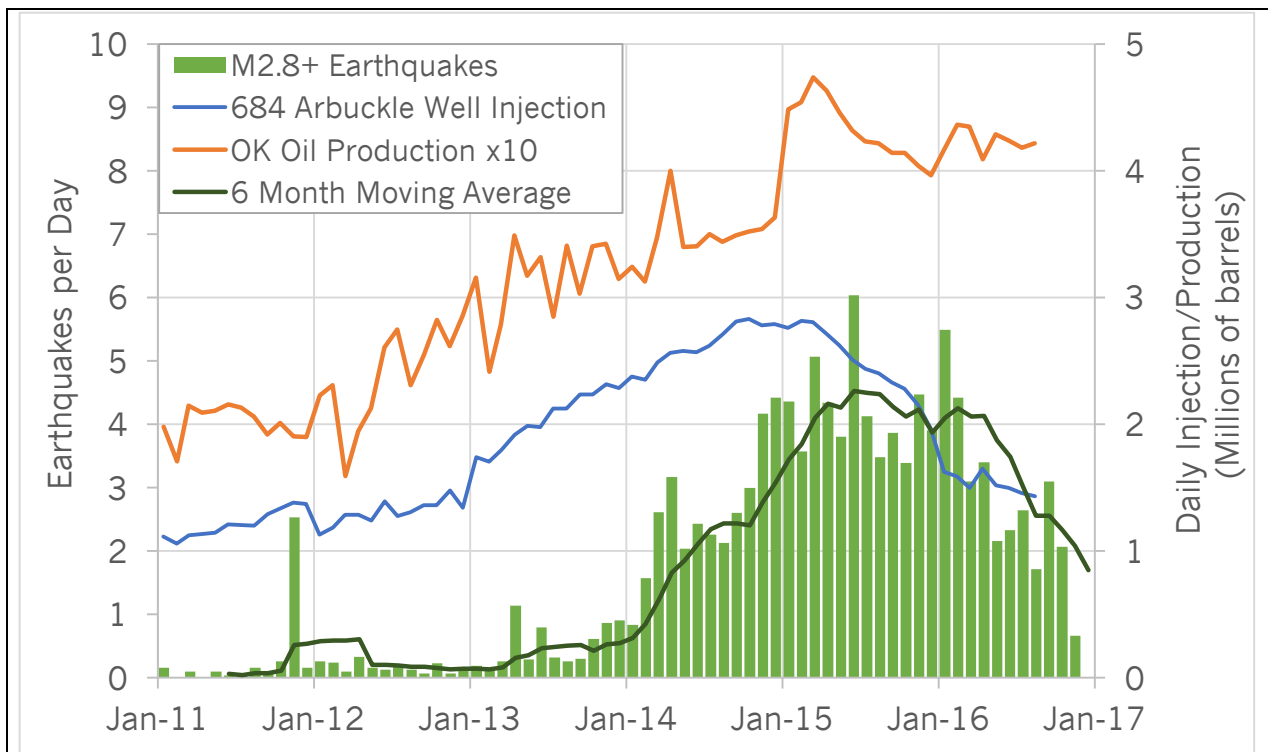


Figure 1.2: Relationship of produced water injection into Arbuckle Group sedimentary rocks to seismic activity. Bars indicate daily frequency of earthquakes of M2.8+ by month from 2009 through November 2016. Note the Prague earthquake swarm in late 2011. Brown line represents a six month moving average. Blue line is monthly injection into 684 wells completed in the Arbuckle Group in the area of increased seismic activity for 2015 through early 2016. Green line represents Oklahoma crude oil production (multiplied by ten to display trends more clearly).

injured several people, and aroused a significant debate about the origin of the earthquakes. After the Prague swarm, earthquake activity slowed in 2012 (2.8+ = 63), but rose again in 2013 (M2.8+ = 184) and still more in 2014 (M2.8+ = 951), leading to strong political debate and protests.

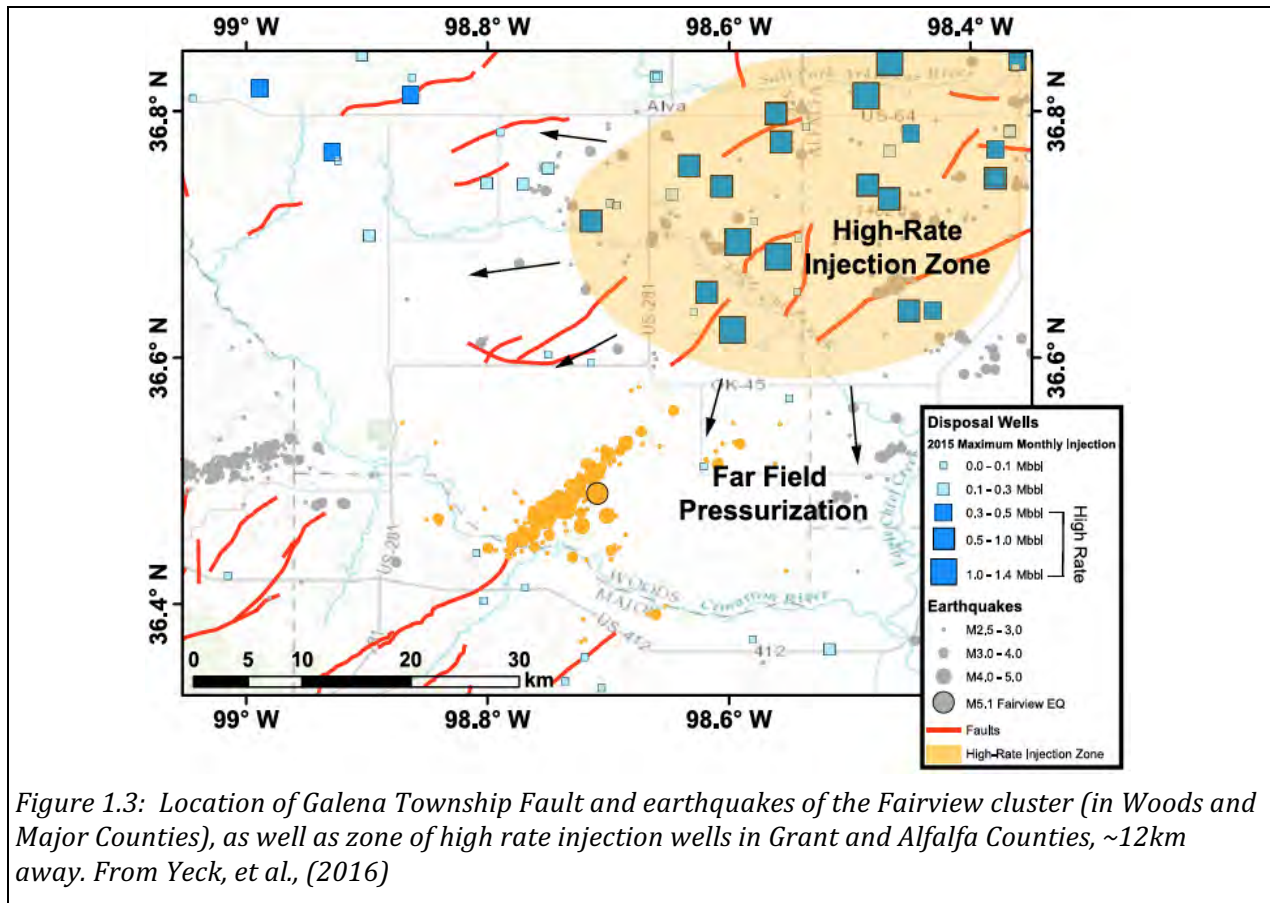
Seismic activity clearly developed in two main areas, one in north central Oklahoma, and the other to the northwest, across the Nemaha Fault. Both areas have seen development of oil and gas plays that produced very large amounts of water, which was disposed of in Underground Injection Class II Salt Water Disposal wells in the same area as the production. Injection volumes reached 1.5 billion barrels in 2014 (Murray, 2015). The rapid increase in injection in the 14 counties where >95% of the seismic activity occurs is also illustrated in Figure 2. Seismicity increased first in the southern part of the central area, then expanded northward then westward into the northwestern area.

By the end of 2014, when 1,533 M2.8+ earthquakes had occurred, the Oklahoma Corporation Commission (OCC) began to act to shut in some disposal wells, and to reduce injection in others in sensitive areas. In early 2015, they requested that operators of about 500 injection wells in the area of greatest seismic activity show they were not injecting directly in to the basement, plug back out of the basement, or cut injection by 50%. Also in early 2015, the Oklahoma Geological Survey (OGS) put out a position statement that clearly attributed the increased seismic activity to deep injection of produced water through pressure communication to the deep basement (Andrews and Holland 2015). Additional actions taken generally in response to earthquakes of M4.0+ called for reduction of injection in many of these same wells.

Figure 1.2 also illustrates injection rates from 684 wells completed in the Arbuckle Group within the seismically active zone that reported injection data for 2011 through 2016 in response to accelerated reporting requested by the OCC. It documents a substantial decrease in injection beginning at the end of 2014, largely driven by market forces reacting to the sharp decline of oil price through 2014. Also shown on the chart is the monthly Oklahoma crude oil production from the U. S. Department of Energy's Energy Information Administration (U. S. Energy Information Administration, 2016). It shows a very modest decline in crude oil production in Oklahoma, in 2015, but increasing production in 2016. This trend suggests that other plays are taking the place of production lost in the water-rich plays that generate much of the salt water disposed in the seismic area of interest.

Despite reductions directed by the OCC, the earthquake count climbed to 1533 M2.8+ earthquakes by the end of 2015. In November 2015, a surge in seismic activity began on a fault in southern Woods County more than 12 km away from the main area of injection in northern Woods, Alfalfa, and Grant Counties. About 75% of all seismic moment released in Oklahoma in January and 85% in February came along what has been labeled the Galena Township Fault (see Figure 1.1). Three M4.0+ earthquakes in the first week in January, an M5.1 earthquake in February, and three M4.0+ aftershocks of that earthquake in July were the most significant events through August 2016.

Figure 1.3 (Yeck *et al.*, 2016) shows the epicenters of earthquakes on the Galena Township Fault, as well as the area of higher injection rate wells to the north. Yeck *et al.* (2016) concluded that seismic activity in this area was driven by injection in the high rate disposal



wells shown in the northern part of the area. They also point out that, whereas seismic events occurred near the high injection rate wells, no earthquake was as large as the main shock on the Galena Township Fault. They conclude that the magnitude of induced earthquakes is determined by the characteristics of the fault, and not the degree of pore pressure enhancement from injection. This inference suggests that changes in injection rate will most likely affect the frequency of earthquakes, not the magnitude.

Elsewhere in the earthquake Area of Interest, earthquake frequency declined. The decline began in mid-2015 in the central area, and somewhat later in the northwest area. In the Central area, which experienced 14 M4.0+ earthquakes in 2015, an M4.2 earthquake on New Years Day 2016 was followed by an interval of 88 days with no M4.0+ earthquakes. The northwest area experienced a pulse of larger earthquakes in late 2015, amid a trend of generally decreasing activity. However, activity on the Galena Township Fault led to an overall increase in M2.8+ earthquakes. Beginning in May 2016, the rate of M2.8+ earthquakes began a rapid decline. The 180-day running average of M2.8+ earthquakes per day peaked in mid-2015 at a value near 4.5. It had declined to about 4.0 by late April. From there, it declined to about 2.3 by the end of September, despite bursts of activity in the Northwestern zone in July and the Pawnee earthquake swarm in September.

Over the Labor Day weekend 2016, a M5.8 earthquake occurred in Pawnee County, on the eastern edge of the earthquake Area of Interest, in a county that had experienced relatively

few earthquakes over the period of increased activity, and whose neighbor, Osage County (administered by the Osage Nation) had experienced almost no earthquakes (Figure 1.4). This earthquake caused localized damage in Pawnee, but was felt throughout much of the U. S. mid-continent. The location of the main shock and early aftershocks placed it on a previously identified fault (see Darold and Holland [2015]). However, subsequent aftershocks defined an additional previously unidentified fault, and the OCC was forced to revise its initial order, shutting in some additional wells, but also changing the wells that were directed to cut back on injection. Additional wells in Osage County were also shut in. The U. S. Environmental Protection Agency, which regulates salt water disposal in the County, followed the lead of the OCC in its action.

Subsequently, a M5.0 earthquake occurred on November 7, 2016 near the town of Cushing Oklahoma, bringing the total of M5.0+ earthquakes for 2016 to three, a number unprecedented in the state's history. All four M5.0+ earthquakes in recent times (including the M5.7 Prague event of 2011) have occurred near the edges of the Area of Interest. The occurrence of three M5.0+ earthquakes against a pattern of decline for nearly all other magnitude groups raises puzzling questions about the trend, at least in the public eye. For example, the number of M2.8+ earthquakes as of November 22 was 967. Simple linear extrapolation would estimate the year end value at ~1100, a reduction of nearly 30% from 2015.

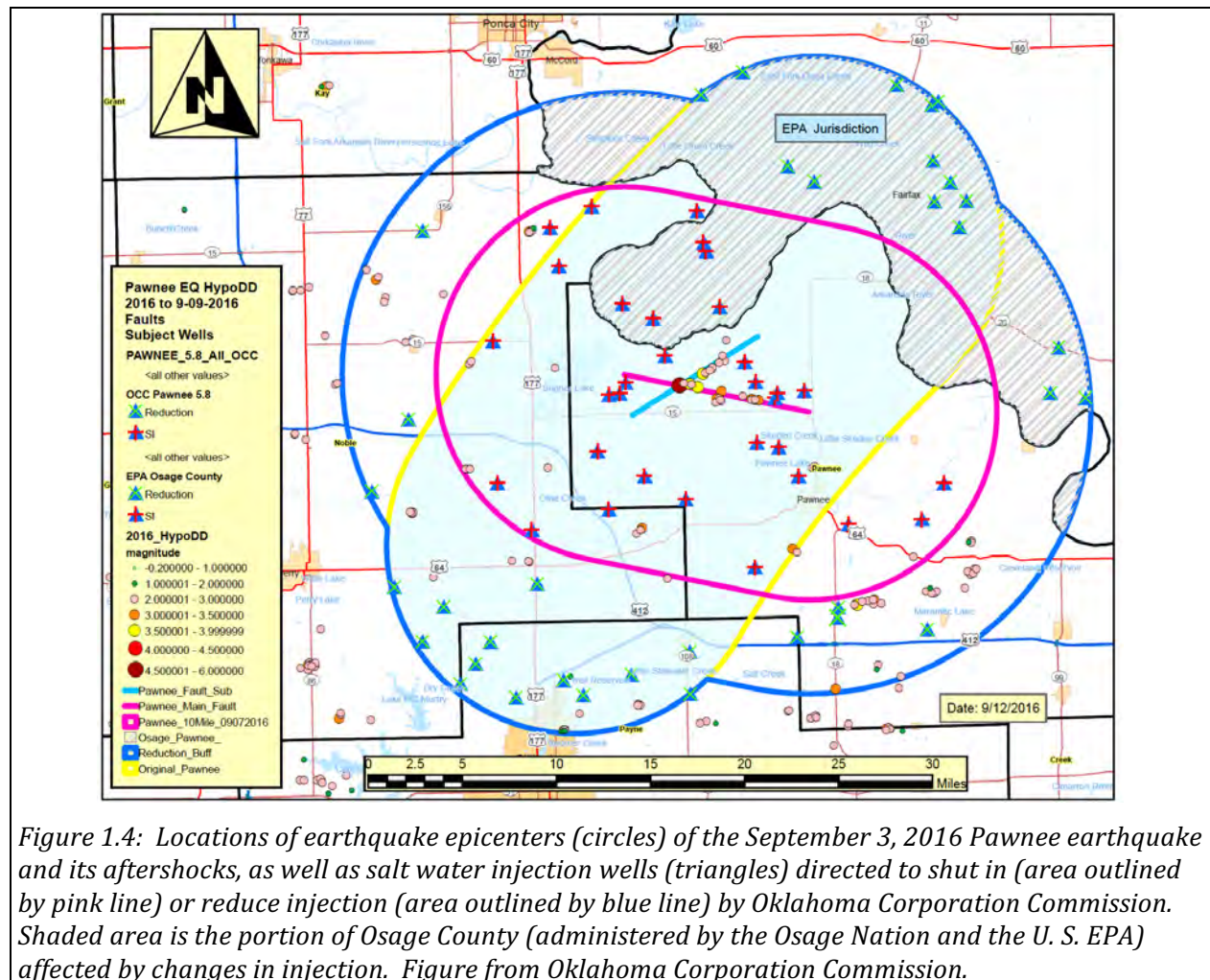


Figure 1.4: Locations of earthquake epicenters (circles) of the September 3, 2016 Pawnee earthquake and its aftershocks, as well as salt water injection wells (triangles) directed to shut in (area outlined by pink line) or reduce injection (area outlined by blue line) by Oklahoma Corporation Commission. Shaded area is the portion of Osage County (administered by the Osage Nation and the U. S. EPA) affected by changes in injection. Figure from Oklahoma Corporation Commission.

For Magnitude 3.0 earthquakes, the current count is 591, which would extrapolate to ~660 by the end of the year – a reduction of more than 200 from the 2015 value of 903.

Actions of the Corporation Commission

The Oklahoma Corporation Commission (OCC) has taken numerous steps to reduce injection of produced formation water across most of the earthquake-prone area. The team addressing the earthquake issue defined an earthquake-prone Area of Interest that encompassed a very large fraction of the earthquakes. This area increased in size as the earthquakes continued, although it has been stable since early 2016. The OCC has issued a series of directives calling for changes in injection practices and quantities in response to the evolving seismic activity (see Table 1.1).

Average depth of the earthquakes has generally been 5.4-5.5 kilometers, indicating that most of the seismicity occurs within the crystalline basement of Oklahoma (Darold et al., 2015). Injection into the Arbuckle Group, the stratigraphic unit that lies directly on the crystalline basement, has been identified as the likely cause of the earthquakes. The largest fraction of the volume of injection has been into this horizon, and increases of pore pressure in the Arbuckle are interpreted to have been transmitted to blind faults in the crystalline basement.

Conclusions

The elevated seismic activity resulting from earthquakes interpreted as induced by oil and gas operations in Oklahoma is highly likely to continue at least through 2017. How much the number of earthquakes will decrease in 2016 is likely to depend upon the activity on the Galena Township Fault and on faults responsible for the Pawnee and Cushing earthquakes. As the largest earthquakes since 2011 happened in February, September and November of 2016 in these zones, there remains large uncertainty about the frequency and magnitude of earthquakes, and their potential for damage. Each of the M5.0+ events has resulted in some damage. However, the results of initial damage from a moderate (say M4.0+) earthquake that is aggravated by cumulative shaking from the numerous smaller earthquakes has not been evaluated, and remains a significant issue for the state.

Acknowledgements

The author acknowledges the support of many members of the staff of the Oklahoma Geological Survey, particularly hydrogeologist Kyle Murray and acting lead seismologist Jefferson Chang. The work of Austin Holland and Amberlee Darold, who built much of the present OGS seismic network and established the framework for understanding Oklahoma earthquakes, can hardly be overstated.

Reference Cited

- Andrews, R. D., and A. A. Holland 2015, Statement on Oklahoma Seismicity, April 21, 2015
- Darold, A. P., A. A. Holland, J. K. Morris, A. R. Gibson, 2015, Oklahoma Earthquake Summary Report 2014, Oklahoma Geological Survey Open-File Report OF1-2015, February 2015
- Darold, A. P., and A. A. Holland, 2015, Preliminary Optimal Oklahoma Fault Orientations Oklahoma Geological Survey Open File Report OF4-2015, July 2015.

Murray, K., 2015, Class II Saltwater Disposal for 2009–2014 at the Annual-, State-, and County- Scales by Geologic Zones of Completion, Oklahoma, Oklahoma Geological Survey Open-File Report OF5-2015, December 2015.

Walsh, F. R. and Zoback, M. D., 2015, Oklahoma’s recent earthquakes and saltwater disposal, *Sci. Adv.* 2015;1: e1500195

Yeck, W. L., M. Weingarten, H. M. Benz, D. E. McNamara, E. A. Bergman, R. B. Herrmann, J. L. Rubinstein, and P. S. Earle (2016), Far-field pressurization likely caused one of the largest injection induced earthquakes by reactivating a large preexisting basement fault structure, *Geophys. Res. Lett.*, 43, doi:10.1002/ 2016GL070861.

Table 1.1: Directives of the Oklahoma Corporation Commission for the earthquake prone area of Oklahoma, with numbers of wells affected and reductions in injection volume

<i>Directive Date</i>	<i># Wells Affected</i>	<i>Shut In</i>	<i>Reduced</i>	<i>Total Reduction (BPD)</i>	<i>Action Area</i>
March 18, 2015	347				Full Area of Interest
June 17, 2015	1	1	0	375	Olmstead
July 15, 2015	211				Expanded Area of Interest
July 28, 2015	3	1	2	x	Crescent
August 3, 2015	23	0	23	x	Logan-Payne Trend
September 17, 2015	13	3	10	6,126	Cushing 3.7
October 16, 2015				x	Cushing 4+
November 16, 2015				x	Fairview
November 19, 2015				x	Cherokee Carmen
November 19, 2015				x	Crescent
December 3, 2015				x	Byron
December 3, 2015				x	Medford
December 29, 2015				x	Edmond
November 7, 2015				x	N Medford
January 12, 2015				x	Fairview Cherokee Trend
February 16, 2016	195		195	400,000	OK Western Reduction Area - reduction to 2012 levels
March 7, 2016	398		398	400,000	Ok Central Reduction Area - reduction to 2012 levels
March 7, 2016	77		77		Wells added to expanded AOI
August 17, 2016	21	2	19	20,000	Luther-Wellston
September 3, 2016	48	27	21	40,000	Pawnee 5.8
November 3, 2016	20	4	16	12,000	Pawnee 4.3
November 7, 2016	72	7	65	33,000	Cushing 5.0
				911,501	

x = Plan Removed with regional plan implementation; Shut-in wells remained shut-in

Description of RPSEA Task 6 – Seismic Monitoring: The Subcontractor shall install and operate 12 seismic stations within study area. Data shall be sent in real time to the Oklahoma Geological Survey (OGS) seismic monitoring system and processed for routine products such as hypocentral location and focal mechanism. The stations shall be laid out on a rough grid in culturally quiet locations. These 12 stations shall be augmented by four portable seismic monitoring systems for detailed studies, as they are available depending on seismicity patterns and particular areas of interest. Data from this seismic monitoring effort shall also be integrated into the 3D Earth Interpretation (Task 9.0) as seismic tomography, hypocenter and stress orientations, and other seismic imaging techniques.

The report appended below summarizes earthquake monitoring activities in Oklahoma during 2015 and 2016, with reference to activities supported by the RPSEA Project.

2. Oklahoma Earthquake Summary Report 2015-16

*Jefferson Chang, Jeremy Boak, Noorulan Ghouse, Fernando Ferrer Vargas, Andrew Thiel
Oklahoma Geological Survey, Sarkeys Energy Center, Rm. N-131
100 East Boyd St., Norman, Oklahoma 73019-0628*

Summary

The Oklahoma Geological Survey (OGS) located 6,668 earthquakes in 2015, in 34 counties in Oklahoma, and 3,922 in 2016 in 30 counties (through November 22; see Figure 2.1); the number for 2015 is the greatest number of earthquakes that have occurred in a single year in Oklahoma's recorded seismic history, whereas the rate in 2016 reflects a significant decline in earthquake frequency. Of the earthquakes reported in 2015, 1533 were of magnitude 2.8 or greater (M2.8+), 903 were M3.0+, and 27 were of M4.0+. Of the earthquakes reported by November 30, 2016, 976 were M2.8+, 596 were M3.0+, and 14 were of M4.0+. Seismicity was concentrated in central and north-central Oklahoma with almost 96% of the earthquakes each year located in twelve counties (Alfalfa, Garfield, Grant, Lincoln, Logan, Major, Noble, Oklahoma, Pawnee, Payne, Woods and Woodward).

The OGS catalog is reasonably complete to a minimum magnitude of 2.0 during much of the time that the OGS has operated a seismic monitoring network - 1977 to about 2013. However, with the increased rate of earthquakes in 2014 and 2015, analysis to that level of detection was not possible and our efforts focused on completeness for a minimum magnitude of 2.5. The seismicity rate for Oklahoma continued to increase in early 2015. A plot of daily rates of earthquakes above M2.8 (figure 2.2) shows a peak in the 180-day moving average above 4.5/day in June of 2015. After that time, the rate declined until early 2016, then rose until April, then declined rapidly to less than 2.4/day. The 30-day moving average shows the episodic nature of the seismicity, whereas the 180-day moving average displays the longer-term trend.

The largest earthquakes in 2015 were magnitude 4.7 events in Grant and Alfalfa Counties. By November 30, 2016, Oklahoma had recorded three earthquakes of magnitude greater than 5 – a M5.1 event February 13, 2016 northwest of Fairview in Woods County, a M5.8

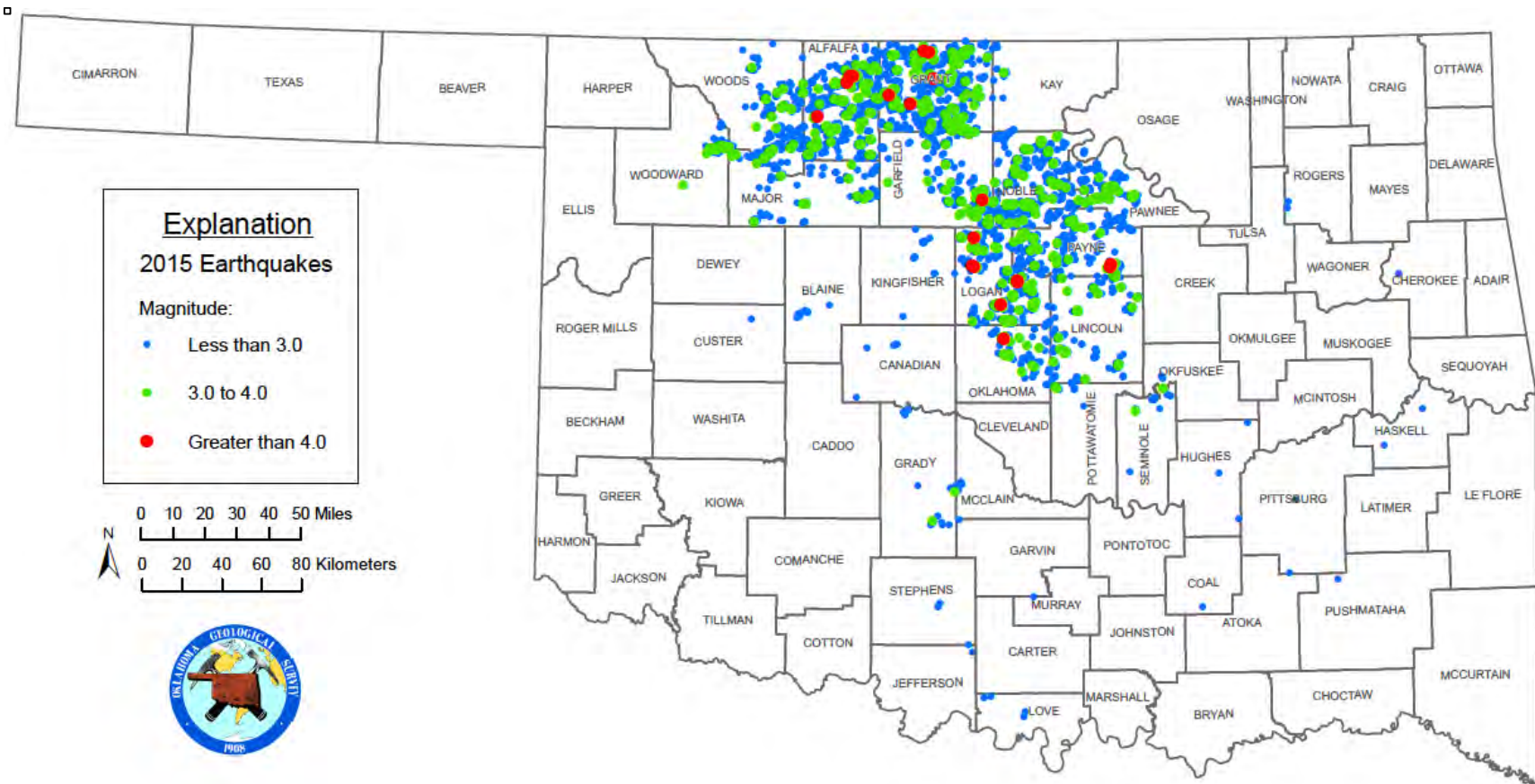


Figure 2.1a: Earthquakes located by the Oklahoma Geological Survey in 2015. Blue dots are earthquakes of magnitude less than 3.0; Green dots are magnitude 3.0-4.0; Red Dots are magnitude greater than 4.0.

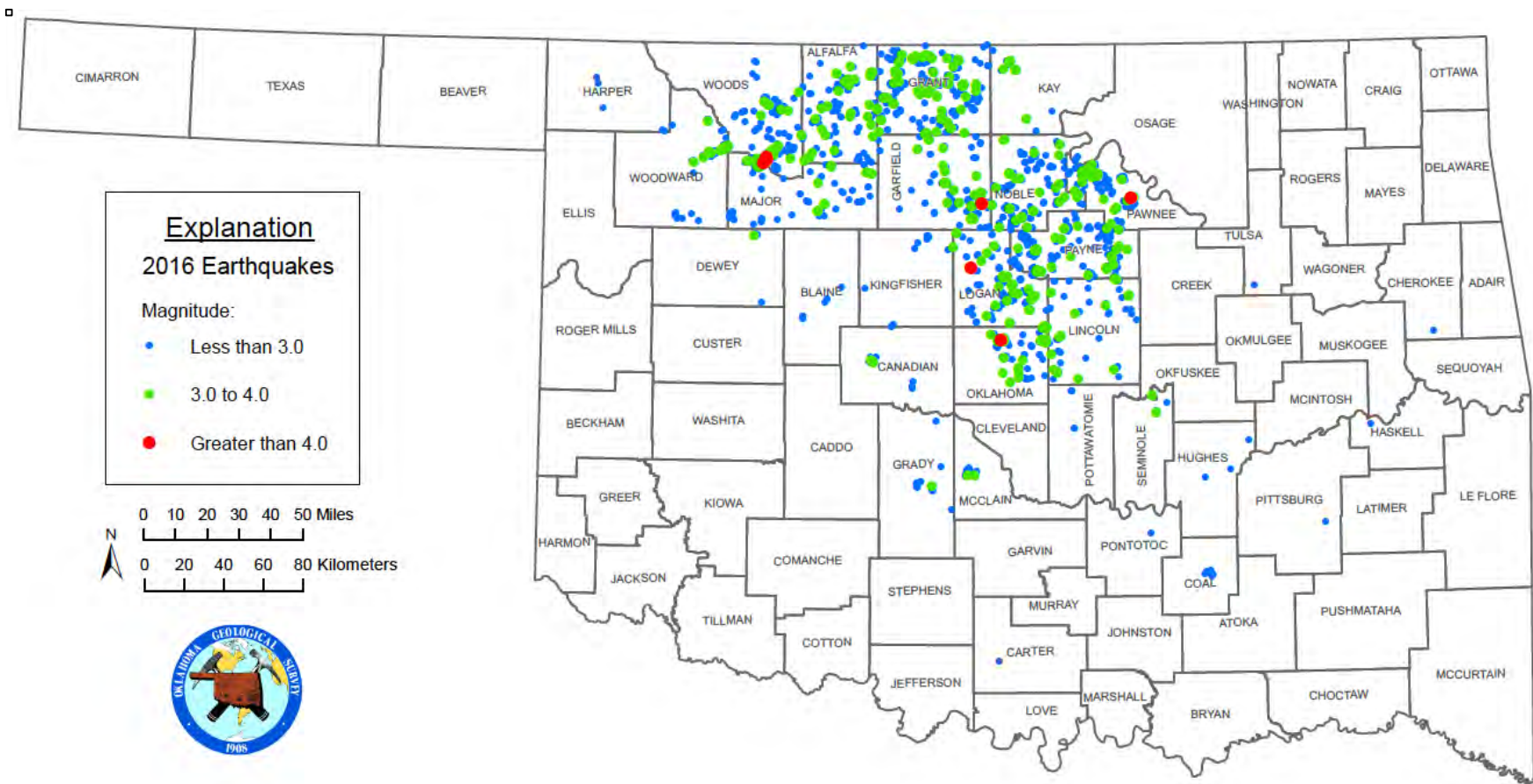


Figure 2.1b: Earthquakes located by the Oklahoma Geological Survey in 2016. Blue dots are earthquakes of magnitude less than 3.0; Green dots are magnitude 3.0-4.0; Red Dots are magnitude greater than 4.0.

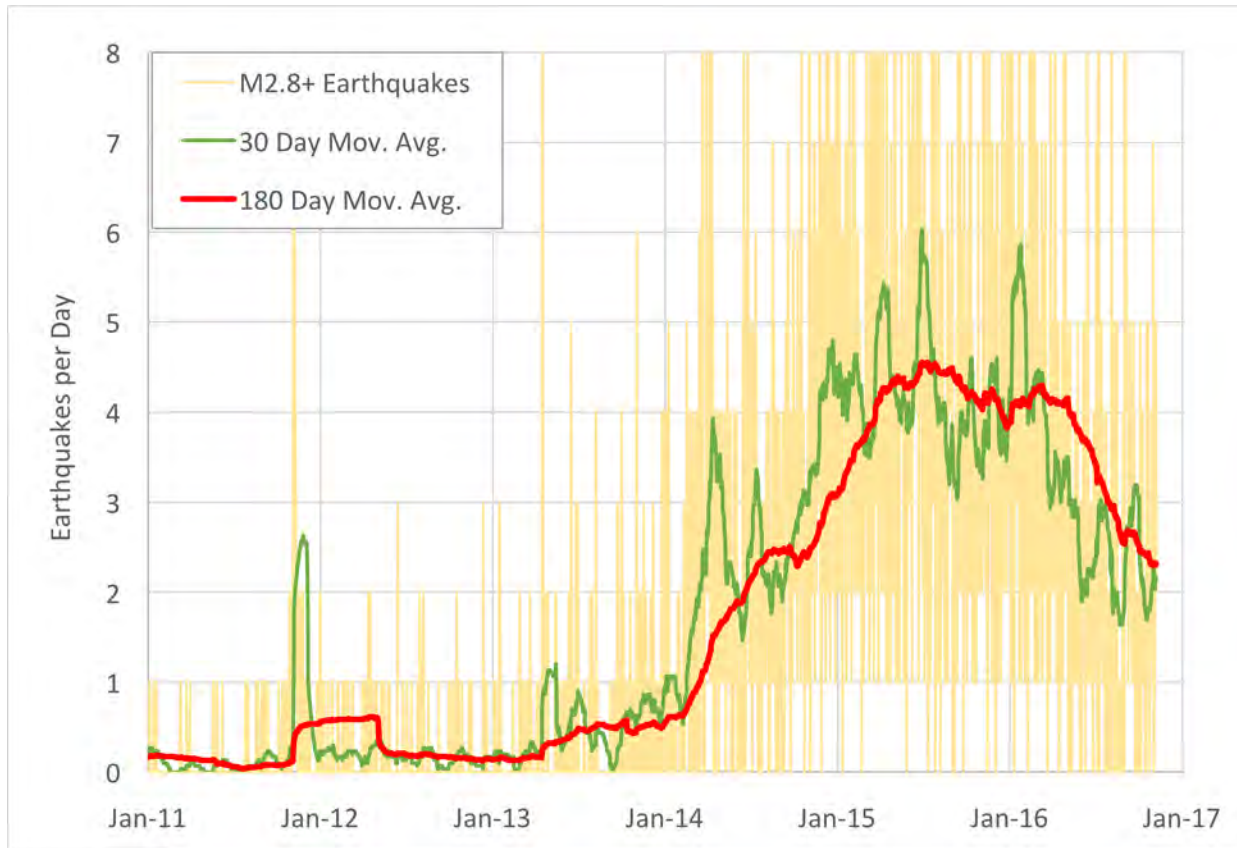


Figure 2.2. Earthquake rate in Oklahoma for earthquakes of M2.8+, showing daily rate as well as 30-day and 180-day moving averages.

event September 3, 2016 near Pawnee in Pawnee County, and a M5.0 event November 6, 2016 near Cushing in Payne County. These three earthquakes represented the largest, second largest and fourth largest earthquakes in recorded history for Oklahoma, accounted for approximately 81% of the seismic moment released in 2016 (to November 30), and ensured that 2016 would be the year of greatest seismic energy release in Oklahoma history.

The February event occurred along what has been informally termed the Galena Township Fault, and extended the trace of a fault previously mapped in Major County into Woods County. The September 3rd event occurred at the intersection of a previously identified fault with a fault that was defined by the seismic activity that followed the main shock. The November 6th event occurred on a fault that had previously been active in October 2015.

Table 2.1 lists the number of earthquakes of magnitude 2.5 or greater (M2.5+) in 2015, by month and by county, with the overall total being 3,309 events. Twenty-five counties are represented, but only seventeen have more than five events of this magnitude. Individual counties and the entire state show remarkable month to month variability, reflecting the episodic nature of seismicity. Grant County showed the highest earthquake frequency for seven of twelve months, and for the entire year, with more than one quarter of all events occurring in this county. Logan County had the highest count for two months, and was second highest for the year. Alfalfa, Garfield, and Payne County led in one month each, and were third, fourth, and sixth in earthquake frequency for the entire year. Noble County, was the fifth in earthquake frequency, but led in no month.

Table 2.1. Number of M2.5+ earthquakes reported, listed by county and month for 2015, sorted by total earthquakes, from most to least.

County	Jan	Feb	Mar	Apr	May	Jun	Jul	Aug	Sep	Oct	Nov	Dec	Total
Grant	106	54	120	75	60	56	49	75	32	47	131	65	870
Logan	54	22	63	76	30	74	56	27	17	12	29	19	479
Alfalfa	49	57	28	23	28	34	44	27	24	13	56	27	410
Garfield	17	7	24	35	26	82	29	21	25	24	17	11	318
Noble	37	23	47	46	22	24	14	14	25	26	18	16	312
Payne	21	16	47	12	15	11	15	16	54	26	10	12	255
Woodward	3	1	34	26	36	7	11	3	12	2	6	4	145
Pawnee	15	2	5	4	8	24	18	5	8	11	4	5	109
Woods	2	3	4	1	10	10	2	8	8	9	22	22	101
Lincoln	6	4	11	6	11	14	10	9	6	5	3	15	100
Oklahoma	3	1	9	8	6	11	6	8	8	6	3	24	93
Major	3	3	1	1	6	6	3	5	13	11	6	3	61
Grady			3			1	2				2	3	11
Pottawatomie	1		1				4	1		2			9
Kay	1	1	3				1	1			1		8
Seminole					1			3	1				5
Kingfisher				1			1				3		5
Okfuskee			1			1					1		3
McClain						1					2		3
Canadian	1									1	1		3
Blaine											3		3
Stephens							1	1					2
Osage				1								1	2
Love	1												1
Pittsburg								1					1
Grand Total	320	194	401	315	259	356	266	225	233	195	318	227	3309

Table 2.2 lists the number of M2.5+ earthquakes for 2016 (to November 30, 2016), with the overall count being 1,992. These numbers were increasing regularly in the latter half of the year as the expanded seismic team sought to drive the completeness level of the catalog down to 2.5 and lower. Twenty-nine counties are represented in the table, but nineteen recorded more than five events, even in the shorter period than for 2015.

Woods County, location of the Galena Township Fault, which produced an M5.1 earthquake in February, topped the list for earthquake frequency. It accounted for slightly more than one fifth of the total number, and led in five monthly counts. Grant County was second

Table 2.2. Number of M2.5+ earthquakes reported, listed by county and month for 2016 (to September 28, 2016), sorted by total earthquakes, from most to least.

County	Jan	Feb	Mar	Apr	May	Jun	Jul	Aug	Sep	Oct	Nov	Total
Woods	101	87	29	24	19	28	44	13	16	17	4	382
Grant	57	31	26	24	19	17	16	17	32	21	12	272
Oklahoma	41	40	9	27	17	7	10	5	11	5	6	178
Garfield	2	28	21	10	23	14	24	26	11	7	2	168
Logan	29	17	9	15	17	12	23	4	13	4	5	148
Pawnee	3	5	2	9	2	8	6		71	18	21	145
Payne	26	28	8	7	11	6	17	4	19	1	12	139
Alfalfa	22	5	26	7	29	9	13	3	9	2	6	131
Noble	12	8	9	14	4	7	10	12	21	7	6	110
Woodward	4	11	14	9	6	14	4	6	7	15	3	93
Major	10	5	7	13	1	6	1	4	4	21	13	85
Lincoln	6	3	7	12	2	2	4	8	3	5	3	55
Kay		1	5	8	4	6	2		1			27
Kingfisher			1	2	1	7				1		12
McClain					3		8					11
Pottawatomie		1	1	1					1		1	5
Grady						2			2	1		5
Coal					1			1	1	1	1	5
Canadian											5	5
Dewey		1				1		3				5
Seminole				1	1				1			3
Hughes			1		1							2
Okfuskee	1											1
Pittsburg		1										1
Blaine									1			1
Osage			1									1
Cherokee				1								1
Harper							1					1
Grand Total	314	272	176	184	161	146	183	106	224	126	100	1992

overall, but did not top the list for any one month. Oklahoma, Garfield and Alfalfa Counties ranked third, fourth and sixth respectively, each leading in one month. Logan County, ranked fifth, did not lead in any month. Pawnee, site of the largest earthquake of the year, led only in September, the month of the M5.8 earthquake.

Earthquake Processing and Analysis

The OGS has used the SEISAN (Havskov and Ottomoller, 1999) earthquake analysis package since 2010. The regional velocity model used to determine the location of earthquakes in Oklahoma is shown in Table 2.3. We currently use a V_p/V_s ratio of 1.73 for the regional velocity model. The regional model does a reasonably good job through most of the state of Oklahoma.

SEISAN has the capability to calculate moment magnitude (M_w) from the shape of the displacement spectra (Abercrombie, 1995; Brune, 1970). The OGS began routinely doing M_w analysis in 2014 for earthquakes of an initial local magnitude (M_L) of 3.8 or greater. There are many smaller earthquakes for which an M_w has also been calculated. In general, M_w 's calculated by the OGS compare quite well to those determined by the United States Geological Survey (USGS) National Earthquake Information Center (NEIC), which generally are only determined for earthquakes of magnitude 4.0 or greater. The M_w magnitudes tend to be smaller than the M_L magnitudes calculated by the OGS.

Both of these calculations are tracked in the earthquake reporting in the OGS catalog, which is available for 2015 and 2016 in a variety of formats at

<http://www.okgeosurvey1.gov/pages/earthquakes/catalogs.php> or directly at <http://wichita.ogs.ou.edu/eq/catalog/2015/> and <http://wichita.ogs.ou.edu/eq/catalog/2016/>.

The OGS earthquake catalog is preliminary and subject to change as further analysis occurs. The information in the catalog may change, and is always the most up-to-date at the above links. For an earthquake to be reported in the OGS catalog, there must be identified phase arrivals from at least four seismic stations included in the location solution and the earthquake must have occurred within Oklahoma. In addition, the OGS routinely relocates earthquakes using HYPODD (Waldhauser and Ellsworth, 2000). These relocations are in the static copy of the catalog. A discussion of parameters used for the relocations and the reasons for these choices is beyond the scope of this report, but we will provide this information to those that may be interested.

SEISAN allows the calculation of first focal mechanisms using a variety of techniques including FPFIT (Reasenber and Oppenheimer, 1985), HASH (Hardebeck and Shearer, 2002), and FOCMEC (Snoke et al., 1984). All these techniques continued to be used to determine focal mechanisms for earthquakes in Oklahoma during 2015 and 2016. During 2015 and 2016, ??? focal mechanisms were determined mostly for earthquakes of magnitude 3.0 and greater.

□ *Table 2.3. Regional 1-D velocity model used in Oklahoma to determine the location of earthquakes*

P-Velocity (km/s)	Depth (km)
2.700	0.0
2.950	0.3
4.150	1.0
5.800	1.5
6.270	8.0
6.410	21.0
7.90	42.0
8.15	50.0
8.5	80.0

The OGS implemented, with the support of the USGS, a continuous waveform buffer (CWB) that allows for the real-time exchange of data from our data server using SEEDLINK, which continues to be used to send data to the Incorporated Research Institutions for Seismology's (IRIS) data management center (DMC). The OGS CWB allows for the continuous archiving of data and data retrieval for earthquake studies and analysis.

In addition, the OGS began operating a quasi-real-time automatic processing system called SeiProc. The SeiProc system regularly performs coincidence triggering on different sub-nets in Oklahoma. Once events are identified, the waveforms are processed by an automatic picker and associator algorithm (Chen and Holland, 2014). After an event has been automatically located using the SEISAN earthquake location algorithm, an M_L is automatically determined for each earthquake.

SeiProc allows analysts to prioritize their efforts by being able to identify and begin analysis on earthquakes with an automatically determined magnitude of 2.5 or greater. Furthermore, it reduces the effort required by analysts for manually locating very small earthquakes. Routinely, locations and magnitudes can change substantially upon re-evaluation by a trained analyst compared to the automatic system. Because the potential for problematic events from the automatic processing system, automatic earthquake solutions are not reported. Thus, to prevent confusion, these data are only used to guide and prioritize the analysis of earthquakes.

Earthquake Magnitudes

The state has seen an increased number of magnitude 4.0 or greater earthquakes in 2015 compared to years prior. However, after further analysis many have magnitudes below 4.0; this is often the case at both the USGS and the OGS. There are many ways to calculate magnitude and the most reliable methods are usually done after the initial reporting of an earthquake and further analysis occurs. The more reliable methods for magnitude determination mostly affect the larger earthquakes and tend to reduce their magnitude slightly.

Most Oklahoma earthquakes are located and reported with an initial M_L and updated to a M_W if further analysis is deemed necessary (*i.e.* the earthquake is estimated at a $3.8M_L$ or greater). The method used by the OGS to calculate M_L and the M_L attenuation relationship used are documented in Darold et al. (2014). Local magnitudes often disagree slightly with other magnitude relationships, as can be seen in Miao and Langston (2007), but are commonly used by regional networks. Magnitude measurements are estimates based on recorded ground motions and have uncertainty that can be characterized (CEUS-SSC, 2012).

The OGS uses the spectral shape in displacement of the P or S phase to determine the M_W for earthquakes using functionality within SEISAN (Abercrombie, 1995; Brune, 1970; Caprio et al., 2011; Ottemoller and Havskov, 2003). The M_W more accurately represents the area of the fault that ruptured and the total energy released (Hanks and Kanamori, 1979; Kanamori and Anderson, 1975), whereas the initial M_L uses measured amplitudes and may more accurately represent the ground shaking of an earthquake experienced by

those that feel it. The OGS initially reported 60 earthquakes at or above a magnitude 4.0 in 2015 and 42 in 2016. However, after completing M_w analysis and using the USGS M_w calculations as the preferred magnitude, the number of reported earthquakes at or above a magnitude 4.0 was reduced to 28 for 2015 and 14 for 2016 (to November 30, 2016).

Improvements to Network from RPSEA Project

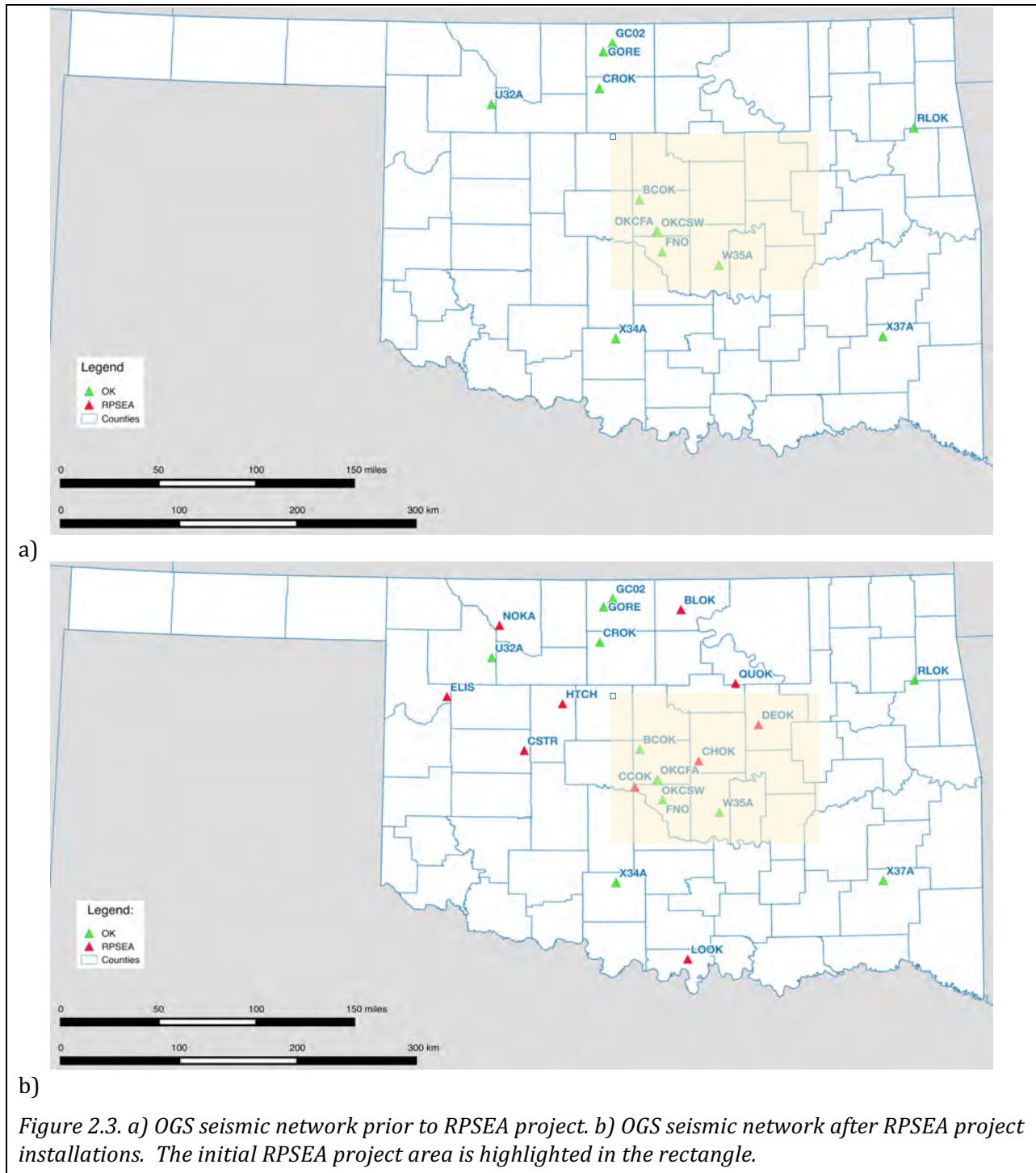
To help expand and prioritize analysis efforts the OGS had developed and implemented an automatic processing and earthquake evaluation system and upgraded the existing data archiving, retrieval, and exchange processes. Additions and upgrades to the OGS seismic monitoring network during 2015 and 2016, continued to dramatically improve earthquake location accuracies and analysis. The configuration of OGS seismic stations is shown in Figure 2.3, both before (2.3a) and after (2.3b) implementation of the system upgrades afforded by the RPSEA Project.

In the first few months of 2014, the OGS added four temporary stations, and one permanent station in response to several earthquake swarms within central and north-central Oklahoma. Instrumentation for three of these temporary stations are generously on loan from the USGS. We received instrumentation for the Oklahoma Risk and Hazard (OKRaH) network in August 2014 and installed 12 temporary stations in central and north-central Oklahoma. These instruments were borrowed from the IRIS Portable Array Seismic Studies of the Continental Lithosphere (PASSCAL), instrument center. Twelve additional stations, acquired using matching funds for the RPSEA Project from the Oklahoma Corporation Commission, were installed during 2015 and 2016.

To meet with the demands of an expanding workload in all areas and to improve communication with the community, the OGS added an acting lead seismologist, a lead seismic analyst, two additional analysts, and a seismic technician in 2015 and 2016. However, the Lead Seismologist (Austin Holland) and Research Scientist (Amberlee Darold) both left the OGS for positions with the United States Geological Survey. Jefferson Chang was promoted to Acting Lead Seismologist during the search for a Lead Seismologist. In August 2016, OGS hired Jacob Walter to the position, with a November 1, 2016 start date.

Oklahoma Risk and Hazard (OKRaH) Network

Oklahoma Risk and Hazard (OKRaH) network consists of a set of temporary seismic stations deployed as part of this RPSEA Project, including cost share contributions from the state of Oklahoma, the University of Oklahoma, and Oklahoma oil and gas operators. For this project, 12 temporary seismic stations are operated in central and north-central Oklahoma within the existing seismic monitoring network operated by the OGS. Each station consists of a sensitive seismometer, a recording device, batteries and a solar panel. All twelve of these stations feed immediately into the OGS seismic monitoring system. The data are incorporated into routine earthquake analysis within Oklahoma or in support of other research efforts. The data are also archived at the IRIS DMC (www.iris.edu) and will be made available to other researchers after the project has been completed. One station (KNG1) is being provided as open data and is available at the IRIS DMC.



The recordings from these instruments, along with the Oklahoma Seismic Network, will be used to improve our understanding of active faults and subsurface rock properties, along with the surface ground motions observed in Oklahoma. Ultimately, we hope to gain a better understanding of potential changes that may be causing some of the earthquakes within

Oklahoma. Further, current, information on the OKRaH network are available on the OGS seismic monitoring website.

OGS Outreach and Education Efforts

The increased rate of seismicity in Oklahoma in 2014-15 added to the potential future risk to the public, therefore the OGS sought to establish a more proactive stance on earthquake education and outreach efforts. This multidimensional approach encompassed presentations to the Federal Emergency Management Agency, local and state emergency management groups in addition to other civic organizations, a strong online presence, active engagement and open dialogue within the academic community, media interviews/ state-ments, and the production of hard copy preparedness materials. It is through these undertakings that the OGS stayed consistently visible and informative to the public.

Website and Social Media

On the OGS website (www.ou.edu/ogs/), a section is devoted to information regarding [Oklahoma earthquakes](#). In 2015 and 2016, the OGS website posted current earthquakes, maps of the seismic monitoring network, earthquake catalogues, current and past research publications, and earthquake preparedness/education material. Moreover, the website allowed for the external reporting of earthquakes by the public ([Report Feeling an Oklahoma Earthquake](#)), asking seismologists questions ([Ask a seismologist](#)) and the posting of frequently asked questions with replies ([OK Earthquake FAQ](#)). The homepage displays a direct link to our Twitter and Facebook accounts.

Two social media accounts, Twitter's [@OKearthquakes](#) and Facebook's [Oklahoma Geological Survey – Earthquake Notices](#), post the latest information on Oklahoma earthquakes as they are located and updated by analysts. The communication includes the date, time, magnitude, closest town, latitude/longitude, and depth of each earthquake.

The number of social media posts generally correlates with the number of earthquakes greater than magnitude 2.4. Analyst hours occur primarily within work days and working hours (8am-5pm); tweets and Facebook posts occur mainly during these times. For earthquake with magnitudes greater than 3.0, analysts are on-call and update earthquake locations as soon as possible, including weekends and holidays.

The Twitter account [@OKearthquakes](#) currently has 3,191 followers; the general OGS account, [@OKgeology](#) has 198 additional followers (total = 3,389 followers). The Facebook account [Oklahoma Geological Survey – Earthquake Notices](#) has 2,168 followers; the Oklahoma Geological Survey account has 590 additional followers (total = 2,758 followers).

Academia

From the most basic to the most advanced levels of education, the OGS seismic group strives to extend itself and its knowledge to students and scholars in all areas concerning Oklahoma earthquake education and on-going research. The OGS worked with multiple primary, secondary, and post-secondary institutions last year and held a two day Workshop on Oklahoma Seismicity, which included numerous presentations and question and answer sessions for technical participants from Federal and state government, academia,

national laboratories, and the oil and gas industry. The function was well attended with over one hundred forty participants.

At the primary and secondary levels of education, the OGS accepted several local public school invitations to teach and/or give presentations about earthquakes. Along with these invitations, level-appropriate materials were created to scaffold learning for young students and preparedness brochures were provided to students, teachers, and parents. Additionally, tours and presentations were held for students at the OGS facilities both in Norman, Oklahoma and Leonard, Oklahoma.

Because the main offices for the OGS are situated at the University of Oklahoma and because educational outreach is highly valued, the OGS employs undergraduate and graduate students to create mutually beneficial relationships of innovation and development. These student-employees help with the maintenance of catalogs, databases, and even employ their own original research at times. In turn, their education and research receives input from professionals and adds a component of practical experience.

Employees of the OGS seismic group published several papers in 2015 and 2016 and attended numerous conferences to share and receive input for recent seismic findings in Oklahoma. They collaborated often with institutions and researchers nation-wide and participated in the USGS Powell Center Working Group on Induced Seismicity. Their publications can be found on the website or in the list provided in *Chapter 9: Technology Transfer Activities*.

Local Communities

Representatives from the OGS seismic monitoring program gave numerous presentations to community organizations all over the state. These presentations provided general, factual information on the increase of Oklahoma earthquakes and vital information about Oklahoma earthquake hazard and preparedness. By sharing this information with civic-minded community organizations, it is the OGS's expectation that community leaders (members of these organizations) will further disseminate it, ultimately establishing more public awareness.

Media

The OGS seismic group offered many interview and media coverage opportunities to local, national and global media. Through media exposure, the OGS gained yet another method of communication and transparency with the public.

Publications 2015-2016

Publications in 2015 and 2016 are listed in *Chapter 9: Technology Transfer Activities*

Concluding Remarks

Earthquakes are not predictable and we do not know what the future holds, therefore, it is not possible to know whether we are going to see an increase or a decrease in 2017 or beyond. The 2016 decrease in earthquakes of a magnitude 4.0 and greater decreases the probability that we could have a damaging earthquake in Oklahoma. On the other hand, the occurrence of three earthquakes of magnitude 5.0 and greater suggests continuing

strong concern about the possibility of damaging earthquakes. Because it is important for Oklahomans to understand how to prepare and what to do during an earthquake, our website has related information and links aimed to educate the public about [earthquake preparedness](#).

Acknowledgements

We would like to thank all those that helped with the monumental task of earthquake analysis in 2015 and 2016, including Stephen Marsh, Jennifer Morris, Noorulan Ghouse, Andrew Thiel, and Junjun Hu. We would also like to thank Isaac Woelfel, our seismology technician, who maintains the seismographs and has worked tirelessly to install new and move existing seismometers during these very challenging years. We also wish to acknowledge Harley Benz, Paul Earle, David Ketchum, Justin Rubinstein, Robert Williams and many others at the USGS for their help, support and productive interactions.

References Cited

- Abercrombie, R. E., 1995, Earthquake source scaling relationships from -1 to 5 ML using seismograms recorded at 2.5 km depth: *J. Geophys. Res.*, v. 100, no. B12, p. 24,015-024,036.
- Aki, M., 1965, Maximum likelihood estimate of b in the formula $\log N = a - bM$ and its confidence limits: *Bull. Earthquake Res. Inst., Tokyo Univ.*, v. 43, p. 237-239.
- Brune, J. N., 1970, Tectonic Stress and the Spectra of Seismic Shear Waves from Earthquakes: *J. Geophys. Res.*, v. 75, no. 26, p. 4997-5009.
- Caprio, M., Lancieri, M., Cua, G. B., Zollo, A., and Wiemer, S., 2011, An evolutionary approach to real-time moment magnitude estimation via inversion of displacement spectra: *Geophys. Res. Lett.*, v. 38, no. L02301, p. 7.
- CEUS-SSC, 2012, Technical Report: Central and Eastern United States Seismic Source Characterization for Nuclear Facilities, EPRI, Palo Alto, CA, U.S. DOE, and U.S. NRC, p. 3176.
- Chen, C., and Holland, A. A., 2014, A Pure-Python Phase Picker and Event Associator: *Seismol. Res. Lett.*, v. 85, no. 2, p. 414.
- Darold, A., Holland, A. A., Chen, C., and Youngblood, A., 2014, Preliminary Analysis of Seismicity Near Eagleton 1-29, Carter County, July 2014: *Okla. Geol. Surv. Open-File Report*, v. OF2-2014, p. 17.
- Gutenberg, B., and Richter, C. F., 1944, Frequency of Earthquakes in California: *Bull. Seismol. Soc. Am.*, v. 34, no. 4, p. 185-188.
- Hainzl, S., Scherbaum, F., and Beauval, C., 2006, Estimating Background Activity Based on Interevent-Time Distribution: *Bull. Seismol. Soc. Am.*, v. 96, no. 1, p. 313-320.
- Hanks, T. C., and Kanamori, H., 1979, A Moment Magnitude Scale: *J. Geophys. Res.*, v. 84, no. 5, p. 2348-2350.
- Hardebeck, J. L., and Shearer, P. M., 2002, A New Method for Determining First-Motion Focal Mechanisms: *Bull. Seismol. Soc. Amer.*, v. 92, no. 6, p. 2264- 2276.

- Havskov, J., and Ottemoller, L., 1999, SeisAn Earthquake Analysis Software: *Seismol. Res. Lett.*, v. 70, p. 532-534.
- Holland, A. A., 2013, Optimal Fault Orientations within Oklahoma: *Seismol. Res. Lett.*, v. 84, no. 5, p. 876-890.
- Kanamori, H., and Anderson, D. L., 1975, Theoretical basis of some empirical relations in seismology: *Bull. Seismol. Soc. Amer.*, v. 65, p. 1073-1095.
- Miao, Q., and Langston, C. A., 2007, Empirical Distance Attenuation and the Local- Magnitude Scale for the Central United States: *Bull. Seismol. Soc. Amer.*, v. 97, no. 6, p. 2137-2151.
- Ottemoller, L., and Havskov, J., 2003, Moment Magnitude Determination for Local and Regional Earthquakes Based on Source Spectra: *Bull. Seismol. Soc. Am.*, v. 93, no. 1, p. 203-214.
- Reasenber, P., and Oppenheimer, D., 1985, Fpfit, fpplot, and fppage: Fortran computer programs for calculating and displaying earthquake fault plane solutions.: U.S. Geol. Survey Open-File Report, v. 85-739, p. 25.
- Snoke, J. A., Munsey, J. W., Teague, A. G., and Bollinger, G. A., 1984, A program for focal mechanism determination by combined use of polarity and SV-P amplitude ratio data: *Earthquake Notes*, v. 55, p. 15.
- Waldhauser, F., and Ellsworth, W. L., 2000, A double-difference earthquake location algorithm: Method and application to the northern Hayward fault: *Bull. Seismol. Soc. Amer.*, v. 90, p. 1353-1368.
- Zoback, M. L., 1992, First- and Second-Order Patterns of Stress in the Lithosphere: The World Stress Map Project: *J. Geophys. Res.*, v. 97, no. B8, p. 11,703- 711,728.

Description of RPSEA Task 6 – Collect Gravity Infill Data: The Subcontractor shall collect additional gravity data to infill existing gravity data. The location of the infill gravity data shall be dependent on the spatial resolution of the existing gravity data and the necessity to validate the density distribution within the 3D geology interpretation as part of the recursive process addressing the misfit between the observed and estimated gravity data.

The report appended below summarizes gravity data collection activities supported by the RPSEA Project.

3. Gravity Data Collection

Stephen Holloway, Kevin Crain

*Oklahoma Geological Survey, Sarkeys Energy Center, Rm. N-131
100 East Boyd St., Norman, Oklahoma 73019-0628*

Introduction

The goal of the gravity collection portion of the RPSEA project was supply data to model the subsurface structure to better understand the structure of the crystalline basement as part of our effort to study the seismicity in the region.

The objectives of the gravity collection fieldwork conducted from June 2014 to July 2016 were several-fold:

- to collect more densely spaced ground gravity measurements to add to a regional gravity database,
- to identify significant gravity anomalies to be incorporated into a geologic model, and
- to identify faults and deeper structures especially in areas of possible induced seismicity.

This gravity fieldwork builds upon the PACES Gravity Database developed by the University of Texas at El Paso, which contains contributions from the U. S. Geological Survey, the National Geospatial-Intelligence Agency, National Oceanic and Atmospheric Administration, industry and academic colleagues. Details of the PACES Gravity Database compilation effort are available in the USGS Open-File Report 02-463 (<http://pubs.usgs.gov/of/2002/0463/>). Our work focused on increasing the spatial density of the gravity measurements in the defined RPSEA study area, which centered on the Prague earthquake sequence. Also, as the earthquake frequency increased and the location of seismicity changed over time, we shifted our focus northward, extending beyond our original study area.

Gravity potential field anomalies reflect variations in the physical properties of rocks at depth. Combined with independent constraints from geologic field mapping, borehole analysis, geomagnetic survey anomalies, and other geophysical observations, gravity studies provide insight into the buried geological structures and the tectonic development of the area.

Global Positioning System (GPS) Data

High-quality GPS location data are required for accurate gravity analysis. Sub-decimeter elevation accuracy is needed to obtain gravity readings that are more accurate than 20 microlgal (μGal , 10^{-8} m/sec²). Horizontal accuracy is not as crucial as vertical accuracy in the gravity data reduction process, although GPS solutions typically provide a horizontal accuracy that is about three times as fine as the vertical accuracy. Both the accuracy and the precision of a GPS solution are important for evaluating the quality of a location determination, but GPS processing software commonly reports only precision estimates.

We employed two GPS units (a base and a rover) to measure high-quality locations at gravity stations. These units utilize dual-frequency carrier-phase antennas and apply differential corrections relative to local base stations after the GPS time-series are recorded. The GPS units used were Topcon GB-1000 receivers with PG-A1 with ground plane antennas. Topcon documentation specifies a horizontal accuracy of 10 mm + 1.0 ppm (x baseline length) and vertical accuracy of 15 mm + 1.0 ppm (x baseline length). So, for example, a baseline of 10 km between the base and rover GPS units would yield a horizontal accuracy of 20 mm and vertical accuracy of 25 mm under ideal conditions.

To further increase our accuracy, the base station measurements are submitted to the National Geodetic Survey's (NGS) Online Positioning User Service (OPUS), which uses the three nearest Continuously Operating Reference Stations (CORS) in the region to calculate differentially a high-precision location of the base station.

The base and rover receivers recorded GPS data every 5 seconds. The GPS rover data were acquired at gravity stations during 5-minute occupations. On some occasions, we lost carrier phase-lock on the rover and had to reacquire it. This necessitates a new 10-minute static wait time before continuing.

We also tested real-time kinematic (RTK) observation mode in prior field sessions but experienced problems with radio shadowing, out of range conditions, significant battery draw, plus the added complication of needing to move the base stations multiple times per day. We ultimately decided that post-processing would give us satisfactory results while utilizing our time efficiently in the field.

GPS observations are recorded as ellipsoidal height and must be converted to orthometric height before being used for geophysical analysis. We first convert the standard GPS output of WGS84 datum to NAD83(2011) to incorporate the CORS station corrections. We then convert ellipsoidal height to orthometric height using NAVD88 (computed using GEOID12B).

Gravity Data

We collected gravity observations at 3,092 locations in north central Oklahoma over 160 field days from June 2014 to July 2016 (Figure 3.1). We used two gravity meters, both Scintrex CG-5 Autograv systems (serial numbers 080940457 and 080940101). These gravity meters compute a gravity reading from a filtered time series of raw readings over a specified interval of time. We used an occupation time of 1 minute, which was recommended by

the manufacturer. At each gravity station, we collected 3 occupations and when subsequent gravity readings were within 0.02 μGal , we accepted the average of the three readings as the value for the station.

We utilized the absolute gravity base station SEC1 that was established in 2005. SEC1 is located in the basement of the Sarkeys Energy Center on The University of Oklahoma campus. It is a small brass cap embedded in concrete opposite the tower elevators on level 1. Absolute g has been estimated at SEC1 to be 979656.483 ± 0.016 mGals. We visited SEC1 at the beginning and end of each gravity field day, taking three sets of three readings and then taking the average to establish our starting and ending absolute values.

After taking our absolute gravity base station readings, we then would drive to a predetermined area and establish a local relative gravity field base station. This location of the field base station was chosen based on several factors including accessibility, security, and a central location for the desired area targeted for that field day. Good practice is to repeat readings at the same field base station over multiple days and tie those readings to the absolute gravity base station. This serves as an added check on the repeatability of readings.

Gravity observations were made adjacent to the field vehicle (Figure 3.2) along public roadways, generally along section-line roads. Stations were located with 2-mile spacing as a compromise between coverage and density both to fill existing gravity coverage gaps and to collect a grid of higher spatial density station spacing.

To process the gravity data, we first correct for instrument drift by comparing the difference between the tide-corrected gravity readings at the gravity base station at the beginning and ending of each day. This is in addition to the built-in tidal and instrument drift corrections. We then apply the standard latitude correction and free-air correction to each reading. At this point, the Free Air gravity anomaly values could be incorporated into our gravity modeling effort.

A total of 9,020 unique gravity readings were reduced, resulting in 3,092 gravity stations with accompanying post-processed GPS coordinates.

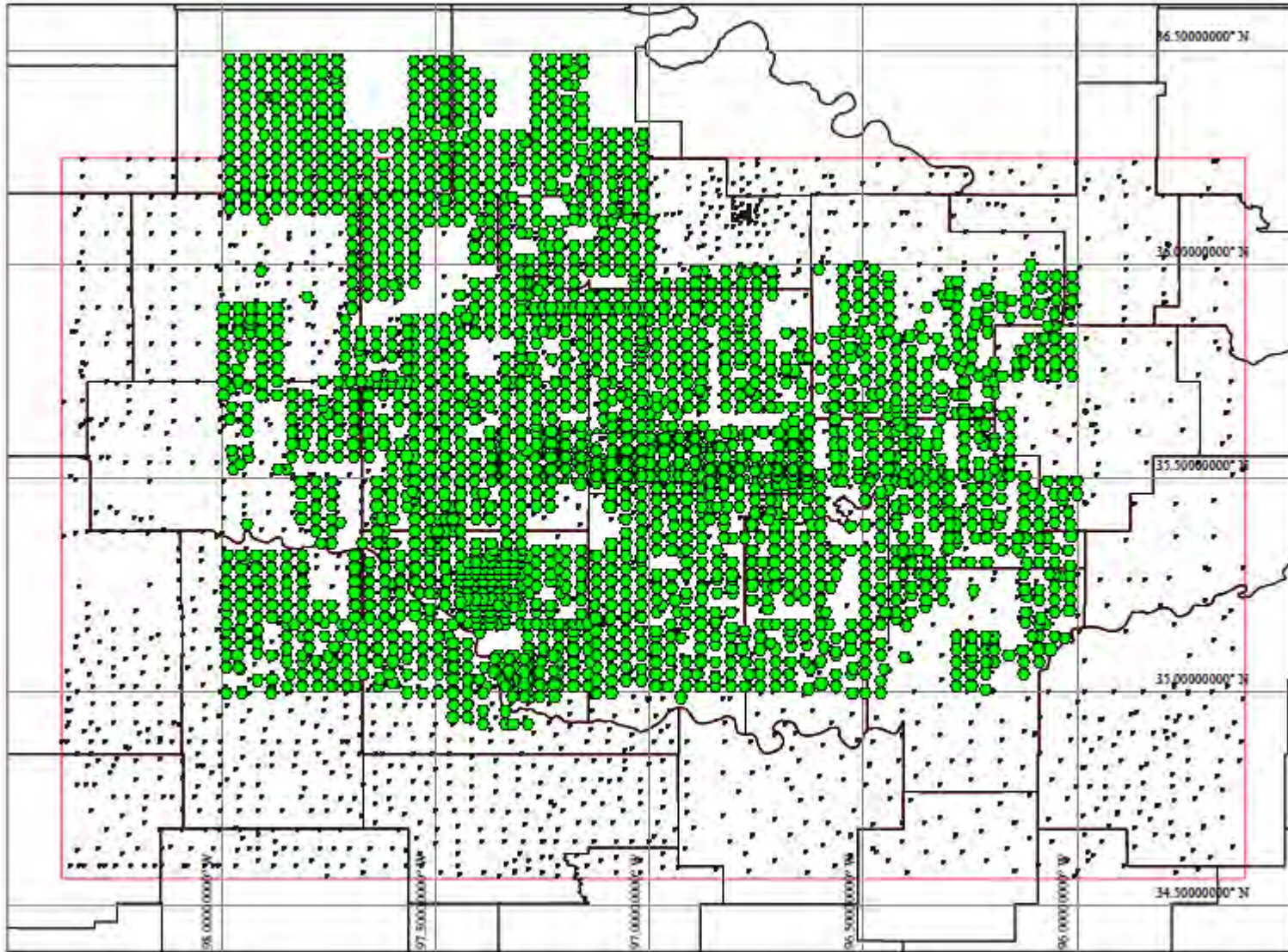


Figure 3.1: Gravity station coverage map for the RPSEA project area (highlighted in red). Gravity stations collected for this project are shown as green dots. Gravity stations from the PACES gravity database are shown as black dots.



Figure 3.2: Scintrex CG-5 gravity meter prepared for taking a reading at a gravity station. The GPS rover antenna is located on the roof secured by a magnetic mount.

Description of RPSEA Task 9 – Construction of Integrated Multi-Variate 3D Geologic Interpretation

This task provides the crucial integrative platform for the integrated analysis. A multi-variate 3-dimensional (3D) earth model based on a 3D geological interpretation initially employing subsurface data, digital elevation, and results that define structures below drilling depths shall be developed. The 3D interpretation shall be based on gravity data that covers the study area uniformly, and shall be iterated based on results such as seismic tomography, seismic data provided by industry, and detailed well log analysis.

The report appended below summarizes a portion of Task 9 comprising a seismic tomography study in Oklahoma, supported by the RPSEA Project.

4. Seismic Tomography of North Central Oklahoma

Chen Chen

*Oklahoma Geological Survey, Sarkeys Energy Center, Rm. N-131
100 East Boyd St., Norman, Oklahoma 73019-0628*

The large number of earthquakes that occurred in Oklahoma and the surrounding region have drawn a great deal of attention since 2009. Many seismometers were deployed in this region to better record the seismicity; these new instruments easily produce large data sets that are almost impossible to process manually. Chen and Holland [2016] developed a *Python* package for automatically detecting earthquakes and making phase picks. The surging seismic activity in Oklahoma provides an excellent opportunity to study deep structures within the crystalline basement, which are helpful to better understand the relationship between the seismicity and geological structures. Prior to 2009, earthquakes in Oklahoma occurred over a broad region, without showing a clear relationship with previously known structures. However, the recent profound seismicity increase may be related to reactivation of faults and/or fractures within the basement, which have been interpreted to be triggered by wastewater injection that increases the pore-pressure, in turn promoting fault slip (for example, Keranen et al., 2013).

Chen derived two velocity models using north-central Oklahoma earthquakes. By using FMTOMO, he created the first velocity model with >8000 earthquakes of magnitude 2.0 or greater (M2+). This model used several cutoffs, such as requiring depths >3.0 km, number of stations with observed arrivals >12, and root mean square (RMS) residuals of travel-time <0.6 seconds (s), that were selected to control the data quality and computation time. To better control the velocity model from the tomographic inversion, Chen filtered the picks with travel-time errors greater than 1.5 s comparing to predicted travel-time based on a one dimensional (1D) velocity model. After filtering the picks, there were 153,119 P- and 145,949 S-picks left. The V_p/V_s ratio used was 1.73.

The reliable region of both P- and S-wave tomography results was estimated with checkerboard tests. The alternatively perturbed velocity anomalies were imposed onto the initial 1D velocity model to create a checkerboard pattern. Positive and negative anomalies of 0.6 km/s, were added to P-wave velocity, and similarly ± 0.3 km/s were added to S-wave velocity alternatively. The model was parameterized with an optimized node spacing of about 0.15° (Δx : ~ 13 km) \times 0.12° (Δy : ~ 13 km) \times 2.8 km (Δz) after several tests with different node spacing. The solution converged well, and the residuals were reduced to a reasonable level after 4 iterations. The checkerboard patterns of the P-wave velocity model shallower than ~ 15 km were recovered for central and north central Oklahoma.

The second velocity model was created by using the SIMUL2000 package with the composite event method, which reduces the volume of the data to improve the computation time. Although the total number of picks is reduced, the composite event method preserves as much of the original phase pick information as possible. In addition, this method makes the composite event distribution more uniform. 8,194 M2+ events were used to start this tomographic processing.

The first target earthquake was selected that contains the most picks from the 1D velocity-relocated data. A close event search algorithm identified the nearby earthquakes within a certain radius (2 km in our case) centered at the target event. For a certain station, the median value of all the picks from the events within the 2-km searching radius (including the target event) was selected instead of taking the mean value. The median value was assigned to the target event as the phase record from that certain station. A larger radius searching (5 km in our case) followed to exclude the events between two spheres (with radius 2 km and 5 km in this case, respectively) for candidate treatment of the next target event in the future. There were 493 composite events with 13,447 P-picks and 11,293 S-picks constructed from 8,194 M2+ events. The first 485 composite events were used to conduct the second velocity modeling study, which has more than 99.5% of the picks from all the composite events.

A 30-km horizontal grid was chosen to invert for the three-dimensional (3D) velocity model, which is about twice the grid size of the FMTOMO model, due to the computation capability restriction. The vertical grid points are not equally spaced, which permits better representation in our initial velocity model. The V_p - and V_p/V_s -ratio-damping parameters were optimized with a series of single-iteration inversions, respectively. For the V_p damping determination, the damping parameters ranged from 50 to 2000 to plot the data misfits versus model variation tradeoff curve, while prohibiting the V_p/V_s ratio inversion. From the V_p tradeoff curve, 300 was chosen as the optimized value because the data misfits can be reduced significantly without introducing too much model variance. By holding the V_p damping fixed at 300, Chen could use a series of V_p/V_s ratio damping parameters from 10 to 1000 to determine the optimized value as 70. Thus, 300 and 70 were chosen as the values for V_p and V_p/V_s ratio, respectively, in the tomographic inversions. Although lower damping values can reduce the data misfits, they can introduce some sharp and strong velocity anomaly features that probably are artifacts.

To better understand the structures in the crystalline basement, velocity models, gravity, and magnetic data were used to examine the geological correlation. On a large scale, the velocity model correlates to gravity anomalies because dense rocks generally have high

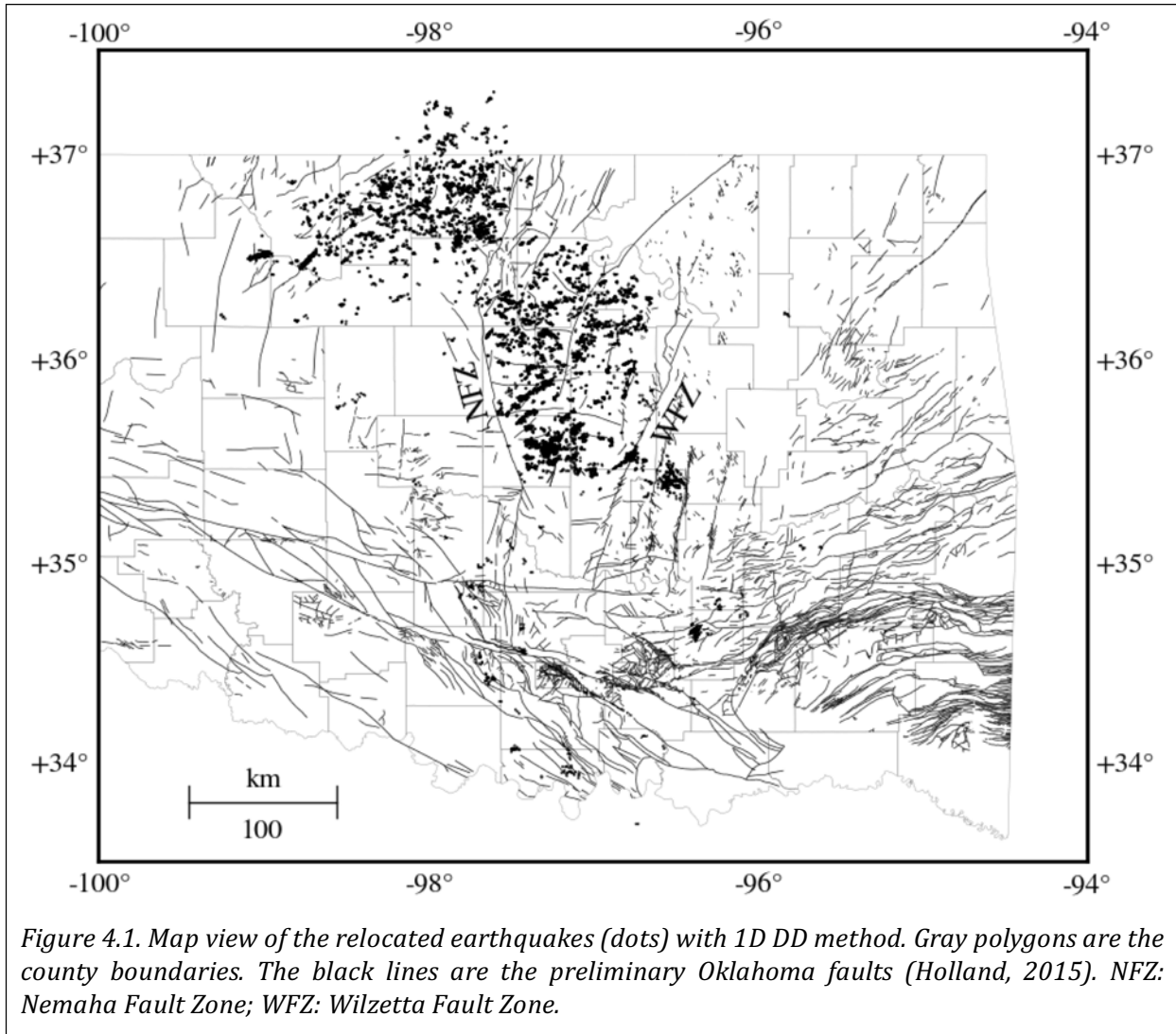
velocities, and vice versa. The velocity models reveal strong lateral heterogeneities within the Precambrian crystalline basement, which indicates complex structures in the upper portion of the crust in the study area, such as igneous intrusions related to the OCM (Osage County Microgranite), the SGG (Spavinaw Granite Group), and the widely distributed COGG (Central Oklahoma Granite Group) unit in north central Oklahoma (Reference). I estimated a low V_p/V_s ratio zone roughly from depth $\sim 3 - 10$ km. The averaged basement top is ~ 3 km in Oklahoma. Therefore, the V_p/V_s ratio can be simplified to three layers: <3 km, ~ 3 to 10 km, and >10 km, although there is a strong variation of V_p/V_s ratio in some cross-sections. Due to the complex fault and fracture structures in the basement, it is considered highly possible that wastewater can penetrate to the deep basement, possibly even down to 10 km or more. Water-filled fractures can be used to explain the low V_p/V_s ratio zone in the upper basement of central Oklahoma.

Earthquake location estimation is one of the most important inverse problems in seismology. Most earthquake location methods are based on exploiting phase arrivals from the seismic waveforms and a selected velocity model. Accurate earthquake location is important for many applications, such as fault studies, hazard assessment, seismic tomography, stress field determination, identification of induced seismicity, and others.

Most of the earthquakes in central Oklahoma are clustered and presented northeast-southwest (NE-SW) or northwest-southeast (NW-SE) trending orientation that is consistent with the \sim East-West maximum horizontal stress state within the region (Holland et al. earthquake summary). With the 3D velocity model, the cataloged earthquakes were relocated. The high-accuracy earthquake locations improved the resolution of fault locations by producing sharper patterns of seismicity. Furthermore, the improved earthquake locations can potentially better explain the relationship between injection wells and induced seismicity. In addition, the improvement of the earthquake locations can help identify primary fault planes from focal mechanisms, crustal deformation, and others.

The 3D velocity relocation strategy is to first relocate the cataloged earthquakes with the single event method, which is used to improve the absolute earthquake locations. Then, a double differential (DD) method follows to improve the relative locations for the clustered nearby events with the 3D velocity model. The DD technique takes advantage of the fact that if the hypocentral separation between the nearby events is much smaller than the event-station distance and velocity variation scale, the ray paths from the event to the common station are similar. In this case, the relative location between nearby events can be improved by the double-differential travel-times and the hypocentral separation, even though the travel-times are biased by the 3D velocity structures. To compare the difference between the 1D and 3D relocation results, the cataloged earthquakes were relocated with a 1D velocity model. Figure 4.1 shows the relocated earthquakes using the 1D DD model.

Although the 1D and the 3D velocity relocations show similar shapes and orientations of clusters, there are systematic shifts between the results. Two large earthquake groups that are separated by Nemaha Uplift have different directions of shift. The earthquakes are shown in Figure 4.2. Most of the clusters in the southern group, which is between the Nemaha Fault Zone (NFZ) and the Wilzetta Fault Zone (WFZ), basically shift westward and northwestward (in greenish color). The clusters in the northern group to the west of the



NFZ mainly shift southward (in reddish color). The dominant shift distance is about 0.5 km, and the average shift amount is 0.7 km. More than 80% of the earthquakes shift less than 1 km. There are only a few events shifting greater than 2 km.

DD method relocation results with the 1D velocity model

Although the 3D velocity model can improve the absolute earthquake locations and relative locations, the DD relocation with the 1D velocity model still has important meaning for this study. The relocated earthquakes are shown in Figure 4.1, which also present clear and narrow clusters. The shapes and orientations of the clusters are almost all consistent with the 3D velocity relocated ones.

After 12 relocation iterations, the RMS travel time residuals reduced to about 0.29 s (Figure 4.3(a)), which is slightly higher than that of the 3D velocity relocation. The slightly higher RMS residuals with more iteration numbers may indicate that the 3D velocity model has the better relocation performance. Figure 4.3(b) shows a histogram of the residuals from

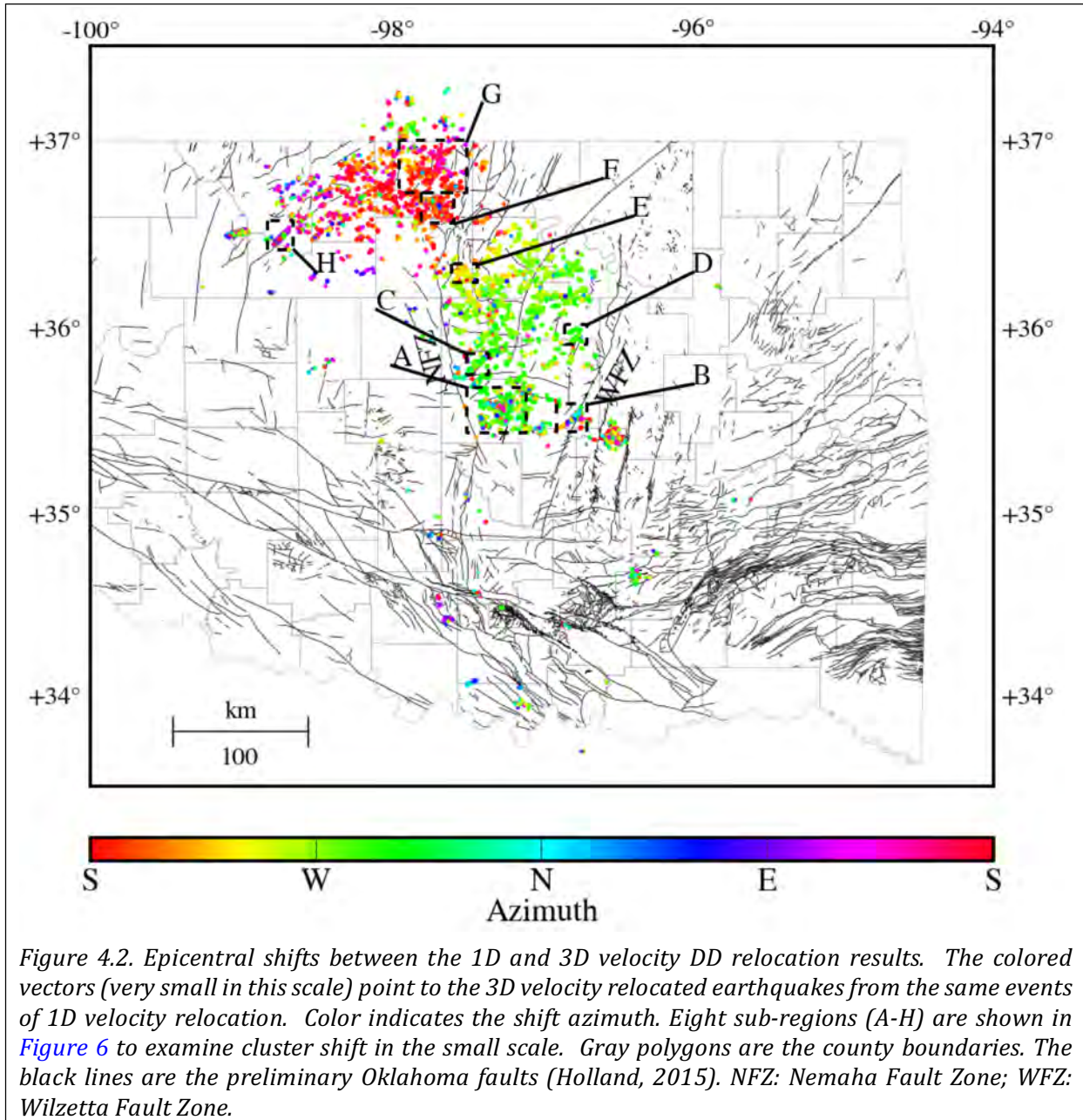


Figure 4.2. Epicentral shifts between the 1D and 3D velocity DD relocation results. The colored vectors (very small in this scale) point to the 3D velocity relocated earthquakes from the same events of 1D velocity relocation. Color indicates the shift azimuth. Eight sub-regions (A-H) are shown in Figure 6 to examine cluster shift in the small scale. Gray polygons are the county boundaries. The black lines are the preliminary Oklahoma faults (Holland, 2015). NFZ: Nemaha Fault Zone; WFZ: Wilzetta Fault Zone.

3D DD relocation results. Figure 4.3(c) shows most earthquake depths are around 5 km. As with the 3D velocity relocation results, evaluation of histograms of location uncertainties suggest that most of the earthquakes have small uncertainties, about 0.4 km for x and y directions and 0.6 km for z direction.

Comparison between the 3D and 1D DD relocations

Although the 1D and the 3D velocity relocations show similar shapes and orientations of clusters, there are systematic shifts between the results. For comparison, we plotted dif-

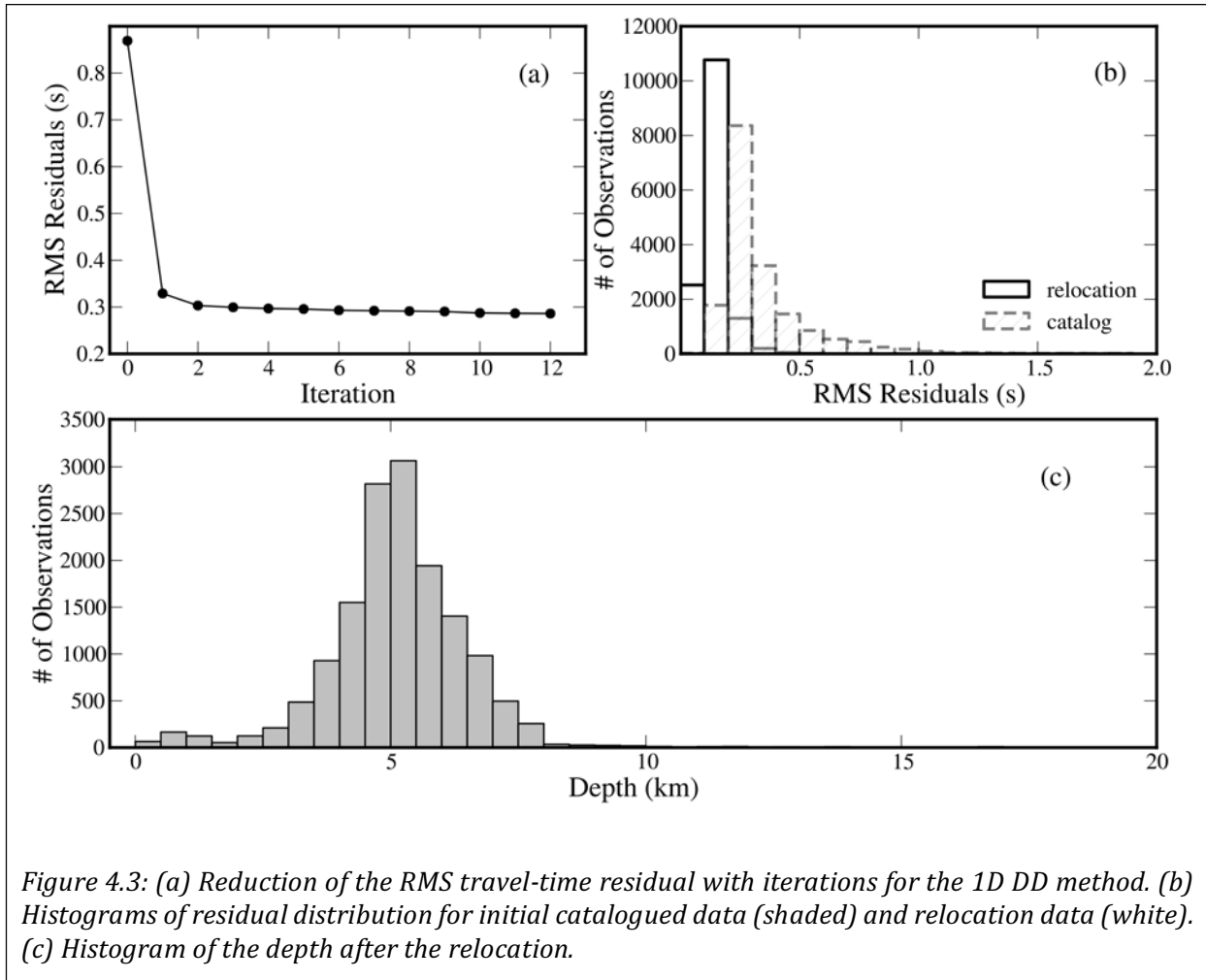
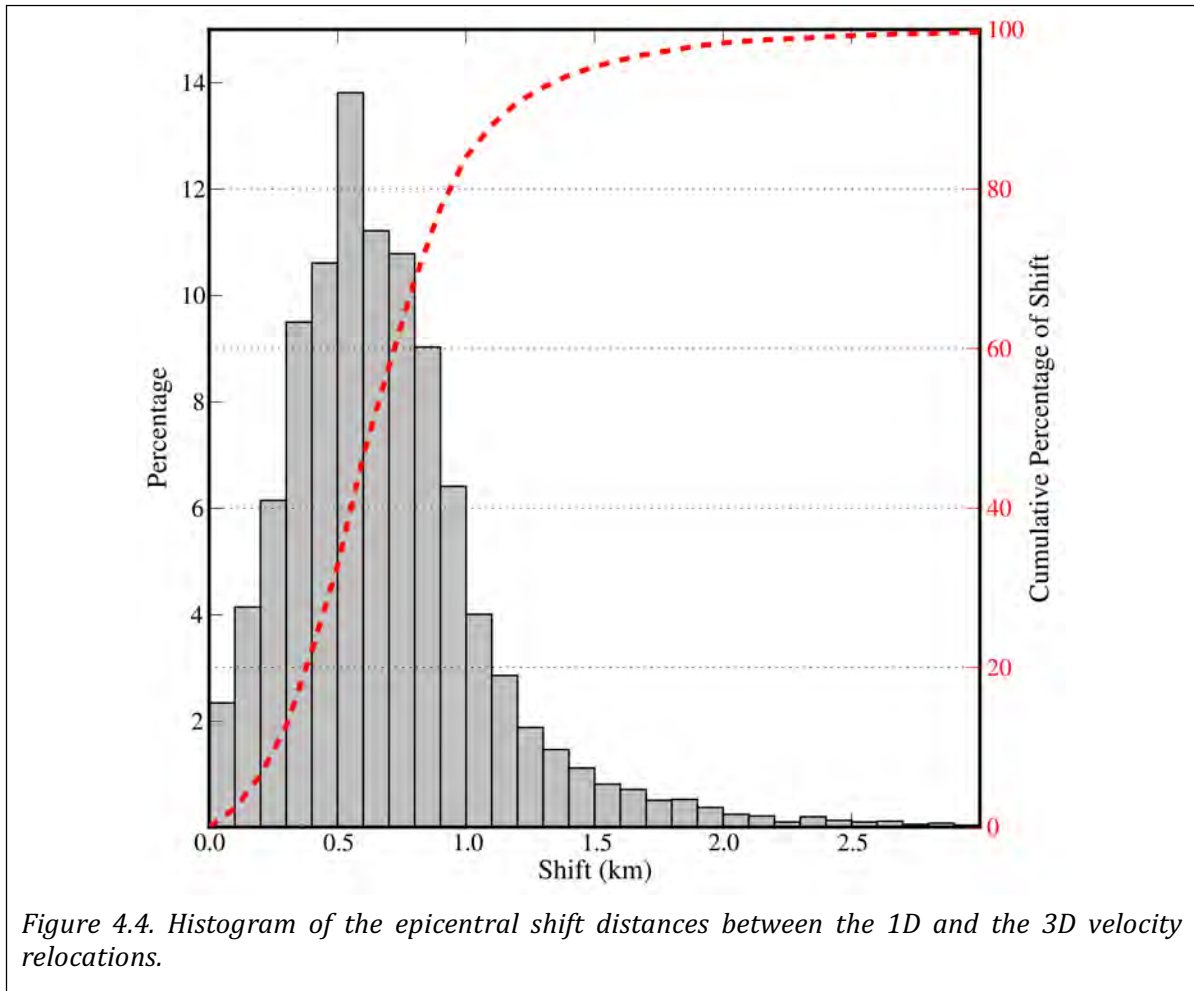


Figure 4.3: (a) Reduction of the RMS travel-time residual with iterations for the 1D DD method. (b) Histograms of residual distribution for initial catalogued data (shaded) and relocation data (white). (c) Histogram of the depth after the relocation.

ferences between the 1D and the 3D velocity DD relocation results in Figure 4.2. The vectors point to the 3D velocity DD relocation from the 1D velocity DD relocation and are color coded for directions of the shift. Two large earthquake groups have different shifting directions (Figure 2). As noted above, most of the clusters in the southern group, which is between the NFZ and the WFZ, basically shift westward and northwestward (in greenish color). The clusters in the northern group to the west of the NFZ mainly shift southward (in reddish color). Figure 4.4 shows the histogram of the epicentral shift distances between the 1D and 3D velocity relocation results. The dominant shift distance is about 0.5 km, and the average shift amount is 0.7 km. More than 80% of the earthquakes shift less than 1 km. There are only a few events with shifts greater than 2 km. Figure 4.5 shows 8 sub-regions (black dashed boxes in Fig. 4.2) to examine cluster shifting in small scales.

Sub-region A in Figure 4.5(a) shows the relocated clusters near the town of Jones, OK. The 3D velocity relocated earthquakes (dots) generally present a systematic shift in orientation compared to the 1D velocity relocation (vector tails). (The symbols are the same for all the sub-regions in Figure 4.5a-i. The vectors point to the 3D DD relocation from the 1D DD relocation.) The prominent shift in directions for the earthquakes in this area is northwest,



although there are a few earthquakes moving in other directions. The clusters in this area do not seem to present clear orientations.

Sub-region B in Figure 4.5(b) shows the Prague sequence, which is the largest seismic sequence that has drawn a great deal of attention (e.g. Keranen, 2013; McNamara, 2015). Three moderate damaging earthquakes (Mw 4.8, 5.7, and 4.8) occurred in early November 2011 near Prague, OK. The aftershocks present a clear NE-SW trending orientation that very likely suggests a rupture, and an interpreted fault was inferred from this sequence. The earthquakes in the sequence tail show more consistent southwest shifting (in yellowish color). The northwestern earthquakes in the sequence shift southward (in reddish color) to the fault, and the southeastern earthquakes in the sequence primarily shift northwestward (in greenish color) to make the sharper seismicity pattern.

Sub-region C in Figure 4.5(c) shows several clusters near Guthrie, OK, where a NE-SW trending fault is to the southeast of the clusters. Most of the earthquakes shift slightly to the west (in greenish color). The largest cluster in this area, with very consistent shifting, presents a clear conjugate-plane pattern (NE-SW and NW-SE). The cluster in the southwest corner appears to show two parallel separated small clusters with the primary northwest

shifting and a few other shifting directions. Several earthquakes at the northeastern corner shift to the northeast (in bluish color).

There are two NE-SW trending clusters around Cushing, OK in Figure 4.5(d). Two earthquake clusters in this sub-region D present relatively consistent northwest shifting orientations. The earthquakes around this region have tremendous meaning to the energy security of United States, where one of the world's largest crude oil storage facilities is located (McNamara et al., 2015). In October 2014, two M4+ earthquakes shook the Cushing oil hub that is a strategic infrastructure of United States. McNamara et al., (2015) inferred a WNW-ESE fault based on their earthquake relocation study (Figure 4.5e) for the southern cluster and made a series of analyses. However, our relocation result shows NE-SW trending orientations for it, which is different than McNamara et al., (2015). We think that more studies may be necessary for further details to demonstrate the fault structures in this area.

Sub-region E in Figure 4.5(f) is close to the gap between two large earthquake groups. Most earthquakes of two obvious clusters in this sub-region shift southwestward (in orange and yellowish colors). These two clusters also present NE-SW and NW-SE orientations, which are consistent with the maximum horizontal stress state in Oklahoma. Only a few earthquakes shift to other directions.

Several parallel NE-SW trending clusters in sub-region F, south of Medford, are shown in Figure 4.5(g). This area is located in the large northern earthquake group. Most of the earthquakes in this area shift southward (in reddish color). The consistent cluster orientations may indicate similar fault strike orientations in this sub-region.

As with sub-region F, clusters in sub-region G, north of Medford, also present systematic southward shifting (in reddish color) in Figure 4.5(h). Some clusters show NE-SW trending orientations, and some of them show NW-SE orientations, which are close to nearby parallel fault segments.

Sub-region H in Figure 4.5(i) shows a NE-SW trending cluster on the Galena Township Fault, in northwestern Oklahoma. The earthquakes in this cluster primarily shift eastward (in purplish color). The cluster aligns well with the mapped fault to the southwest. This fault may be blamed for the most moderate earthquakes in this cluster, which occurred in early 2016.

Discussion

Demonstrating the relationship between the earthquakes and geological structures in Oklahoma is important, because the seismicity has been very active in this region since 2009. The 3D velocity model can improve the earthquake locations, which helps to correlate the seismicity with the mapped faults, interpret unmapped faults, and determine the connection between the earthquakes and the wastewater injection wells. Some of the relocated clusters present narrower and more linear trends, which may indicate the potential faults that are related to the clusters. Therefore, the correlation between the earthquake locations and faults may be used to decide where to build large-scale structures with low risk, such as high-rise facilities, oil storage infrastructures, pipelines, and others. In addition, the correlation may provide information to evaluate insurance rates of residential buildings in Oklahoma as well (Luza and Lawson, 1982).

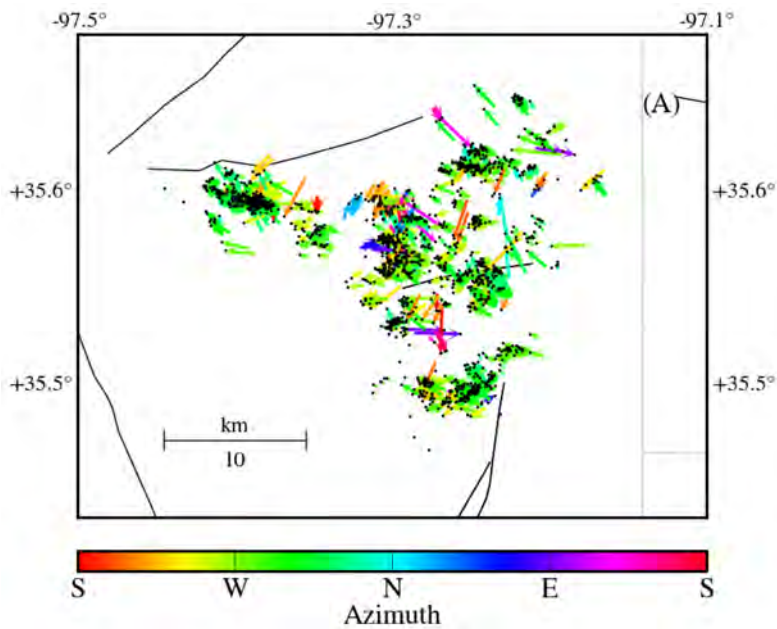


Figure 4.5(a). Sub-region A in Figure 3 (Jones area). Epicentral shifts between the 1D and 3D velocity DD relocation results (black dots). The colored vectors point to the 3D velocity relocated earthquakes from the same events of 1D velocity relocation. Color indicates the shift azimuth. The thick black lines are the preliminary Oklahoma faults (Holland, 2015). The gray lines are the county boundaries.

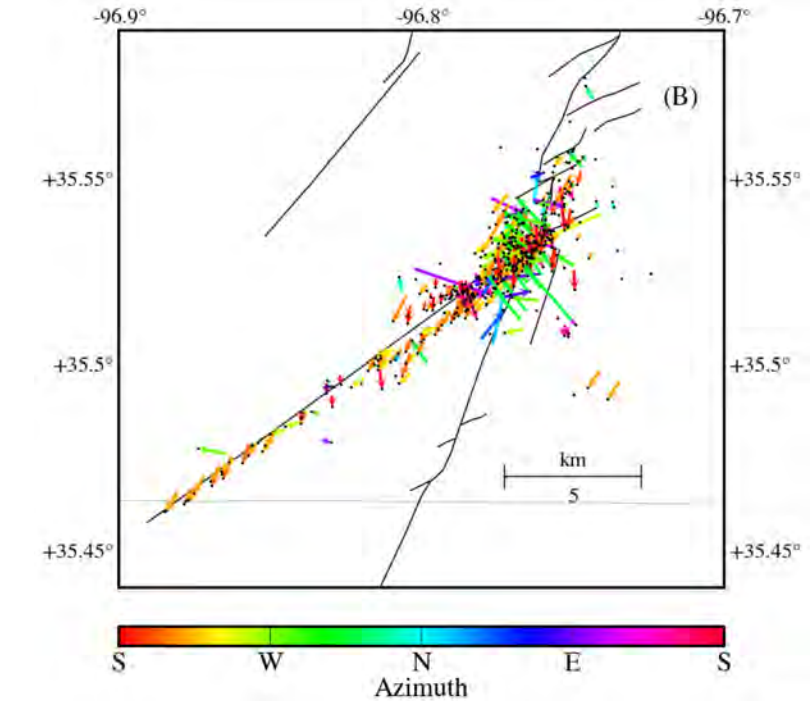


Figure 4.5(b). Sub-region B in Figure 3 (Prague area). Epicentral shifts between the 1D and 3D velocity DD relocation results (black dots). The colored vectors point to the 3D velocity relocated earthquakes from the same events of 1D velocity relocation. Color indicates the shift azimuth. The thick black lines are the preliminary Oklahoma faults (Holland, 2015). The gray lines are the county boundaries.

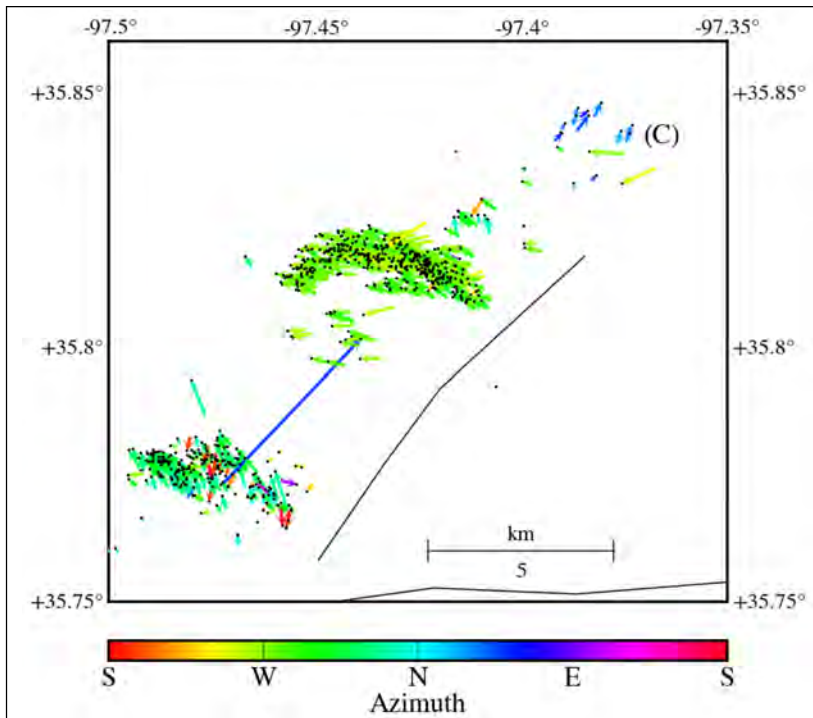


Figure 4.5(c). Sub-region C in Figure 3 (Guthrie area). Epicentral shifts between the 1D and 3D velocity DD relocation results (black dots). The colored vectors point to the 3D velocity relocated earthquakes from the same events of 1D velocity relocation. Color indicates the shift azimuth. The thick black lines are the preliminary Oklahoma faults (Holland, 2015).

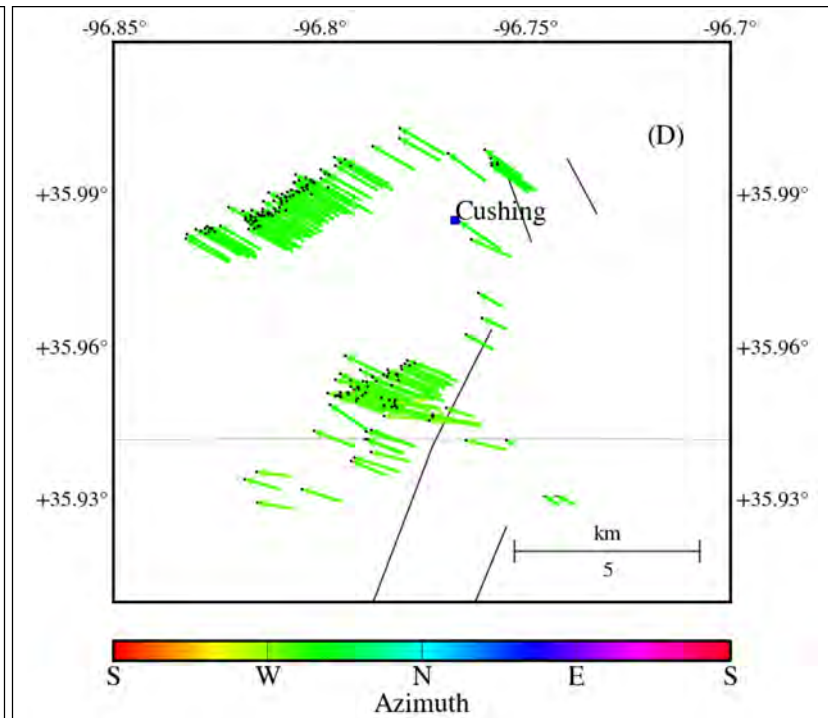


Figure 4.5(d). Sub-region D in Figure 3 (Cushing area). Epicentral shifts between the 1D and 3D velocity DD relocation results (black dots). The colored vectors point to the 3D velocity relocated earthquakes from the same events of 1D velocity relocation. Color indicates the shift azimuth. The thick black lines are the preliminary Oklahoma faults (Holland, 2015). The gray lines are the county boundaries.

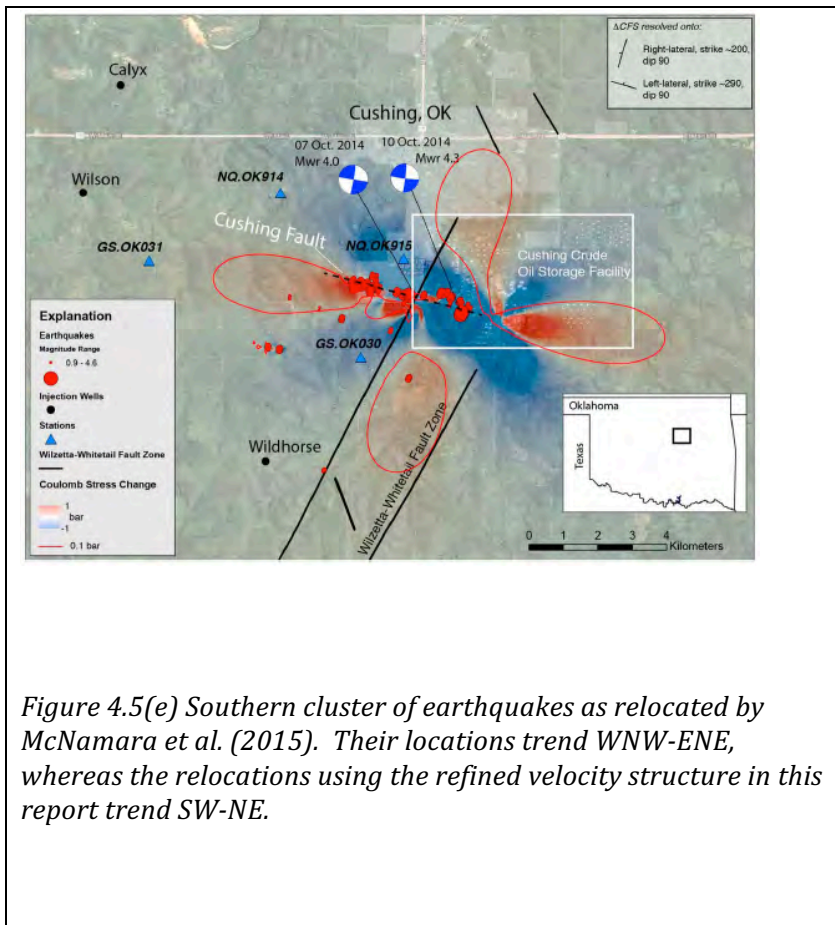


Figure 4.5(e) Southern cluster of earthquakes as relocated by McNamara et al. (2015). Their locations trend WNW-ENE, whereas the relocations using the refined velocity structure in this report trend SW-NE.

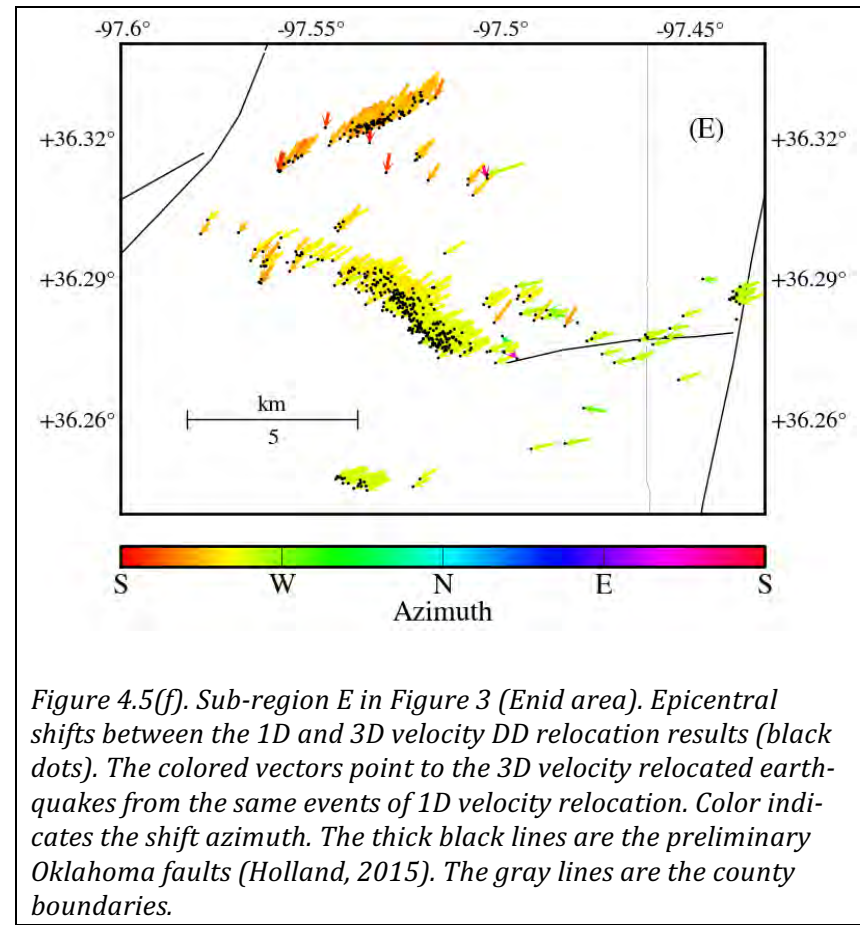


Figure 4.5(f). Sub-region E in Figure 3 (Enid area). Epicentral shifts between the 1D and 3D velocity DD relocation results (black dots). The colored vectors point to the 3D velocity relocated earthquakes from the same events of 1D velocity relocation. Color indicates the shift azimuth. The thick black lines are the preliminary Oklahoma faults (Holland, 2015). The gray lines are the county boundaries.

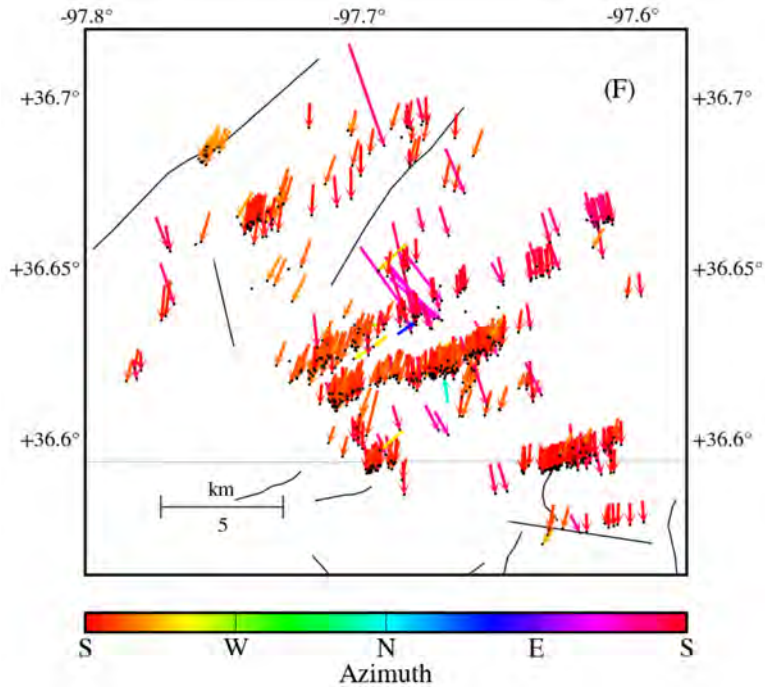


Figure 4.5(g). Sub-region F in Figure 3 (S Medford area). Epicentral shifts between the 1D and 3D velocity DD relocation results (black dots). The colored vectors point to the 3D velocity relocated earthquakes from the same events of 1D velocity relocation. Color indicates the shift azimuth. The thick black lines are the preliminary Oklahoma faults (Holland, 2015). The gray lines are the county boundaries.

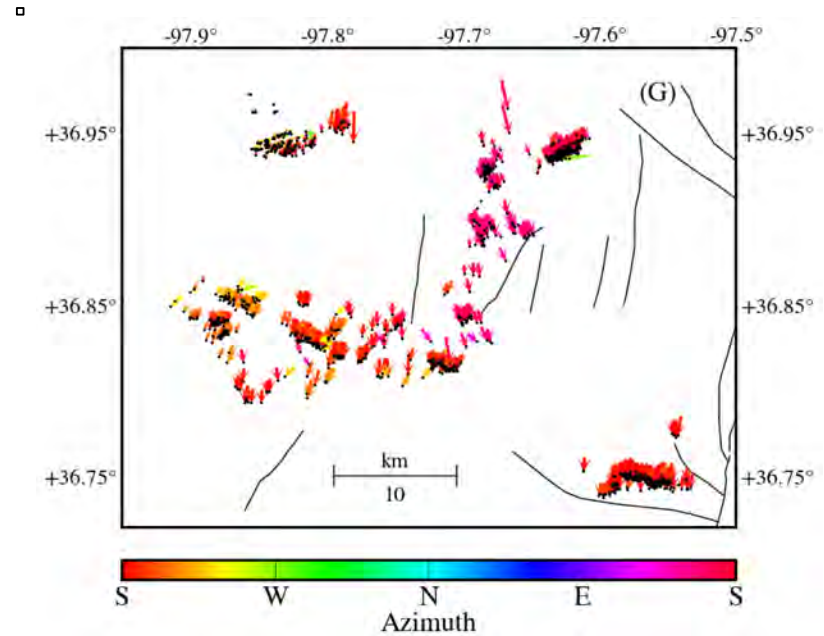


Figure 4.5(h). Sub-region G in Figure 3 (N Medford area). Epicentral shifts between the 1D and 3D velocity DD relocation results (black dots). The colored vectors point to the 3D velocity relocated earthquakes from the same events of 1D velocity relocation. Color indicates the shift azimuth. The thick black lines are the preliminary Oklahoma faults (Holland, 2015).

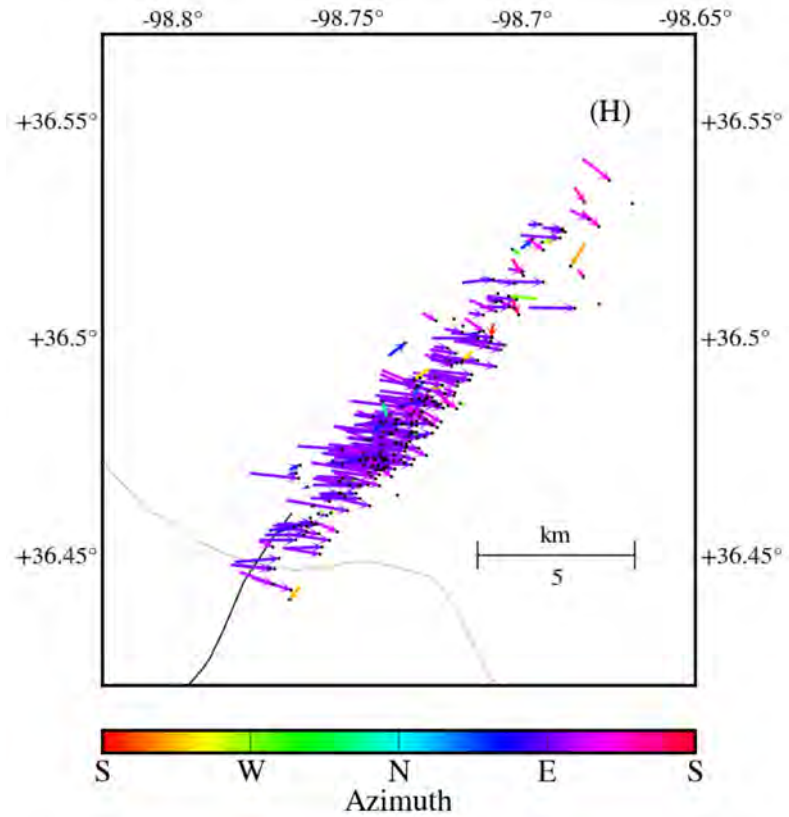


Figure 4.5(i). Sub-region H in Figure 3 (Galena Township Fault Area). Epicentral shifts between the 1D and 3D velocity DD relocation results (black dots). The colored vectors point to the 3D velocity relocated earthquakes from the same events of 1D velocity relocation. Color indicates the shift azimuth. The thick black lines are the preliminary Oklahoma faults (Holland, 2015). The gray lines are the county boundaries.

Most of the clusters present narrower linear trends with NE-SW or NW-SE orientation after the 3D velocity relocation, which are consistent with the favorable fault orientations in central Oklahoma (Holland, 2013). Several studies suggest that recent earthquakes in Oklahoma were caused by reactivation of ancient faults that cut through the Arbuckle Group and extend into the upper basement (e.g. Holland, 2013; Alt and Zoback, 2014; McNamara et al., 2015). (Holland, 2013; Sumy et al., 2014; McNamara et al., 2015) studied the Prague sequence with a variety of focal mechanism data to show that most of the earthquakes in the Prague sequence display strike-slip motion, which is consistent with the knowledge that Wilzetta Fault is a vertical or near vertical fault, at least in the shallow sedimentary section and upper basement. However, not all the clusters have been well studied in Oklahoma. For many relocated clusters, there is no identified fault nearby, but some of the clusters may associate with large geological structures in central Oklahoma, given that they align well with mapped faults. Due to the strong heterogeneity in the basement, basement faults may be complicated that are difficult to associate with the seismicity increase.

References

- Alt, R., and M. Zoback, 2014, Development of a detailed stress map of Oklahoma for avoidance of potentially active faults when siting wastewater injection wells, AGU Fall Meeting 2014, abstract.
- Holland, A. A., 2013, Optimal fault orientations within Oklahoma, *Seismol. Res. Lett.*, 84, 876–890.
- Holland, A. A., 2015, Preliminary fault map of Oklahoma, Oklahoma Geol. Surv. Open File Rep., OF3-2015
- Keranen, K. M., H. M. Savage, G. A. Abers, and E. S. Cochran, 2013, Potentially induced earthquakes in Oklahoma, USA: Links between wastewater injection and the 2011 MW 5.7 earthquake sequence, *Geology*, 41, 699–702, doi:10.1130/G34045.1.
- Luza, K. V., and J. E. Lawson, 1982, Seismicity and tectonic relationships of the Nemaha Uplift in Oklahoma, part IV, Oklahoma Geological Survey Special Publication, 82-1.
- McNamara, D. E., H. M. Benz, R. B. Herrmann, E. A. Bergman, P. Earle, A. Holland, R. Baldwin, and A. Gassner, 2015, Earthquake hypocenters and focal mechanisms in central Oklahoma reveal a complex system of reactivated subsurface strike-slip faulting, *Geophys. Res. Lett.*, 42, 2742–2749, doi:10.1002/2014GL062730.
- McNamara, D. E., G.P. Hayes, H. M. Benz, R. A. Williams, N. D. McMahon, R. C. Aster, A. Holland, T. Sickbert, R. Herrmann, R. Briggs, G. Smoczyk, E. Bergman, and P. Earle, 2015, Reactivated faulting near Cushing, Oklahoma: Increased potential for a triggered earthquake in an area of United States strategic infrastructure, *Geophys. Res. Lett.*, 42, 8328–8332, doi:10.1002/2015GL064669.
- Sumy, D. F., E. S. Cochran, K. M. Keranen, M. Wei, and G. A. Abers, 2014, Observations of static Coulomb stress triggering of the November 2011 M5.7 Oklahoma earthquake sequence, *J. Geophys. Res. Solid Earth*, 119, 1904–1923, doi:10.1002/2013JB010612.

Zoback, M. L., 1992, First- and second-order patterns of stress in the lithosphere: The world stress map project, *J. Geophys. Res.*, **97**, 11703–11728, doi:10.1029/92JB00132.

Description of RPSEA Task 9 – Construction of Integrated Multi-Variate 3D Geologic Interpretation

This task provides the crucial integrative platform for the integrated analysis. A multi-variate 3-dimensional (3D) earth model based on a 3D geological interpretation initially employing subsurface data, digital elevation, and results that define structures below drilling depths shall be developed. The 3D interpretation shall be based on gravity data that covers the study area uniformly, and shall be iterated based on results such as seismic tomography, seismic data provided by industry, and detailed well log analysis.

The report appended below describes a portion of Task 9 comprising development of a three-dimensional model of the Project area and its surroundings derived from gravity measurements and geological information, supported by the RPSEA Project.

5. Gravimetric Determination of Basement Geologic Structure

Kevin Crain

Oklahoma Geological Survey, Mewbourne College of Earth and Energy, University of Oklahoma, Norman OK 73019

Abstract

Most Oklahoma earthquakes occur within the crystalline basement. This study investigates whether we can identify crystalline basement geologic structures that may concentrate seismicity. The paper also seeks to identify the differences in basement geologic character that do and do not host earthquakes.

In the holistic view, gravity data measure the gravity field generated by the universe's unique density distribution at the time and location of the observation. In the real world this study will be using the observed free-air gravity data. The study uses the free-air gravity because it does not have an embedded geologic model, as is the case in the simple or complete Bouguer gravity model (Nettleton, 1976).

The geologic character of the upper crystalline basement can be estimated and tested using a geologically and statistically constrained density inversion of three dimensional (3D) free-air gravity data and a geologically consistent 3D density distribution of known and expected geologic features above and below the upper crystalline basement. The gravity data are four dimensional (4D) point data collected at unique locations and times and reflect the Earth's unique density distribution at the time of observation. The geologic model is a container populated with the density distribution of a geologically consistent expected model Earth. The density inversion estimates the density distribution that minimizes the misfit between the observed and estimated free-air gravity data. If the residual free-air gravity anomaly (RFAA), is consistent, then the estimated density distribution may be correct but if the RFAA is inconsistent the results are not correct.

Using published formation isopach models, a 3D geologic model is built that is consistent with known and expected geologic characteristics. As more geologic information becomes

available, the expected geologic formation model can be improved to reflect these data while maintaining consistency with both the regional and local geologic model.

Therefore the 3D geologic model represents the published 3D geologic data constrained by observed and expected formation boundaries and rock types. Then, using expected rock type to density relationships, a geologically consistent expected 3D density distribution model can be built. Using the expected 3D density distribution model, the expected gravity effect of the model at each 3D gravity station location is calculated with SIGMA. SIGMA is a newly developed, efficient, and extremely rapid 3D gravity, gravity gradiometry calculation algorithm at the 3D gravity data point locations (Chang and Crain, 2015).

Then with a geologic model and statistically constrained density inversion, the updated density distribution model estimates a density distribution that minimizes the misfit between the observed free-air and estimated free-air gravity data. The density inversion is a geologically and statistically constrained linear inversion with geologic and statistical constraints (Jackson, 1979, Tarantola and Valette, 1982, Baker, 1988, and Crain, 2006).

The resulting RFAA reflects basement geologic mass distributions that indicate complex basement rock type distribution and geologic structures that are consistent with the available data, and should provide insight into the distribution of earthquakes.

Introduction

Definitively determining the geologic structure of the basement requires rock in hand. Given the expense of drilling to the basement, much less to the depths of earthquakes within the crystalline basement, and the lack of accessible seismic reflection surveys, geophysical measurements remain the most cost effective methods to investigate basement rock properties.

Approximately 25 to 30 percent of the state of Oklahoma has exploration 3D seismic reflection surveys and probably 90 percent of Oklahoma has 2D seismic surveys. However, these data are not available publicly, and this study must rely on published data to build the 3D geologic volume. Therefore, this study must rely on potential field methods, such as magnetic and gravity measurements available publicly.

Of the potential field methods, the most cost effective geophysical method is aeromagnetic data and that should be the first choice. But given the cost to acquire new high-resolution aeromagnetic surveys, the Oklahoma Geological Survey has used low-resolution public domain aeromagnetic data, (Bankey 2002), and gravity data from the Pan American Center for Earth & Environmental Studies [PACES], (Hinze 2004), followed up with newly acquired gravity data (Chapter 3) to investigate targeted anomalies. Fully investigating the geologic character of the basement using gravimetric methods requires more than one iteration of expected geologic models.

The modeled domain must be substantially larger than the study area to accurately represent the three-dimensional effects of rock masses on the gravity field at a given point. The study area is shown as a rectangle in the figures in this paper. The modeled area includes much of Oklahoma, but also parts of adjacent Kansas, Arkansas, and Missouri. The Project area near the Prague earthquake, is shown as a smaller rectangle. Figure 5.1 shows a map of the observed Free Air Anomaly (FAA).

The RFAA in Figure 5.3 illustrates the complexity of the basement geology between the mid-continent rift, MCR in Kansas, and the Southern Oklahoma Aulacogen, SOA. Associated with the two rifts, MCR, and SOA, are parallel geologic structures like the Nemaha Uplift and Amarillo Uplift and the Anadarko basin. Also, there are additional associated structures throughout Oklahoma like the Wilzetta Fault zone and their many conjugate fault zones.

The anomalies in the RFAA show complex and previously un-mapped long-lived structures with expected tectonic implications. Specifically in Figure 5.3, at the Kansas – Oklahoma Border, at the southern end of the MCR, there appear to be two branches of gravity highs

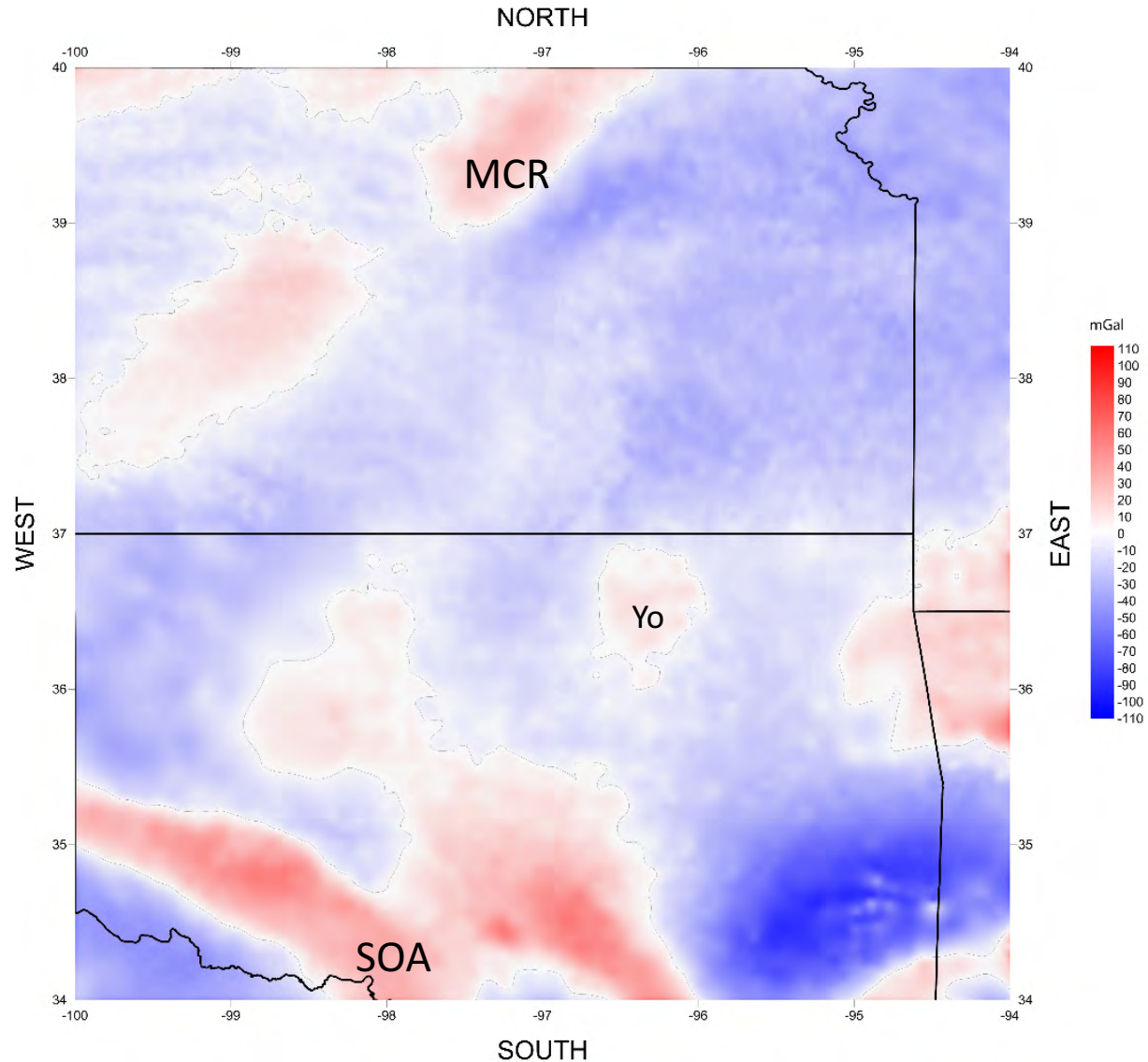


Figure 5.2. Estimated free-air anomaly over the same region as in Figure 1 is the result of the density inversion estimating the model densities that minimize the misfit between the observed and estimated free-air gravity.

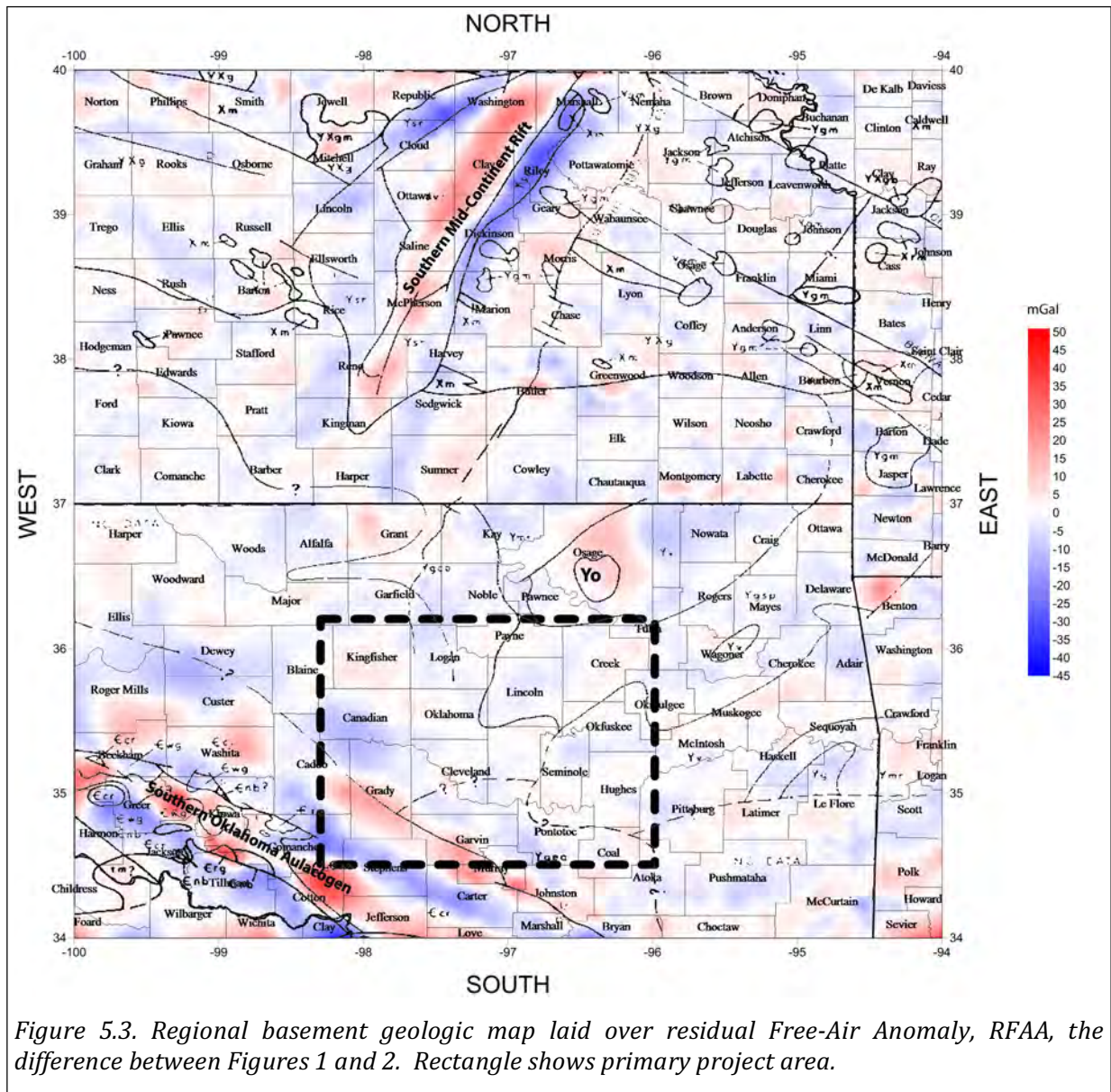


Figure 5.3. Regional basement geologic map laid over residual Free-Air Anomaly, RFAA, the difference between Figures 1 and 2. Rectangle shows primary project area.

(red) which previously are unmapped and have earthquake activity in or very near them. Therefore, given the complexity of the basement structures, we should investigate the geologic features not only due to the earthquakes but the influence of the basement geology even in areas without earthquakes.

Geologic and Gravity Model

As previously stated the EARTH's gravity field results from the unique density distribution of the Universe including the sun, moon, and planets, commonly lumped into the "tides" correction and the EARTH's geologic structure. The observed gravity data are point measurements of the Earth's continuous gravity field measured at discrete point locations. For this study, we assume a static density distribution to model the observed

gravity field at their discrete data locations using a geologically consistent 3D geologic model, with known and expected rock density distributions and their uncertainties.

The observed free-air gravity at any location measures the gravity effect of the density distribution of geologic features. The initial phase of interpreting the observed free-air gravity is removing the gravity effects of known and expected regional 3D geologic units. Then the RFAA represents the gravity effect of the unmodeled, mismodeled, or unexpected density distributions within the upper crust model that is currently using a geologically consistent uniform single density.

The RFAA is the difference between the observed free-air anomaly and the estimated free-air anomaly calculated using estimated model densities returned by a geologically and statistically constrained density inversion that minimizes the misfit between the observed and estimated free-air anomaly.

Modeling the RFAA requires density distributions consistent with expected and assumed geologic features they represent. Using a geologic and statistically constrained density inversion to minimize the misfit between the residual gravity and the estimated residual gravity allows progressive refinement of the documentable geological model. If the results are statistically consistent, then the resulting model may be correct, but any inconsistent results are definitely incorrect.

The initial phase of the interpretation is to image the gravity effect of the unknown density distribution within the upper crust. The initial model is composed of four individual geologic models from the surface topography to 100 km below mean sea level (BMSL), as shown in Figure 5.4. Degree of detail decreases with depth, reflecting the lack of available data regarding the deeper levels of the crust and mantle. Each element of the geologic models has geologic and statistical constraints used by the density inversion when estimating the densities that minimize the misfit between the *prior* and *posterior* model densities. The first model unit comprises the sedimentary rocks above the crystalline basement. The second model unit is the upper crust. The third model unit is the lower crust. The fourth model unit is the mantle.

Figure 5.5 shows the near surface sedimentary rock above the crystalline basement. The current sedimentary rock model is a uniform density volume at the average density of the sediment. The expected volume is defined by two surfaces. The top surface is the surface topography at one arc-second resolution (~30 m grid spacing), and the bottom surface, the crystalline basement, is defined by a 30 arc-second grid topography (~1 km grid). The most prominent features of the sedimentary section are the thick sections in the Arkoma and Anadarko Basins in the southern margin of the block. In addition, the Nemaha Fault shows up as a ridge running roughly north-south through the middle of the block.

The upper crust beneath the sedimentary section is the rock volume of interest because it is hosting most Oklahoma earthquakes. This unit is shown in Figure 5.6. The initial model assumes the rock in the upper crust is granitic, with a constant density, and any density variations within the upper crust should show up as anomalies in the RFAA. The expected volume is defined by two surfaces. The upper surface is the basement surface below the sedimentary column. The bottom surface is at 25 kilometers BMSL.

The deep crust model, Figure 5.7, is an estimated density distribution using 0.10-degree square prisms extending from 25 km to 42 km BMSL. Individual cell densities are estimated rock densities between 2.9 to 3.0 g/cm³ appropriate for the depth of 25 to 42 km BMSL and returned by the density inversion minimizing the misfit between the observed and estimated FAAs. The expected deep crust geologic model, below 16 km BMSL, reflects a geologically constrained density distribution consistent with expected and accepted geologic features, boundaries, and depths.

The mantle model, Figure 5.8, is a multi-density model extending from 42 km to 100 km BMSL. Each density prism is the nearest neighbor area with the EarthScope transportable array station in the center and the density returned by the density inversion. The expected density of the mantle was set to 3.3 g/cm³ and the density uncertainty set to $\pm 3\%$.

Figure 5.9 shows the RFAA with geologic boundaries, and illustrates the complexity of the geologic architecture assumed to occur in the upper crust. There are distinct differences in the geologic interpretation between Kansas and Oklahoma. Kansas used aeromagnetics and drill hole samples to help define their geologic model, whereas Oklahoma defined the

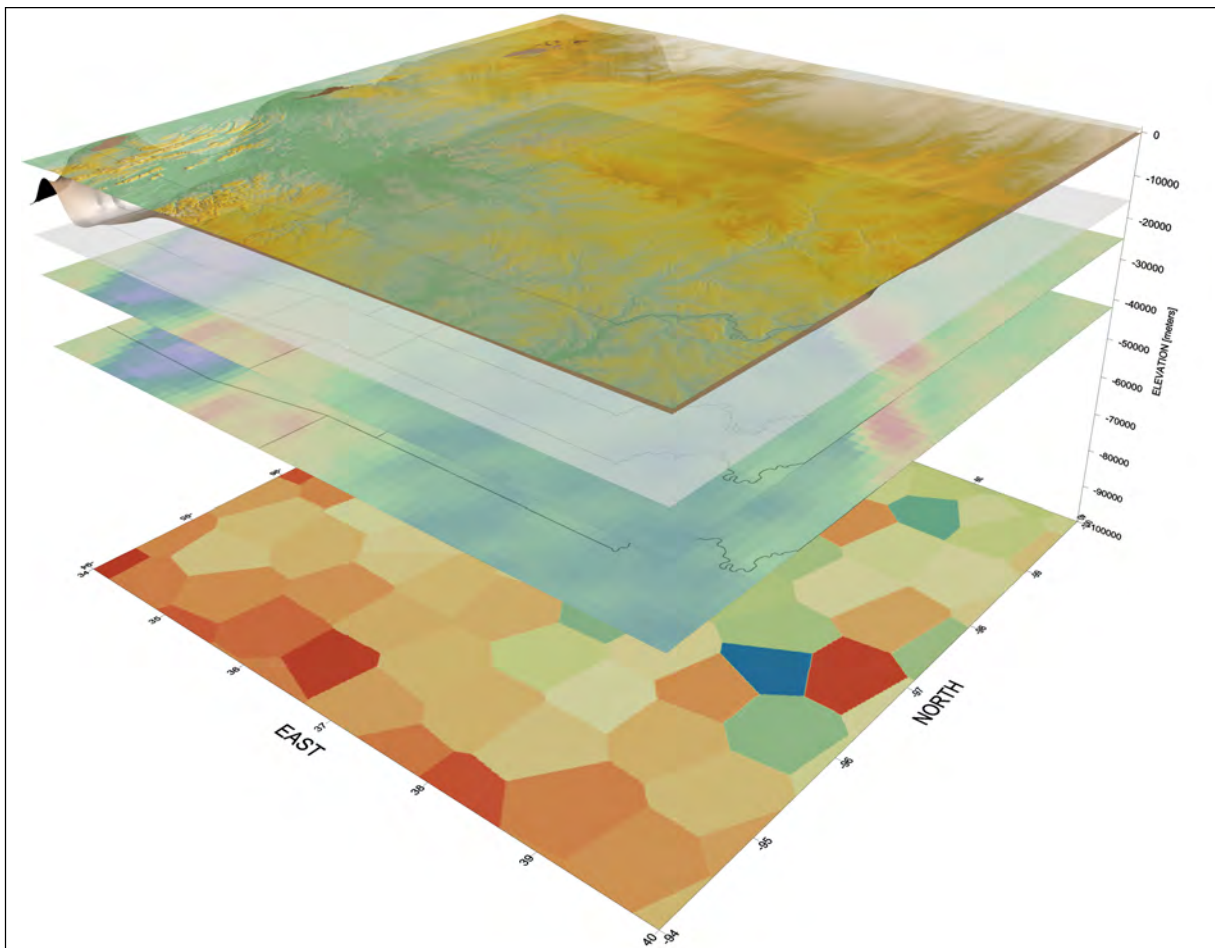


Figure 5.3. 3D geologic model units from the surface topography to 100 km below sea level.

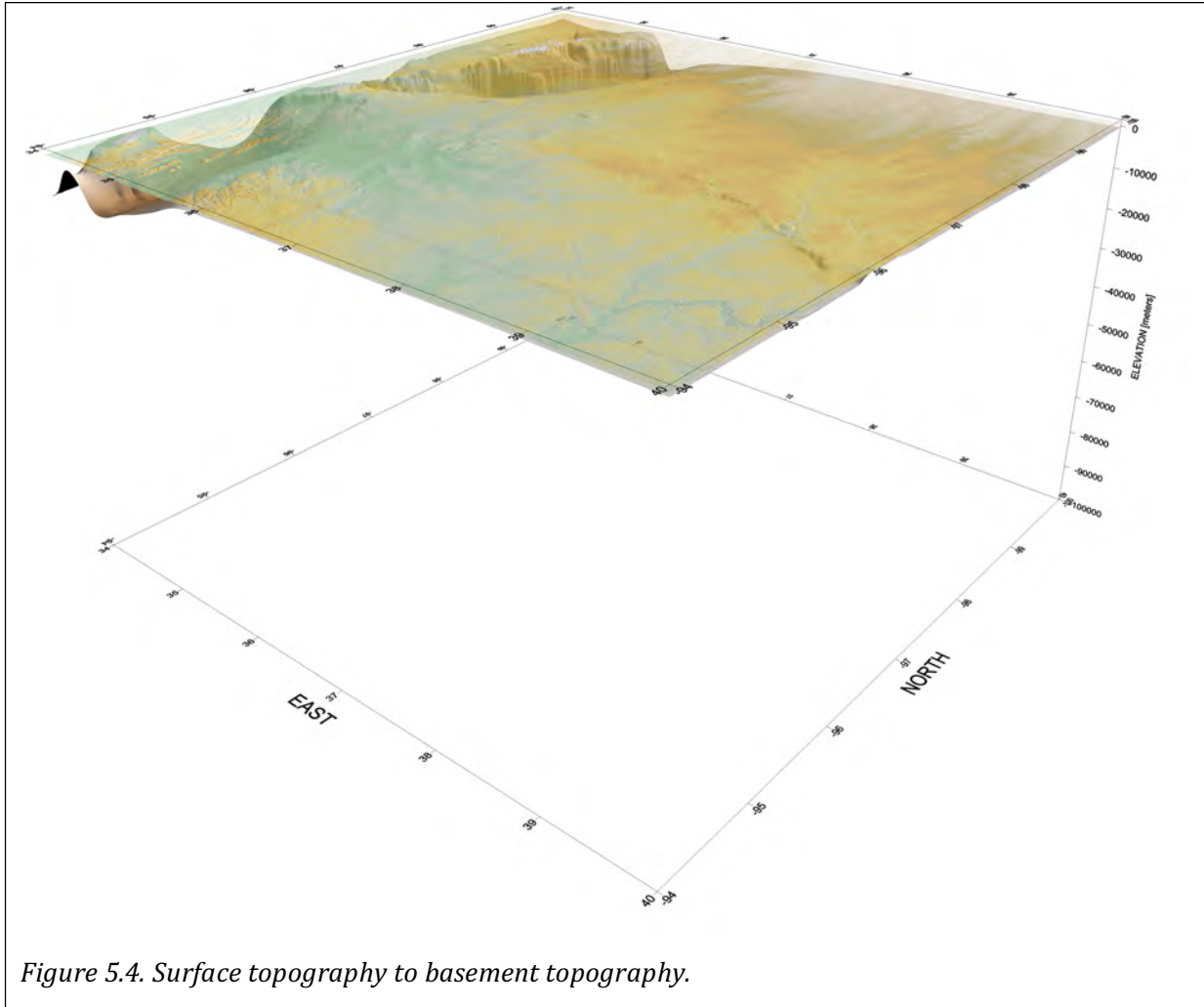


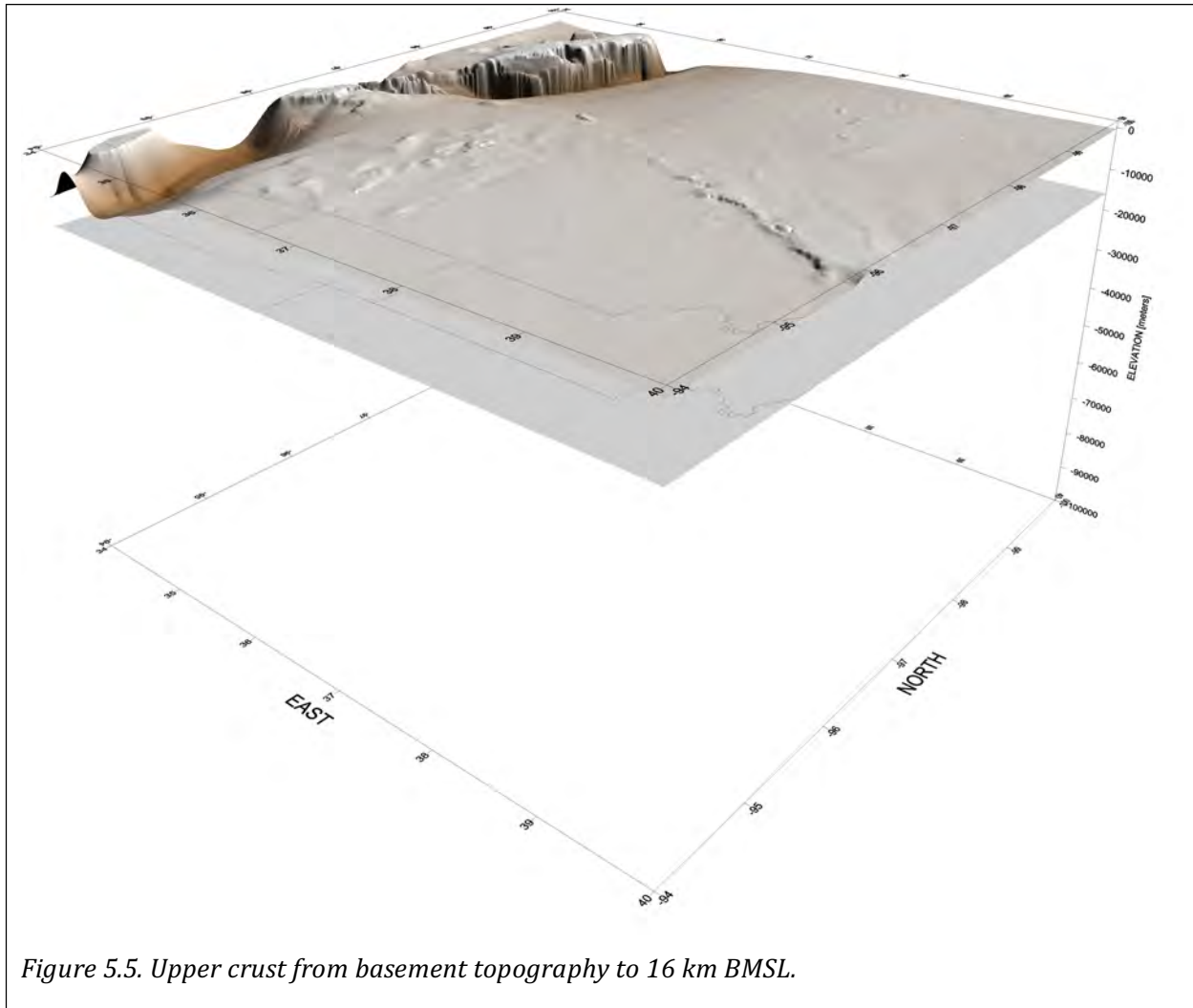
Figure 5.4. Surface topography to basement topography.

basement geology solely on the basis of outcrop and drill hole samples. The lack of data has left large areas of Oklahoma with no data defining the geologic units.

With increased earthquake activity in the crystalline basement/upper crust; one may ask are there geologic structures in the basement that reflect earthquake seismicity? Figure 5.10 shows the RFAA and magnetic intensity, along with their first vertical derivative. The first vertical derivative commonly shows the edges of geologic structures if there is a rock type difference or possibly an elevation offset in the rock. The majority of the current faults are strike-slip faults, and therefore there are areas without distinct signatures in the first vertical derivative maps. An additional problem is the spatial resolution of the data. In most of the state of Oklahoma both the gravity and magnetic data spacing are at the scale of the earthquake clusters or larger.

Future work

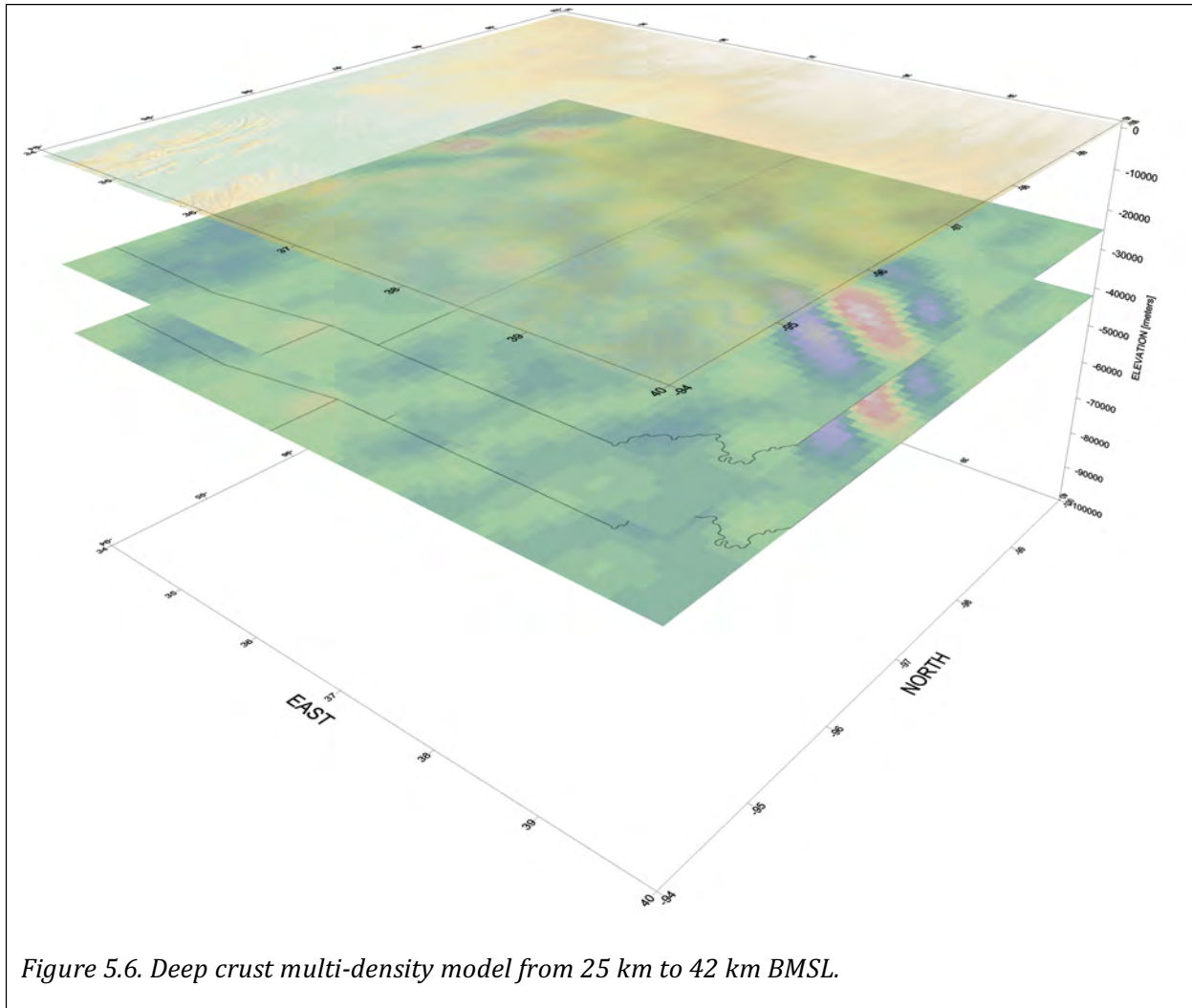
Improving the accuracy of the density model requires integrating additional geologic formation and structural data. We currently have limited access to more comprehensive data, though if it becomes available, the regional 3D geologic model can be updated integrating these data into the regional model. The ability to update the geologic models in



a piecewise manner allows improving the geologic model whenever data becomes available while maintaining model consistency at all geologic model scales.

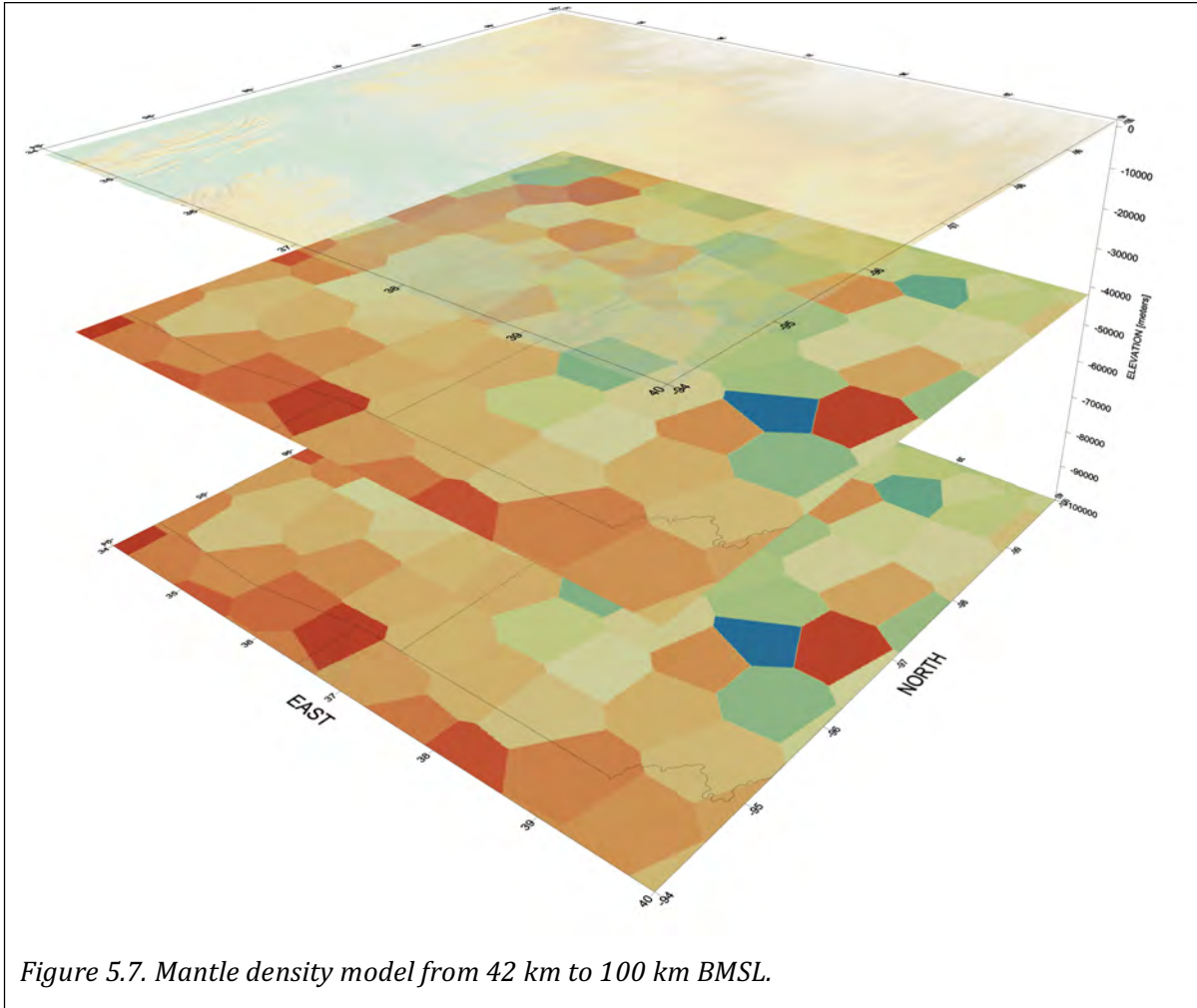
A second improvement of the sedimentary model would integrate well-log density data into the model formation volumes. An additional improvement would be with the aid of industry data to locally update the regional geologic models with detailed seismic and well-log formation tops and formation density data. Another improvement would be to use 2D seismic depth sections and 3D seismic volumes to improve the formation tops and basement topography.

Future investigations targeting local gravity/magnetic anomalies should target local geologic features and require acquiring additional high-resolution gravity data along with updating the regional geologic model. Each new targeted local geologic model will specifically address gravity anomalies revealed in the regional RFAA and combined, they would improve the overall understanding of the geologic structure and the observed free-air gravity anomaly, while maintaining geologic model consistency at both regional and local scales.



In the future, removing the gravity effect of the regional sedimentary geologic model unit should use 3D geologic volumes and their expected densities converted from their expected rock types. We are currently working on updating the sedimentary model using isopach maps from Tulsa Geological Society Special Publication 3 (Rascoe and Hyne, 1988), producing a multi-layer geologic volume with expected and volumetrically consistent rock density distributions. Any additional formation top elevations and rock densities can integrate into the regional geologic model with individual updates maintaining geologic consistency of the regional geology model. Initially, the regional formation tops and new updated average formation densities will update the geology density distribution model. Figure 5.10 shows that there are areas within Oklahoma where earthquakes show correlation with the gravity and magnetic anomalies. Additionally, in Figures 5.10, large scale, and 5.11, small scale, there are apparent geologic structures in Oklahoma without earthquake activity.

Figure 5.11 illustrates the data aliasing problem in Woodward and Woods counties. The current gravity data, white dots, where the data spacing is similar to that of much of the



gravity data in Oklahoma and the inter-station spacing is similar to the current earthquake cluster spacing in these counties. The Woodward and Galena Township earthquake clusters are on the scale of 14 to 16 km, and the gravity data spacing is 10 to 14 km. Both the RFAA and magnetic data and their first vertical derivatives show indications of geologic structure within the region of the earthquake clusters. However, making definitive statements about geologic structure is impossible due to data aliasing.

Conclusion

The residual gravity anomaly aligns with previously known geologic features in the basement in areas of the Southern Mid-Continent Rift and Southern Oklahoma Aulacogen. Also, the basement geologic structures are commonly coincident with known and previously unknown structures in the basement revealed by earthquake activity.

The residual gravity anomaly and magnetic data commonly indicate many of the areas of earthquake activity have basement structure associated with them. The residual gravity anomaly and magnetic maps show the structure for a large volume. At the same time, there are earthquake clusters that appear to be internal to basement geologic units without

There are also places where the residual gravity anomaly hints at geologic structure but does not seem to be able to resolve the structure; this is more often the result of aliased signal due to sparse data undersampling the gravity and magnetic signal. The only solution to aliased data is to acquire higher resolution geological and geophysical data.

Using the 3D data and model format allows updating the data, and geologic model in a piecewise way as new geological and geophysical data become available. The piecewise modeling philosophy is valuable for testing multiple hypotheses for the basement geologic units and structures. This approach also facilitated integration of results of multiple studies into the model to improve the understanding of the basement, and its impact to Oklahoma.

Within Oklahoma, there is a statewide need to acquire new high-resolution gravity and magnetic data to improve the spatial resolvability of the features found in the residual gravity. The Woodward and Woods County earthquake cluster areas clearly illustrate the need to acquire new high-resolution gravity, magnetic and geologic data along with improved geologic models of the sedimentary formations and structures above the crystalline basement. Acquiring new geophysical and geological data can improve the imaging of the basement geologic structure associated with the faults delineated by the earthquakes and at the same time, enhance the understanding of the basement geologic features in areas that have distinctive geologic characteristics, but do not host earthquakes.

References

American Association of Petroleum Geologists (AAPG) and the United States Geological Survey (USGS), Basement Rock Project Committee, 1967, Basement Map of North America, Between Latitudes 24° and 60°N, 1:5,000,000.

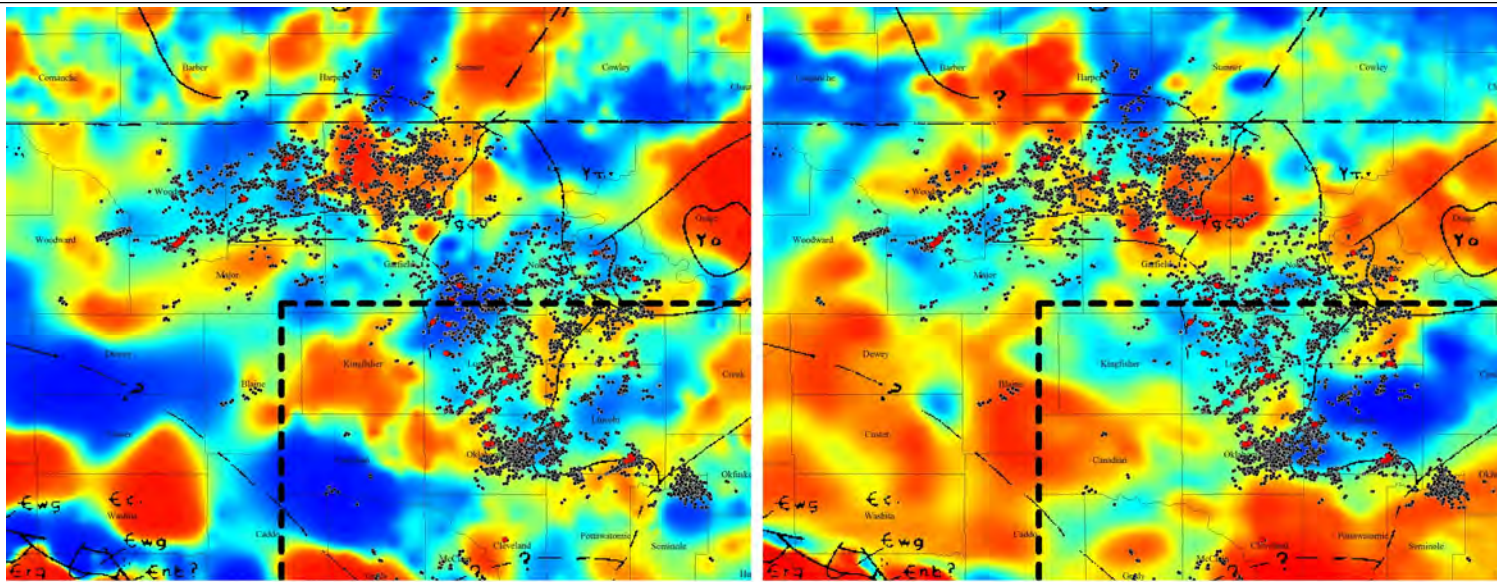
Baker, M. R., 1988, Quantitative interpretation of geological and geophysical well data: Doctoral Dissertation, Univ. of Texas at El Paso.

Bankey, V., Cuevas, A., Daniels, D., Finn, C., Hernandez, I., Hill, P., Kucks, R., Miles, W., Pilkington, M., Roberts, C., Roest, W., Rystrom, V., Shearer, S., Snyder, S., Sweeney, R. E., Velez, J., Phillips, J.D., Ravat, D.K.A., 2002, Digital data grids for the magnetic anomaly map of North America, USGS Publications Warehouse, <http://pubs.er.usgs.gov/publication/ofr02414>

Blakely, R. J., 1996, Potential Theory in Gravity and Magnetic Applications, Cambridge University Press, 461 p.

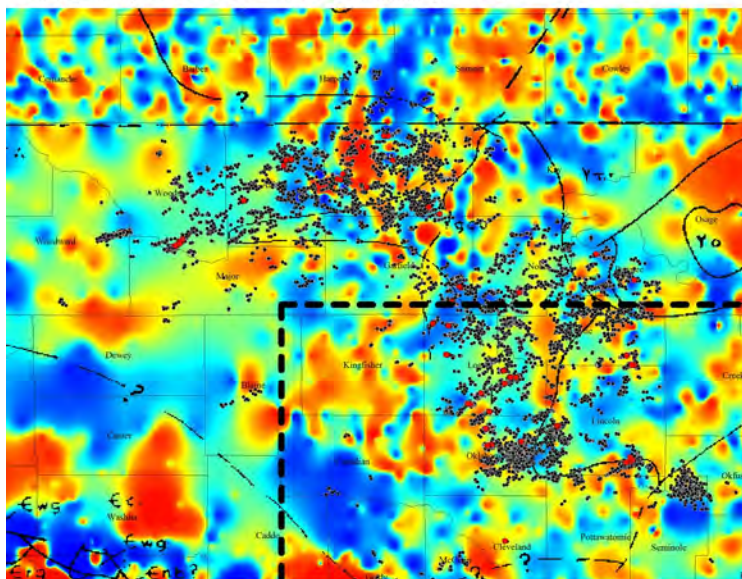
Chang, J. C., and Crain, K., 2015, Gravity Modeling with Vertical Line Elements, AGU Potential Fields Workshop, Keystone, Colorado, August 2015

Crain, K., 2006, Three Dimensional Gravity Inversion with *a Priori* and Statistical Constraints: Doctoral Dissertation, Univ. of Texas at El Paso.



Earthquake epicenters over residual free-air anomaly, red dots ≥ 4.0

Earthquake epicenters over magnetic anomaly, red dots ≥ 4.0



Earthquake epicenters over first vertical derivative residual free-air anomaly, red dots ≥ 4.0

Earthquake epicenters over first vertical derivative magnetic anomaly, red dots ≥ 4.0

Figure 5.9. Earthquake epicenters with geologic boundaries, over public domain gravity and magnetic data. Left side, RFAA, and RFAA first vertical derivative. Right side, magnetic survey, and magnetic first vertical derivative. The red dots are earthquakes magnitude 4 and larger.

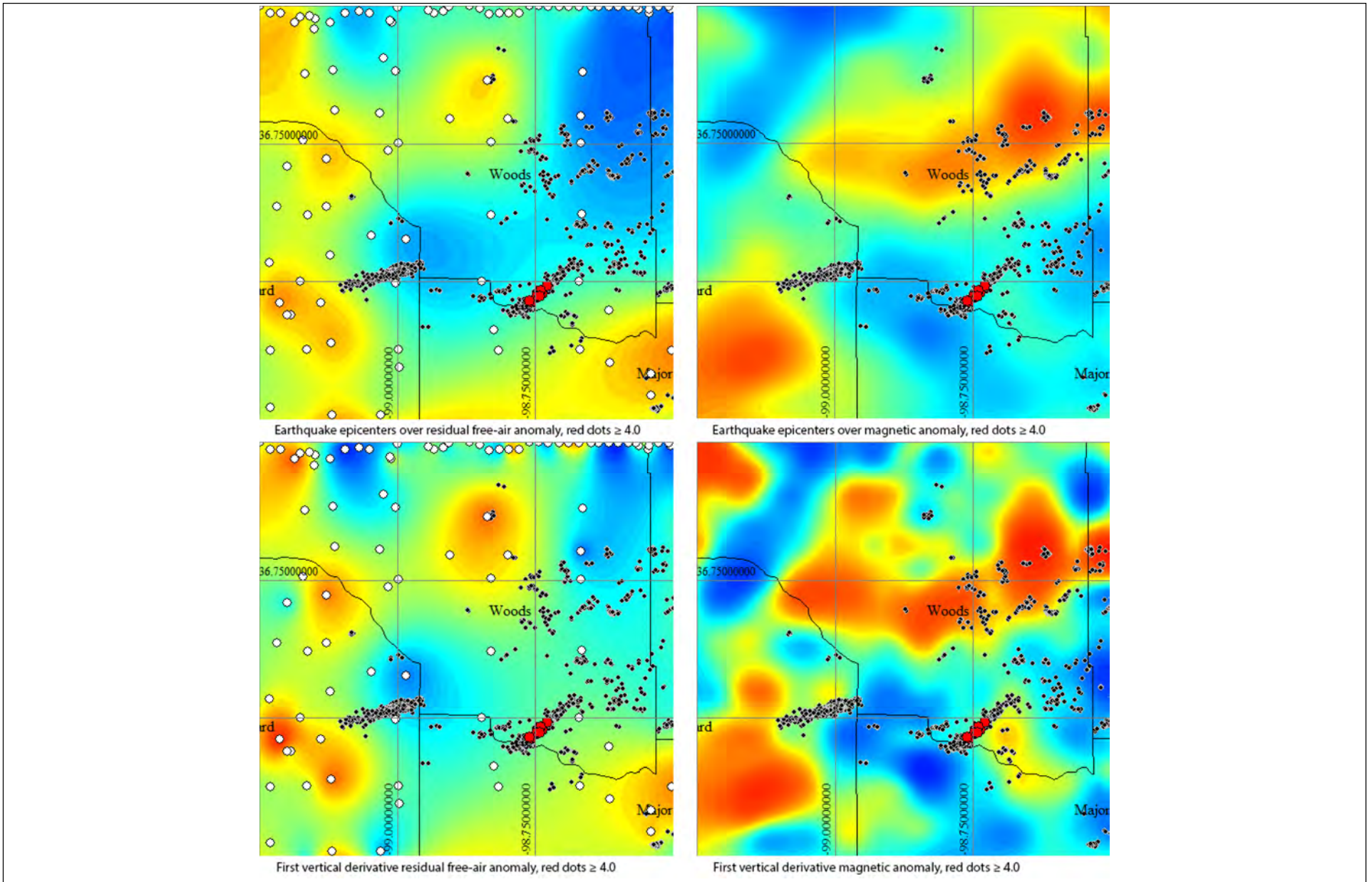


Figure 5.10. Woodward and Woods counties earthquake epicenters over gravity and magnetic. Left side, RFAA, and RFAA first vertical derivative. Right side, magnetic, and magnetic's first vertical derivative, left side and magnetic's and first vertical derivative. The red dots are

- Danes, Z. F. 1960, On a Successive Approximation Method for Interpreting Gravity Anomalies, *Geophysics*, 25, 1215-1228. doi: 10.1190/1.1438809
- Denison, R. E., and Merritt, C. A., 1964, Basement Rocks and Structural Evolution of Southern Oklahoma, Oklahoma Geological Survey, Bull. 95, 302 p.
- Denison, R. E., 1981, Basement Rocks in Northeastern Oklahoma, Oklahoma Geological Survey, Circular 84, 88 p.
- Dicken, C. L., Pimley, S. G., Cannon, W. F., 2001, Precambrian basement map of the north Mid-Continent, U.S.A., A digital representation of the 1990 P.K. Sims map, U.S. Geological Survey; Open-File Report 2001-21, pubs.er.usgs.gov/publication/ofr0121
- Hammer, S., 1974, Approximation in gravity Interpretation Calculations, *Geophysics*, v39, 205-222. doi: 10.1190/1.1440422
- Hinze, W., et al., 2005, New standard for reducing gravity data: The North American gravity database, *Geophysics*, Vol. 70, No. 4, p. J25-J32.
- Jackson, D. D., 1979, The use of a priori data to resolve non-uniqueness in linear inversion: *Geophys. J. R. Astron. Soc.*, 57, 137-157.
- Nettleton, L. L., 1976, *Gravity and Magnetics in Oil Prospecting*, McGraw-Hill Press.
- Rascoe, B., and Hyne, N., eds. *Petroleum Geology of the Mid-Continent*, Tulsa Geological Society, Special Publication number 3, 1988.
- Tarantola, A., Valette, B., 1982, Generalized non-linear inverse problems solved using least squares criterion: *Rev. of Geophys. And Space Physics*, 20, 219-232.

Description of RPSEA Project Task 10 – 4D Integrated Multiscale Reservoir and Geological Modeling: A field-scale model representative of the Osage County gravity anomaly (the reference model) shall be developed using an ensemble of models that are progressively updated. A set of predictions shall be generated through coupled numerical simulation of water movement in the subsurface and the localized stress changes associated with water injection. These predictions shall be compared to observations of seismic activity in the region that have previously been attributed to water disposal and by reconciling these differences in the model to create an improved representation of the preferential flowpaths, geomechanical properties and fault characteristics in the subsurface. The improved model shall be tested against 4D geophysical monitoring analyses and further refined. This shall directly address the key challenges related to improved quantification, sensitivity and resolution of monitoring technologies. By sequentially calibrating reservoir performance models to all available monitoring data, improved prediction and delineation of the injected water becomes possible.

The report appended below summarizes the mathematical basis for evaluating pressure response in injection wells, as part of this task supported by the RPSEA Project.

6. Interpretation of Low Frequency Pressure Measurements in Injection and Production Wells

Deepak Devegowda

*Mewbourne College of Petroleum and Geological Engineering, Sarkeys Energy Center
100 East Boyd St., Norman, Oklahoma 73019-0628*

The intent of this chapter is to delineate a mathematical procedure for reservoir characterization and pressure response analysis to identify highly conductive fluid migration pathways in the subsurface from injection well pumping tests. Pumping tests on produced water disposal wells are a necessary first step to identify fluid migration pathways in the vicinity of the injection well. These fluid migration pathways may include fractures, intersecting faults or high permeability zones. In this work, we document a low frequency asymptotic approach based on Vasco and Karasaki (2006) to interpret these pumping tests.

6.1 Subsurface Characterization from Dynamic Data

The economic impact of inaccurate predictions of future petroleum reservoir performance is substantial. Therefore making proper characterization of the reservoir and uncertainty analyses in production forecasts are crucial aspects in any reservoir development strategy. This goal is equally applicable to produced water disposal wells at various disposal sites. Accurate characterization of the subsurface is critical to predicting the ultimate fate of the injected water and its potential to induce seismicity. This goal is achieved through the use of history matching algorithms which reconcile reservoir/subsurface models to measurements such as pressure or injection/production data or time lapse seismic information.

The workflow depends on constructing an appropriate initial subsurface simulation model and adjusting the values of the uncertain model variables so that the model performance is in reasonable agreement with actual measurements. These approaches can be broadly

classified into two distinct categories: gradient based algorithms and stochastic approaches. Regardless of the approach, all previously recorded data is simultaneously used to update the reservoir model. The first class of algorithms generally utilizes parameter sensitivities or gradients of an appropriately constructed objective function to arrive at a solution to the inverse problem. To generate multiple history matched model realizations, these techniques involve the repeated application of the procedure to each realization of the reservoir, a procedure which can be computationally demanding. Furthermore, these approaches rely on the development of code that may not be capable of handling diverse types of dynamic data.

On the other hand, stochastic algorithms like the Markov Chain Monte Carlo (MCMC) approach, simulated annealing and genetic algorithms rely on statistical approaches to arrive at solutions to the inverse problem. However, these approaches are slow to converge and require excessive turn-around times for model calibration. The associated difficulties with both categories of history matching algorithms are further compounded when it is necessary to assimilate data frequently.

Because of the increased deployment of permanent sensors or downhole monitors, it is increasingly important to maintain 'live models' that are progressively updated as soon as data is obtained. In any case, there is a strong need to seek solutions that provide reasonably accurate solutions in a computationally feasible framework. In this work, we describe an approach developed by Vasco and Karasaki (2006) that relies on a low frequency approximation of the pressure diffusivity equation that can address the challenges associated with noisy pressure measurements acquired during a pumping test to characterize high conductivity fluid migration pathways in the subsurface.

6.2 Methodology

Vasco and Karasaki (2006) have investigated an asymptotic solution of low frequency transient pressure variations to estimate hydraulic fracture conductivity. The inversion of hydraulic fracture tomography can be used to estimate permeability. In 2000, Vasco and his colleagues investigated the high frequency asymptotic solution for pressure variation equations. These equations propose solutions for transient pressure amplitude and arrival time through the use of diffusive travel time tomography. The use of this approach is conducted through applying constant rate tests that are run for specific periods of time. The uses of these tests are governed by utilizing the time derivative to estimate arrival time. Computing the time derivative is usually troublesome due to regional and well effects that cause initial time variations.

This method is usually surrounded by great number of data and noise accompanying data acquisition. Therefore, the low frequency asymptotic approach uses the frequency domain to reduce the amount of data needed to find solutions. Using both the forward and the inverse solutions require only two problems, which are expressed by the steady state pressure equations.

This study focuses on using the low frequency approximation to the diffusivity equation because of the following assumptions:

1. The high frequency variations are sensitive to noise in the measurements.
2. The low frequency responses correspond to lateral and vertical variations in the reservoir properties.
3. Working in the frequency domain reduces the number of observations needed significantly.
4. The method is easily generalized and can be applied to many different reservoir and testing scenarios.

6.3 The Pressure Diffusivity Equation

The following equation defines the final form of pressure variations $P(x, t)$:

$$\nabla(K\lambda_t) \cdot \nabla P + K\lambda_t \nabla \cdot \nabla P = C \frac{\partial p}{\partial t} \quad (1)$$

Where the term (λ_t) denotes the total mobility defined as

$$\lambda_t = \frac{S_n k_{rn}}{\mu_n} + \frac{S_w k_{rw}}{\mu_w} \quad (2)$$

Total mobility does not vary significantly with position, \mathbf{x} ; thus it will be treated as a constant. The term $C(x, t)$ or coefficient (C) does not vary with time, t , due to the saturation constraint ($S_n + S_w = 1$) mentioned above. The coefficient, C is given by:

$$C = \frac{d\phi}{dP} + \phi c_n S_n + \phi c_w S_w \quad (3)$$

6.4 The Low Frequency Asymptotic Solution

In this study, the low-frequency asymptotic solution to the diffusivity equation shown in Equation 1 is employed to quantify, interpret, and invert pressure variations in the low frequency domain. A low-frequency approach is adopted in this work because several of the high-frequency variations in pressure may be because of changes in well operating conditions or responses to localized changes in reservoir/aquifer properties. Low frequency variations on the other hand are likely to be responding to a larger scale reservoir/ injection volume surrounding the injection well. Transforming the pressure pressure to the frequency domain also reduces the volume of observation data to a much smaller set of observations and eliminates noise in the measurements of pressure.

One essential part of the asymptotic inverse problem technique are the sensitivity calculations. These calculations are required to study reservoir parameter variations and their consequent effect on dependent reservoir parameters. Fundamentally, implementing different methods of sensitivity calculations provides additional authentication of the proposed approach and verification of its validity. Sensitivity calculations are discussed later in the chapter.

The main purpose of the asymptotic approach is to find a solution for the diffusive pressure component that emulates the characteristics of the wave propagation model. Many, including Virieux et al. (1994), have studied the asymptotic approach in deriving the diffusivity equation in the frequency domain. The following notation describes the general form of

the solution to the diffusion equation in the frequency domain. The use of this equation is discussed later in the chapter.

$$\hat{P}(x, \omega) = w(x, \omega) \frac{e^{-\sqrt{i\omega} \sigma(x)}}{\sqrt{\omega}} \quad (4)$$

Virieux et al. (1994) explains that the diffusion equation when transformed depends on the expression $\exp(\sqrt{\omega})$. A similar factor $\exp(\omega^{1/3})$ appeared in the asymptotic solution of wave propagation model of the Hilbert Transform. As a result of Virieux et al. (1994) observations, the diffusion equation in the frequency domain was defined in that specific form.

The asymptotic solution for the equation describing the diffusive component, pressure, is transformed to the frequency domain using a Fourier transform integral described in Equation 5. Working in the low frequency or long period domain requires transforming $P(x, t)$, pressure variations as a function of location, x , and time, t , to $\hat{P}(x, \omega)$. The term $\hat{P}(x, \omega)$ is defined as the pressure variation in the frequency domain as a function of location, x and frequency, ω .

$$\hat{P}(x, \omega) = \int_{-\infty}^{+\infty} e^{-i\omega t} P(x, t) dt \quad (5)$$

To describe the behavior of pressure variations in the frequency domain, the pressure is transformed through a Fast Fourier transform. As a result, the pressure equation shown in Equation 1 in the frequency domain becomes:

$$\nabla(K\lambda_t) \cdot \nabla \hat{P} + K\lambda_t \nabla \cdot \nabla \hat{P} = \omega C \hat{P} \quad (6)$$

The permeability is represented by the term $K(x)$ and the pressure variations in the frequency domain is defined by the term \hat{P} . Pressure variations can also be described in the frequency domain through power series representations:

$$\hat{P}(x, \omega) = \frac{e^{-\sqrt{\omega} \sigma(x)}}{\sqrt{\omega}} \sum_{n=0}^{\infty} P_n(x) \omega^n \quad (7)$$

The function $\sigma(x)$ is defined as the phase and ($n = 0, 1, 2 \dots$). This form of the pressure equation is adopted from the representation of the diffusivity equation in the frequency domain in a homogeneous medium for an impulsive source (Virieux et al., 1994). This type of equation is dominated by the first few terms for when the magnitude of the frequency, ω is small. The solution of the pressure equation in uniform media is described by some form of a modified Bessel function of the zeroth order $K_0(\sqrt{\omega} \alpha r)$. The term α is a constant depending on medium properties and r is the distance from the source. The solution of Equation 6 is an adaptation of the modified Bessel function for small frequency, ω (Vasco and Karasaki, 2006). The solution to the pressure variation and the diffusion equation in the frequency domain is:

$$\hat{P}(x, \omega) = w(x, \omega) \frac{e^{-\sqrt{\omega} \sigma(x)}}{\sqrt{\omega}} \quad (8)$$

The expression $w(x, \omega)$ depends on the orders of the frequency magnitudes and is defined by its series form as:

$$w(x, \omega) = \sum_{n=0}^{\infty} P_n(x) \omega^n \quad (9)$$

The pressure variation term in Equation 9, $P_n(x)$, is a function of location, x . Note that, to work in the low frequency domain, only the smallest magnitudes of frequency where ($\omega \ll 1$) were used. Therefore, the representation of the pressure $\hat{P}(x, \omega)$ in Equation 8 is significantly controlled by the first few terms. Accordingly, the final form of Equation 6 can be used to adequately represent the pressure variations in the low frequency domain. This is shown in Equation 9 where the term $P_0(x)$ is defined as the zeroth-order amplitude of the pressure variations.

$$\hat{P}(x, \omega) = \frac{e^{-\sqrt{\omega} \sigma(x)}}{\sqrt{\omega}} P_0(x) \quad (10)$$

To use the equation above to calculate the low frequency pressure variations for a given model, the terms $P_0(x)$ and $\sigma(x)$ need to be calculated. By using the expressions given above in Equation 5, we obtain a new set of terms characterized by different orders of frequency, ω . The mathematical operations conducted are summarized below. The terms (∇) and $(\nabla \cdot \nabla)$ are spatial derivatives that are defined as the gradient and the Laplacian expressions, respectively. A step-by-step detailed mathematical formulation of the solution can be found in Vasco and Karasaki (2006). The gradient and the Laplacian respectively are given by:

$$\nabla \hat{P}(x, \omega) = \frac{e^{-\sqrt{\omega} \sigma(x)}}{\sqrt{\omega}} \left(\nabla w(x, \omega) - \sqrt{\omega} \nabla \sigma(x) w(x, \omega) \right) \quad (11)$$

$$\nabla \cdot \nabla \hat{P}(x, \omega) = \frac{e^{-\sqrt{\omega} \sigma(x)}}{\sqrt{\omega}} \left(w(x, \omega) \omega \nabla \sigma(x) \nabla \sigma(x) - \sqrt{\omega} \nabla \cdot \nabla \sigma(x) w(x, \omega) - 2 \sqrt{\omega} \nabla \sigma(x) (\nabla w(x, \omega)) + \nabla \cdot \nabla w(x, \omega) \right) \quad (12)$$

Substituting Equations 11 and 12 for $\nabla \hat{P}(x, \omega)$ and $\nabla \cdot \nabla \hat{P}(x, \omega)$ in to Equation 6 generates the following equation:

$$K(x) \lambda_t \left(w(x, \omega) \sqrt{\omega} \nabla \sigma(x) \nabla \sigma(x) - \nabla \cdot \nabla \sigma(x) w(x, \omega) - 2 \nabla \sigma(x) \nabla w(x, \omega) + \omega^{-1/2} \nabla \cdot \nabla w(x, \omega) \right) + \nabla K(x) \lambda_t \left(\omega^{-1/2} \nabla w(x, \omega) - \nabla \sigma(x) w(x, \omega) \right) = \sqrt{\omega} C(x) w(x, \omega) \quad (13)$$

The generated equation above represents the final form of Equation 6 after substitution, factoring out the exponent term, and dividing both sides by the term $\sqrt{\omega}$. Substituting the expression for $w(x, \omega)$ defined in Equation 10, we get a sum of infinite number of expressions with varying orders of frequencies $\sqrt{\omega}$. Let us recall that we are aiming to work in the low frequency domain. Therefore, only frequencies ($\sqrt{\omega}$) of small magnitudes are considered.

The solution to deriving an equation of pressure variations in the low frequency domain is done through examining the terms of Equation 13. The terms combined with the smallest orders of the term $\sqrt{\omega}$, are selected. The solutions to terms with $^{-1}\sqrt{\omega}$, $^0\sqrt{\omega}$, and $^1\sqrt{\omega}$ frequencies are discussed below.

Terms of order $^{-1}\sqrt{\omega}$

Examining terms with the smallest order $^{-1}\sqrt{\omega}$ provides the equation defining the zeroth-order amplitude of the pressure variations $P_0(x)$.

$$K(x)\lambda_t \nabla \cdot \nabla P_0(x) + \nabla [K(x)\lambda_t] \cdot \nabla P_0(x) = 0 \quad (14)$$

The expression above is a first order differential equation that resembles the equation governing the static pressure. Note that the solution of the zeroth-order amplitude $P_0(x)$ equation depends on the total mobility λ_t and the permeability $K(x)$. In addition, Equation 14 is independent of frequency, thus, only one solution per well point is needed.

Terms of order $^0\sqrt{\omega}$

Examining terms with the second smallest order of frequency $^0\sqrt{\omega}$, provides an equation needed to solve for the phase coefficient $\sigma(x)$.

$$K(x)\lambda_t P_0(x) \nabla \cdot \nabla \sigma(x) + \nabla [K(x)\lambda_t] \cdot P_0(x) \nabla \sigma(x) + 2 K(x)\lambda_t \nabla P_0(x) \cdot \nabla \sigma(x) = 0 \quad (15)$$

This equation shows the dependency characteristics of the phase coefficient on the zeroth-order amplitude $P_0(x)$, the total mobility λ_t , and the hydraulic permeability $K(x)$. To solve for the phase parameter, Equation 13 must be solved first. The equation above can be rewritten in a more compact form using the coefficient and their derivatives.

$$\Omega(x) \nabla \cdot \nabla \sigma(x) + \mathbf{Y}(x) \cdot \nabla \sigma(x) = 0 \quad (16)$$

Where the terms $\Omega(x)$ and $\mathbf{Y}(x)$ denote the scalar and vector coefficients mentioned above and are given by:

$$\Omega(x) = K(x)\lambda_t P_0(x)$$

$$\mathbf{Y}(x) = \nabla [K(x)\lambda_t] P_0(x) + 2 K(x)\lambda_t \nabla P_0(x) \quad (17)$$

The equations required to solve both the zeroth-order amplitude $P_0(x)$ and phase coefficient $\sigma(x)$ are both independent of the frequency. As a result only one solution per well is needed for each parameter.

Terms of order $^1\sqrt{\omega}$

Examining terms with the largest order of frequency $^1\sqrt{\omega}$, provides an equation relating the zeroth-order amplitude $P_0(x)$, the phase coefficient $\sigma(x)$, and the amplitude term $P_1(x)$.

$$\nabla \cdot [K(x)\lambda_t \cdot \nabla P_1] = [C(x) - K(x)\lambda_t \nabla \sigma \cdot \nabla \sigma] P_0 \quad (18)$$

Solving for amplitude term $P_1(x)$ requires solutions for both Equations 17 and 18. Equation 18 is identical to the equation of static pressure. The only differences noted are the deviations of the phase coefficient from the diffusive travel-time. Solution of the diffusive travel time in high frequency domain is described by the eikonal equation represented by the right side of Equation 18.

In order to estimate the pressure variations in the frequency domain, both the zeroth-order amplitude pressure and the phase coefficients must be calculated using Equations 12 and

15. The equations governing $P_0(x)$ and $\sigma(x)$ are independent of the frequencies, therefore only one solution per well needs to be calculated.

6.5. Model Parameters Sensitivity Calculations

The main purpose of the sensitivity calculations is to relate variations of a specific model parameter at point y to observations recorded at point x . In this study, the model parameters are the permeability values within the model at each grid location and the observations are pressure measurements recorded at an observation well during a pumping test. In this study, the perturbations in hydraulic permeability δk_j or $\delta k(y)$ located at point y are related to the observed values of the derivative of the pressure $\delta \hat{P}(x, \omega)$ in the well located at point x . There are two methods that were used in this study. The low-frequency asymptotic approach allows us to calculate the sensitivities of changes in pressure to changes in gridblock permeability values semi-analytically. Numerical sensitivities are also calculated to demonstrate the validity of the semi-analytical sensitivity. The semi-analytic sensitivity calculations are discussed in the next few sections.

6.5.1 Semi-Analytical Sensitivity Calculations

The sensitivities are calculated through the comparison of hydraulic permeabilities at point y altered slightly from base or background permeability with value $K^b(y)$. The same method is used to compare changes created at the pressure at point x to a background or base model that has a pressure of $\hat{P}^b(x, \omega)$. Equations 19 and 20 define the comparison made between the permeabilities and pressure before and after perturbations:

$$\delta K(y) = K^b(y) - K(y) \quad (19)$$

$$\delta \hat{P}(x, \omega) = \hat{P}^b(x, \omega) - \hat{P}(x, \omega) \quad (20)$$

The reader is referred to Vasco and Karasaki (2006) for further details of the sensitivity computation. The final expression for the sensitivity for a single source-well is related to the square of the pressure gradient and is given by:

$$\frac{\delta \hat{P}(x, \omega)}{\delta k(y)} = -2 \nabla P_0(x, y) \cdot \nabla P_0(x, y) e^{-\sqrt{i\omega} \sigma(y, x)} \quad (21)$$

6.5.2 Comparison with Numerical Sensitivity Calculations

The semi-analytic sensitivities derived in Equation 21 are now compared with numerical sensitivities. Note that numerical sensitivities are derived by perturbing each gridcell permeability value by a small value and solving the full field simulation to obtain changes in the predicted bottomhole pressure at the observation well. Therefore if there are N parameters in the model, computation of the numerical sensitivities would necessitate $N+1$ full simulation runs. This can rapidly become computationally prohibitive and underscores the significance of semi-analytic sensitivity computations.

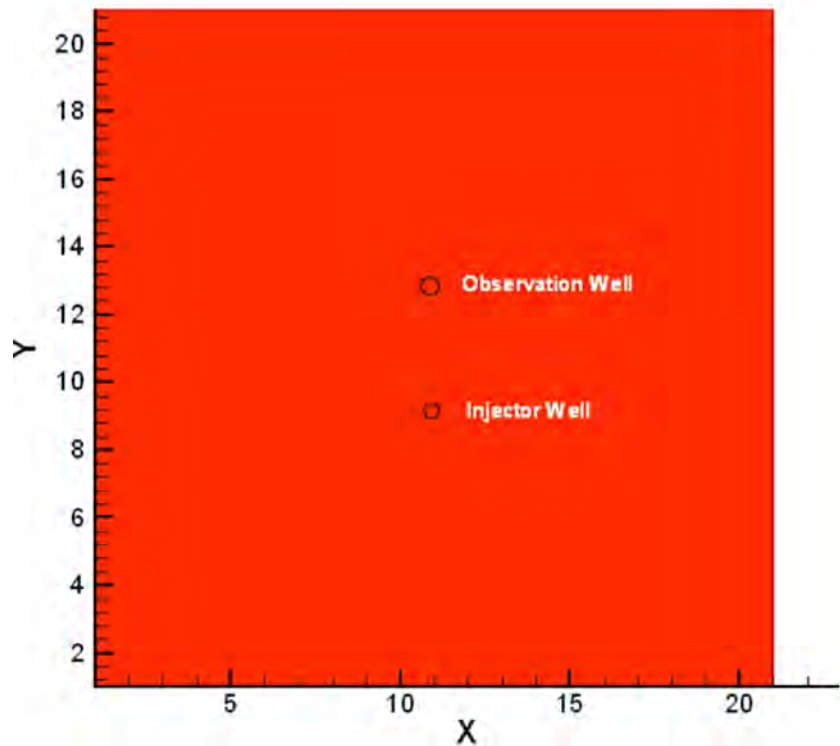


Figure 6.1: Arrangement of the wells in the test study. The north boundary is a constant pressure boundary of 2000 psia.

We consider a model defined on a $21 \times 21 \times 1$ grid with a producing well located in the center of the field in the middle of mesh (See Figure 6.1). The uniform permeability of the reservoir formation is 8.12 millidarcies and the uniform porosity is 10%. The boundary to the north of the field is a constant pressure boundary of 2000 psia.

The numerical sensitivities were calculated by perturbing the permeability of each of the grid blocks by 5% and re-computing the pressure variations at the observation well. This process is repeated 441 times, once for each grid block. Finally, the numerical sensitivities can be computed once the differences in wellbore pressure in the frequency domain are known for the corresponding changes in grid block permeability. The total time required to implement this method is approximately 40 minutes of running time. Figure 6.2 shows the semi-analytic sensitivities derived using Equation 21.

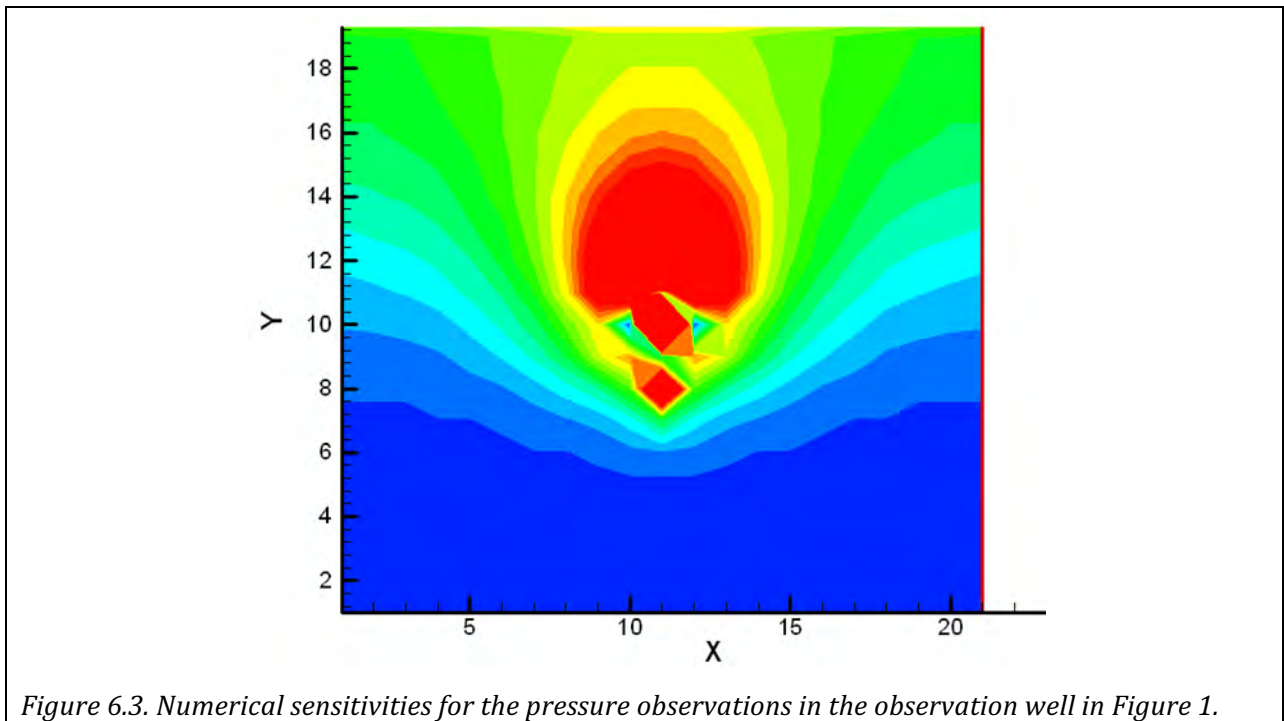
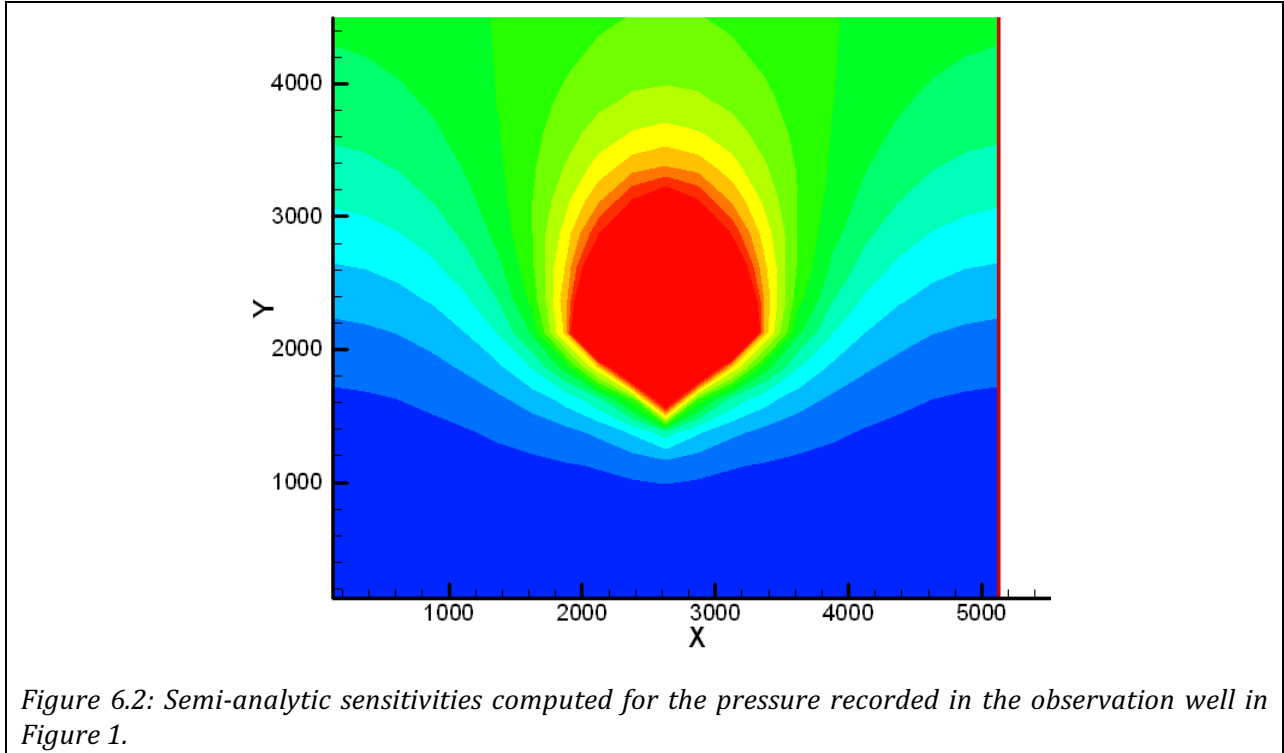
Figure 6.3 shows the numerical sensitivities calculated for the same model. Comparing the two methods used, it can be noticed that the sensitivities shown in Figures 6.2 and 6.3 are very similar and therefore provide validation for the analytic approach to compute sensitivities via Equation 21. The total computation time for the sensitivities in Figure 6.2 was 4 seconds.

6.6 Results and Conclusions

In conclusion, the use of the asymptotic low-frequency approach to interpret pressure measurements is promising and allows for rapid assessment of subsurface heterogeneities.

Additionally, it also provides a mechanism by which noisy measurements may be filtered to use only those measurements with meaningful information content.

The approach described in this chapter allows for a high-resolution reconstruction of conductive pathways in the subsurface for fluid migration. Consequently, in the absence of



other geophysical measurements or geologic interpretation, it provides a sound approach to addressing concerns over the migration of injected water and its role in induced seismicity. The methodology described here borrows heavily from Vasco and Karasaki (2006) but is very promising to determine the fate of injected water in salt water disposal operations.

6.7 References

1. Gradshteyn, I. S., and I. M. Ryzhik. 1980, Table of Integrals, Series, and Products, Elsevier, New York.
2. Oliver, D. S. 1993. The influence of non-uniform transmissivity and storativity on draw-down. *Water Resources Research* **29**(1): 169–178. <http://dx.doi.org/10.1029/92WR02061>.
3. Vasco, D. W. 2000. An algebraic formulation of geophysical inverse problems. *Geophysical Journal International* **142**(30): 970–990. <http://dx.doi.org/10.1046/j.1365-246x.2000.00188.x>.
4. Vasco, D. W. 2004. Estimation of flow properties using surface deformation and pressure data: A trajectory-based approach. *Water Resources Research* **40** (10): 1-14. W10104. <http://dx.doi.org/10.1029/2004WR003272>.
5. Vasco, D. W., and K. Karasaki. 2001. Inversion of pressure observations: An integral formulation. *Journal of Hydrology* **253**(1–4): 27–40. DOI: [http://dx.doi.org/10.1016/S0022-1694\(01\)00482-6](http://dx.doi.org/10.1016/S0022-1694(01)00482-6).
6. Vasco, D. W., and K. Karasaki. 2006. Interpretation and inversion of low-frequency pressure observations. *Water Resources Research* **42**(5) W05408. <http://dx.doi.org/10.1029/2005WR004445>.
7. Vasco, D. W., H. Keers, and K. Karasaki. 2000. Estimation of reservoir properties using transient pressure data: An asymptotic approach. *Water Resources Research* **36**(12), 3447–3465. <http://dx.doi.org/10.1029/2000WR900179>.
8. Vera, F. and Economides, C. 2014. Describing Shale Well Performance Using Transient Well Analysis. *SPE Journal* **10** (2): 24-28. SPE-0214-024-TWA. <http://dx.doi.org/10.2118/0214-024-TWA>.
9. Virieux, J., Flores-Luna, C., and Gibert, D. 1994. Asymptotic theory for diffusive electromagnetic imaging. *Geophysical Journal International* **119** (3): 857-868.

Description of RPSEA Project Task 10 – 4D Integrated Multiscale Reservoir and Geological Modeling: A field-scale model representative of the Osage County gravity anomaly (the reference model) shall be developed using an ensemble of models that are progressively updated. A set of predictions shall be generated through coupled numerical simulation of water movement in the subsurface and the localized stress changes associated with water injection. These predictions shall be compared to observations of seismic activity in the region that have previously been attributed to water disposal and by reconciling these differences in the model to create an improved representation of the preferential flowpaths, geomechanical properties and fault characteristics in the subsurface. The improved model shall be tested against 4D geophysical monitoring analyses and further refined. This shall directly address the key challenges related to improved quantification, sensitivity and resolution of monitoring technologies. By sequentially calibrating reservoir performance models to all available monitoring data, improved prediction and delineation of the injected water becomes possible.

The report appended below summarizes work on modeling of induced seismicity under part of RPSEA Task 10, with reference to activities supported by the RPSEA Project.

7. Modeling Pore Pressure Variations and Potential for Induced Seismicity Adjacent to Water Disposal Wells.

Deepak Devegowda

Mewbourne School of Petroleum and Geological Engineering, Mewbourne College of Earth and Energy, University of Oklahoma, Norman OK 73019

The objective of this study is to deduce a temporal and spatial correlation between salt-water injection and earthquake frequency using numerical models. Studies of seismicity in the vicinity of salt-water disposal (SWD) wells often rely on identifying statistical relationships between SWD well location, injected water volume, rate of injection and the timing of seismicity. For instance, by plotting well head pressure measurement and salt water injection rate through time (Figure 7.1), the Oklahoma Geological Survey report a strong temporal and spatial correlation between salt water disposal wells and occurrence of the earthquake activity that is clearly distinct from background seismicity rate (Darold A.P. et al. 2014) in Oklahoma. Relative proximity of injection sites to earthquake event locations suggests a close link between the two; however, such analyses may have limited utility for predictive purposes. For instance, some of the key concerns are:

- Is there a critical injection rate below which seismicity may be managed?
- What is the optimal distance for injection wells from a fault?
- Does the fault transmissibility play a role in governing induced seismicity?

In this study, we employ numerical modeling to explain hypocenter locations of induced seismicity in the Precambrian basement that are located more than a kilometer below the injection zone and to investigate pore pressure diffusion that triggers fault slip in the crystalline basement specifically in relation to events in Oklahoma.

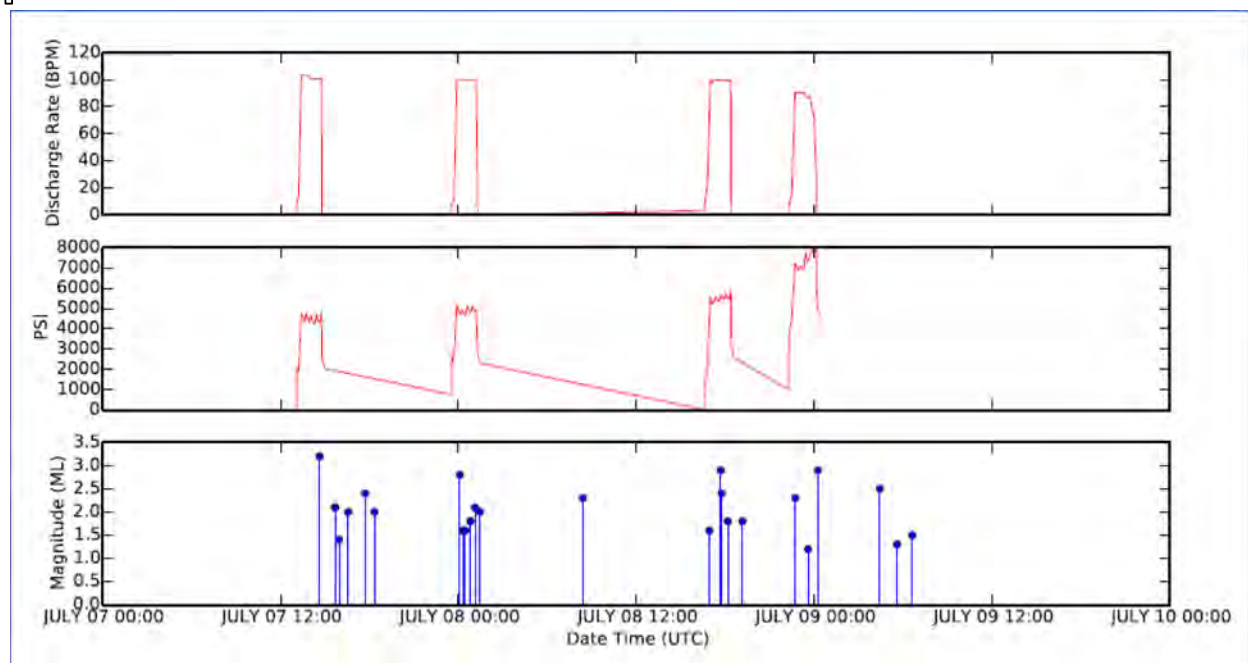


Figure. 7.1: Plot showing temporal correlation between the salt water disposal and earthquake data from Carter county (Darold A.P. et al 2014)

7.1 Literature Review

Whereas there has been a low level of background seismicity historically in Oklahoma, there has been a sharp increase in seismicity of about 300 times since 2009 in a portion of the state (Figure 7.2). Rates of salt-water disposal (SWD) from oil and gas operations have been increasing since 2005, and in 2013, are ten times as large as the volumes recorded in 2000 (Table 7.1). This in turn has raised concerns about the link between oil and gas activity and seismicity in the region. In Oklahoma, produced water disposed in a saline aquifer through vertical SWD wells extend to a total depth of 2.2 km to about 3.5 km in the Arbuckle group, with some wells terminated adjacent to, or in the Precambrian basement. Hypocenter depths of the earthquakes under a magnitude of 2.5 M_L in 2014 are mostly located within the brittle upper crust at the depth of \sim 2 to 5 km into the crystalline basement. We now provide a brief description of the Arbuckle group and the basement relevant to the modeling exercises.

Geology: The Arbuckle group of central-south Oklahoma has a variable thickness of 600 to 3500m, consists dominantly of interbedded thin carbonate mudstone, interclast calcarenite, laminated dolomite or dolomitic limestone with few laterally consistent sandstone beds (Fritz D. Richard et. al. 2013). The Arbuckle Group history has included multiple phases of diagenesis and therefore some units have a complex porosity network controlled by diagenesis, depositional environment, paleokarst formation with fault overprints. Porosity of the upper Arbuckle Group ranges as high as 25%-65% (William E Ham, 1973), although much of the Group is less porous. Below the Arbuckle is igneous basement rock of Precambrian age made up of rhyolite with very low porosity (10- 15%) and permeability

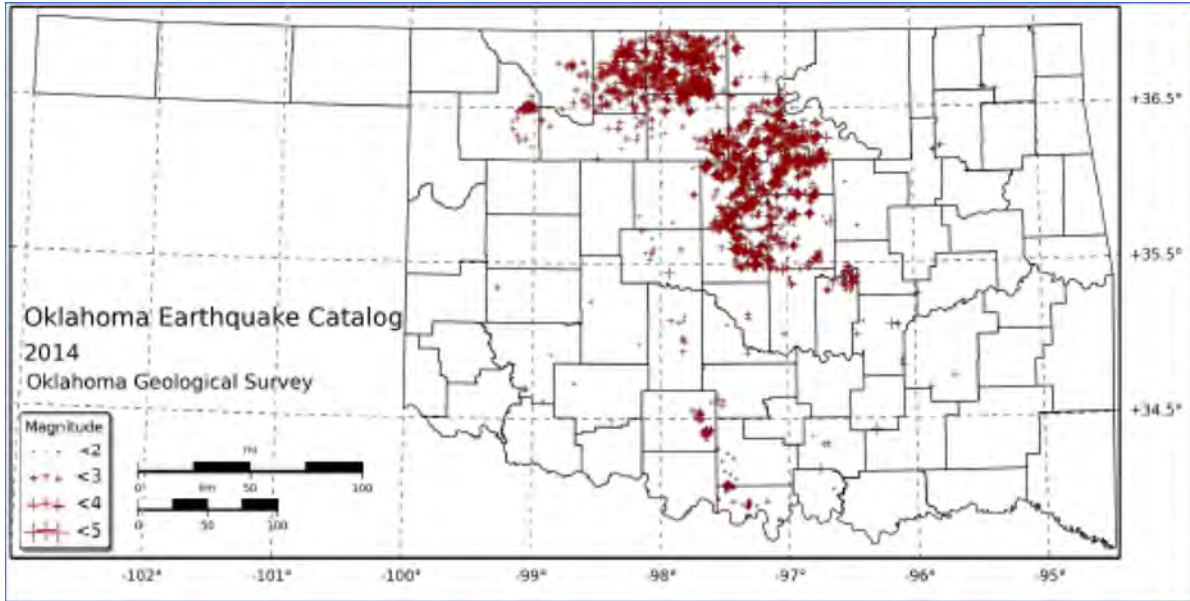


Figure 7.2: Earthquakes in Oklahoma reported by OGS in 2014 (Oklahoma Earthquake Summary Report 2014, OGS Open file report-2015). The greatest number of earthquakes have occurred in Central and north-central Oklahoma but an increase is observed in Northeast Oklahoma from 2015.

Table 7.1: Salt Water Disposal (SWD) volume in Mbbl per zone

Zone	2009 (Mbbl)	2010 (Mbbl)	2011 (Mbbl)	2012 (Mbbl)	2013 (Mbbl)	2014 (Mbbl)
Arbuckle	434,230	449,406	525,027	566,047	842,631	1,046,913
Basement	1,368	771	621	1,379	820	2,162

(10^{-15} - 10^{-18} m²) (Morgan et. al. 2015). The thickness of this crystalline basement unit ranges from about 2600m to more to 3500m.

Hydrogeology: The Arbuckle Group consists in large part of aquifer quality rock. Because of poor quality of the aquifer water and due to the presence of strong confinement above the aquifer, low porosity, permeability and great depth, it is economically impractical to use this water. The Arbuckle Group can accept a large amount of water without increasing wellhead pressure, although the cause of this underpressure is still poorly understood. One explanation could be that SWD well completion intervals include karstified sections or fractures that have higher permeability than the matrix permeability, which allows the Arbuckle SWD wells to behave as if they were underpressured in Oklahoma (Morgan et. al 2015).

Structural Description of the Arbuckle: The southern central part of the Arbuckle group is highly faulted and folded with major fault orientation in the north-west direction. Fig. 7.3 & 7.4 show the position of SWD wells and faults with optimal orientation (those likely to have an earthquake). The focal mechanism distribution is dominated by strike-slip motion on steeply dipping faults. Optimal orientation of faults ranges between 45°-60°, 105°-120° and 135°-150°, and represent orientations most likely to have an earthquake, given the

roughly East-West stress field in much of Central Oklahoma. Moderately optimal orientation ranges between 15°-45°, 60°-75°, 90°-105° and 120°-135° and represent fault orientations moderately likely to have an earthquake. All other orientations of fault strike are sub-optimal orientation and have a low likelihood to have an earthquake (Murray 2014, OGS OF5-2015). These results do not indicate that earthquakes cannot occur on sub-optimal fault strikes, but suggest that they are less likely (Murray 2014, OGS OF5-2015). Fig. 7.4 Shows that major faults trends in north central Oklahoma deduced from focal plane solutions are for strike slip motions on subvertical faults (Darold and Holland 2015).

Absolute Stress Magnitude and Critically Stressed Crust: Stress in the lithosphere can be determined by the earthquake focal mechanism, which are the most ubiquitous indicators of principal stress orientation. Mechanisms of stress determination include the pattern of seismic wave radiation from the focal point of the earthquake. Different types of earthquakes (Strike slip, Normal and Reverse fault) define the magnitude of vertical stress, maximum horizontal stress and minimum horizontal stress (Zoback and Zoback, 2002). We are using a simple model of stress magnitude variation with depth where the fault is in a state of frictional equilibrium. This describes a critically stressed crust in which the differences between frictional and shear stresses are very close to the values required for slip for optimally oriented pre-existing faults (Zoback and Zoback, 2002).

7.2 Known Mechanisms of Fluid Injection-Induced Seismicity

Pore pressure can play a two-fold role in the earthquake process by:

1. Decreasing the effective stress and/or
2. Altering the rock chemically to reduce the coefficient of friction on the fault.

Failure criteria for frictional sliding govern the frictional strength of a preexisting fault. Because of friction, a certain shear stress value must be achieved in the rock before frictional sliding is initiated, and defining this critical stress is the failure criterion for frictional sliding (Byerlee's law). We are taking cohesion as zero for preexisting faulted rock.

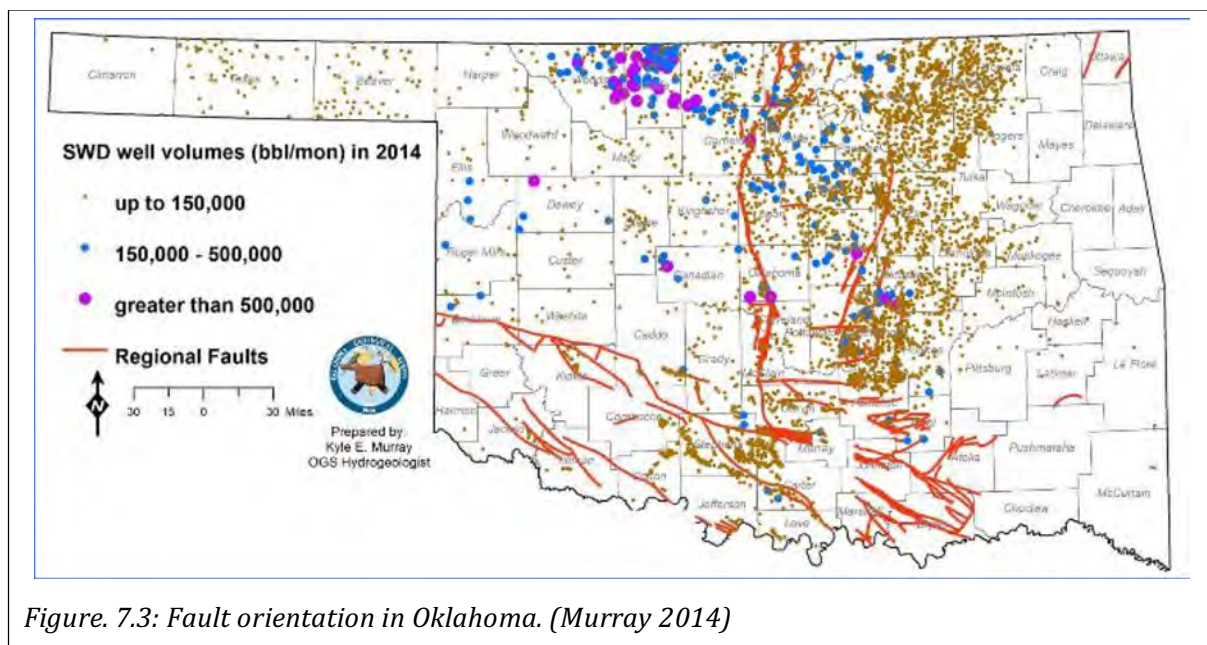


Figure. 7.3: Fault orientation in Oklahoma. (Murray 2014)

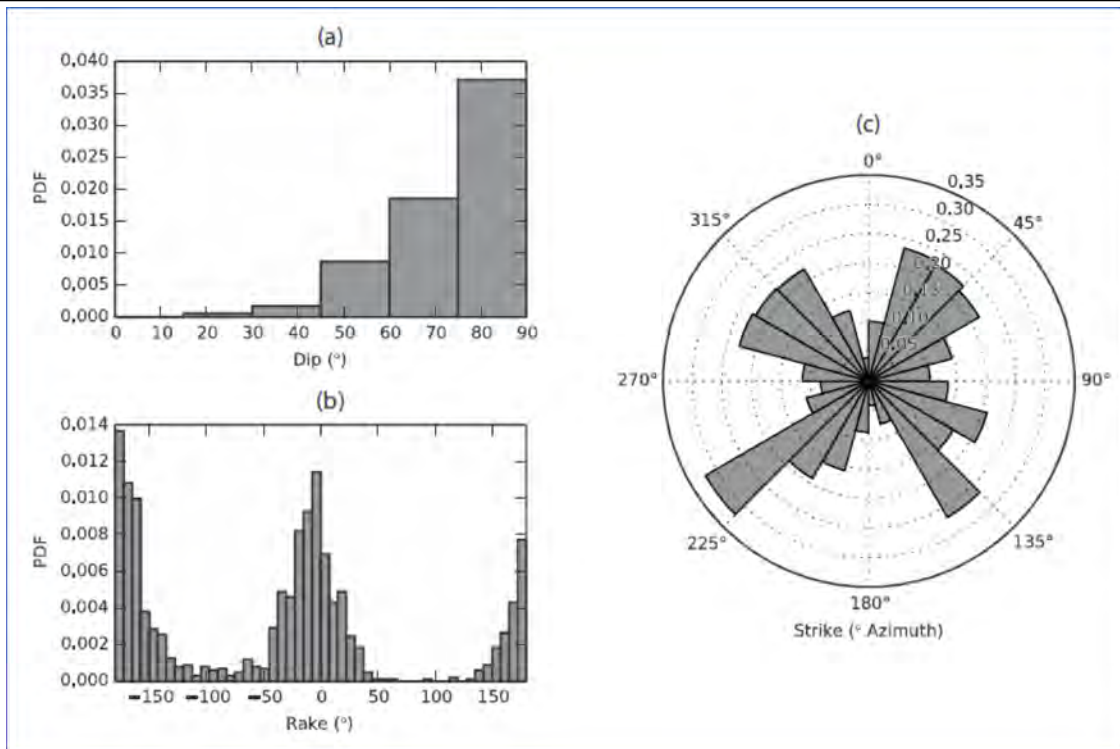


Figure 7.4: Probability density function of the a) Dip of the fault b) fault rake c) fault orientation (Darold and Holland, 2015)

Fault slippage occur when shear force on the fault plane is greater than the frictional force, i.e. $\tau = S_0 + \mu^* \sigma_e$ (where, τ = shear stress, S_0 = cohesive force, which is zero in case of preexisting faults. μ = coefficient of fault friction & σ_e = Effective normal stress). Effective normal stress, $\sigma_e = (\sigma_n - P_p)$, where σ_n = Lithostratigraphic normal stress and P_p = pore pressure. An increase in the pore pressure is accompanied by a net decrease in the effective normal stress and this shifts the Mohr's circle to the left. Failure occurs at the point where Mohr's circle intersects the failure envelope with slope (μ).

Salt water is either disposed into the sedimentary upper Arbuckle Group or in the basement rock. Low porosity and permeability of the basement rock acts as a barrier to the migration of injected water both laterally and vertically. Note that the Arbuckle sedimentary unit is under-pressured. Low permeability of the basement matrix (10^{-15} - 10^{-18} m²) requires faults with high permeability (10^{-12} m²) to create high permeability pathways for increase in pore pressure.

Increase in the pore pressure in the basement rock away from the well bore is due to pore pressure diffusion (P. Talwani and Acree S, 1984): $\partial p / \partial t = D \Delta^2 p$, where D is hydraulic diffusivity. Permeability is directly proportional to diffusivity. This explains the time lag between earthquake and water injection (~8-10 yrs.) and also hypocentral location of earthquake at large distance (Horizontally~10km) and depth (vertically~3.5-5 km) from the injection well.

7.3 Pore Pressure Modeling

This section describes the pore pressure modeling work attempted in this study to assess changes in pore pressure laterally and vertically in the reservoir as a function of water injection rate and duration of injection. For this section of the flow simulation modeling, we have not accounted for local stress changes. The underlying motivation for this part of the study was to investigate the role of reservoir properties such as permeability, fault transmissibility, injection rate and duration of injection to quantify the impact on pore pressures. An increase of 0.01 to 0.1 MPa of stress is sufficient to trigger earthquakes when faults are near failure condition or where earth's crust is critically stressed. (R. A. Harris, et al, 1995, Keranen et al, 2015).

7.3.1 Model Grid Specification

The following data provide an overview of the model grid employed to understand pore pressure variations in response to fluid injection in the Oklahoma City Field. Because we do not have access to a geologic model, the study is restricted to the best possible representation of the geology of the field. The model is shown in Figure 7.5.

1. Total study Area: 35* 35 km (Area of Oklahoma City)
2. Depth= 2km to 8 km (Keranen et al, 2015)
3. Total number of grid cell in x, y, z direction = (i, j, k) : (175, 175, 25)
4. Oil-Water Contact (OWC) at 2000m below the surface. Water is injected in the salt-water aquifer. There is no oil in the model.
5. Position of well on grid: (X, Y) = (90,100). This would represent a well located in the center of the study area.
6. Number of parallel faults used: 4. Distance from the wells:
 - a. Fault 1: 11.6 km from the well;
 - b. Fault 2: 5 km from the well;
 - c. Fault 3: 1.6 km from the well;
 - d. Fault 4: 13 km from the well;
 - e.

7.3.2 Simulation Case Studies

The model described in a previous section is run for two different values of the fault transmissibility multiplier. These are 0.5 and 1. The salt water injection rates are chosen to be 18,000, 30,000, 54,000 and 75,000 sm³/month. The duration of water injection is 10 years. The resulting changes in the stress on different faults (in MPa) with different injection rates is shown in Figure 7.6 as a function of time for a fault transmissibility of 1.

With the model run time of 10 years, an excess pore pressure of up to 0.018 MPa develops on the nearest fault. As noted earlier, this may be sufficient to trigger seismicity for critically stressed faults. Figures 7.7 to 7.9 document pore pressure variations in a vertical slice of the subsurface. The pore pressure under certain injection rates can exceed the criterion for failure of critically stressed faults. With a fault transmissibility multiplier of 0.5, changes in the pore pressure are similar to the cases studied above and do not show appreciable differences.

7.4. Coupled Flow and Geomechanics Simulation

In this section, we describe a coupled flow and geomechanical simulation to investigate changes in stress with increases in volumes of water injected. From the pore pressure modeling results shown in a previous section, at higher injection rates, the increase in the pore pressure exceed the threshold value to trigger slippage. Because our analysis is restricted to the Oklahoma City Field, the stress condition and fault strike is similar to those shown in Figure 7.3. The modeling is restricted to 75000 sm³/d and the objective is to estimate the time to slippage for a pre-existing fault. Because of friction, a specific value of shear stress must be present in a rock before frictional sliding is initiated on pre-existing fractures. Failure criterion for frictional sliding is similar to the Mohr-Coloumb failure criteria and plots as a as a straight line on the Mohr's diagram as seen in Figure 7.11. This empirical relationship is described by Byerlee's law (Ben and Stephan, 2004). Cohesion is zero for preexisting faulted rock.

The plastic model formation properties were derived from Gere and Timoshenko (1997). For the Arbuckle limestone, these are:

1. Elastic moduli: 0.005E+6 MPa
2. Poisson's Ratio: 0.27
3. Cohesion: 0.001. The value is taken to be small for pre-existing faults.

For the basement (granitic rock), these are:

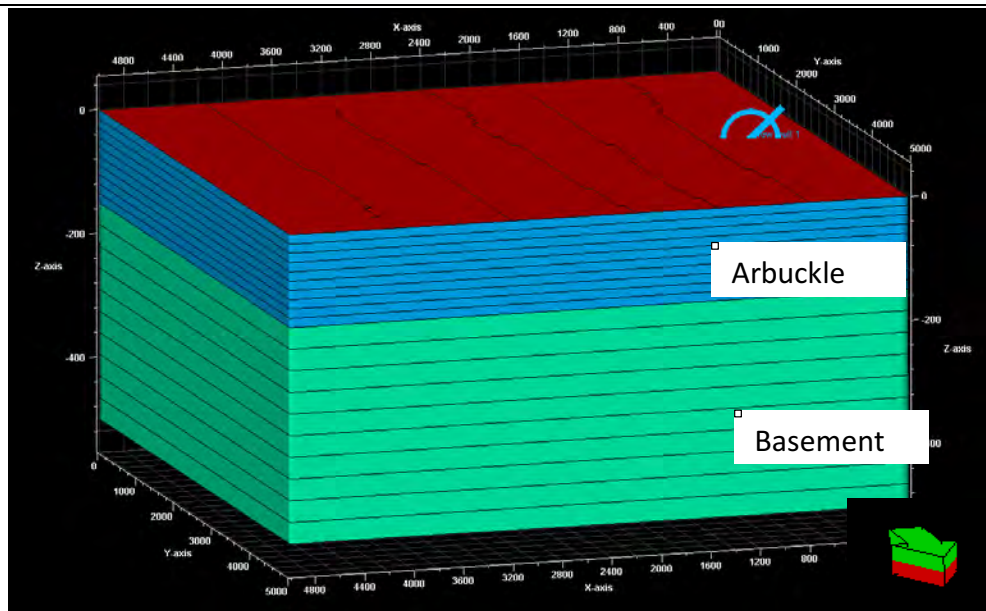
1. Elastic moduli: 0.01E+6 MPa
2. Poisson's Ratio: 0.23
3. Cohesion: 0.001.
4. Initial stress values are given at the top of the reservoir i.e. 6,561.68 ft below surface are given as in Table 7.2.

□ *Table 7.2: Values specified for the horizontal maximum and minimum stresses as well as the corresponding gradients.*

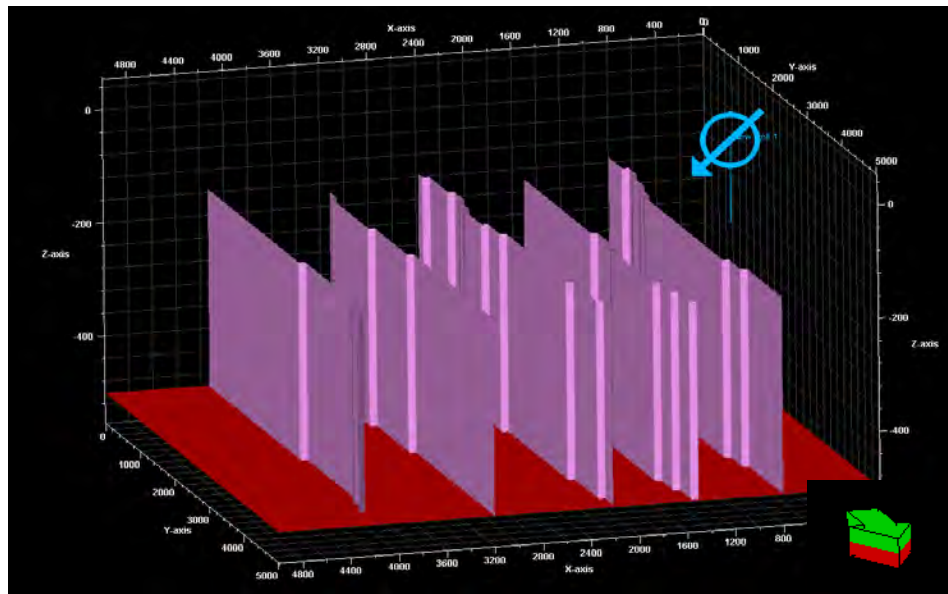
	$S_{\text{horizontal, max}}$	$S_{\text{horizontal, min}}$	S_{vertical}
Stress at the top of the reservoir, psi	5500	4280	6562
Stress gradient, psi/ft	-1.5	-0.618	-1.0

The vertical lithostratigraphic stress gradient= 1psi/ft (Zoback and Zoback, 2003). The horizontal stresses are obtained from Zoback and Zoback (2003). The relative magnitude of the principal stresses, S can be related to the faulting style currently in the region. Because Oklahoma predominantly has strike slip faults, we have modeled strike slip faults in the basement with no faults in the Arbuckle. The relationship between the principal stresses is given by:

1. Arbuckle, normal faulting: $S_{\text{vertical}} > S_{\text{horizontal, max}} > S_{\text{horizontal, min}}$
2. Basement, strike-slip fault: $S_{\text{horizontal, max}} > S_{\text{vertical}} > S_{\text{horizontal, min}}$

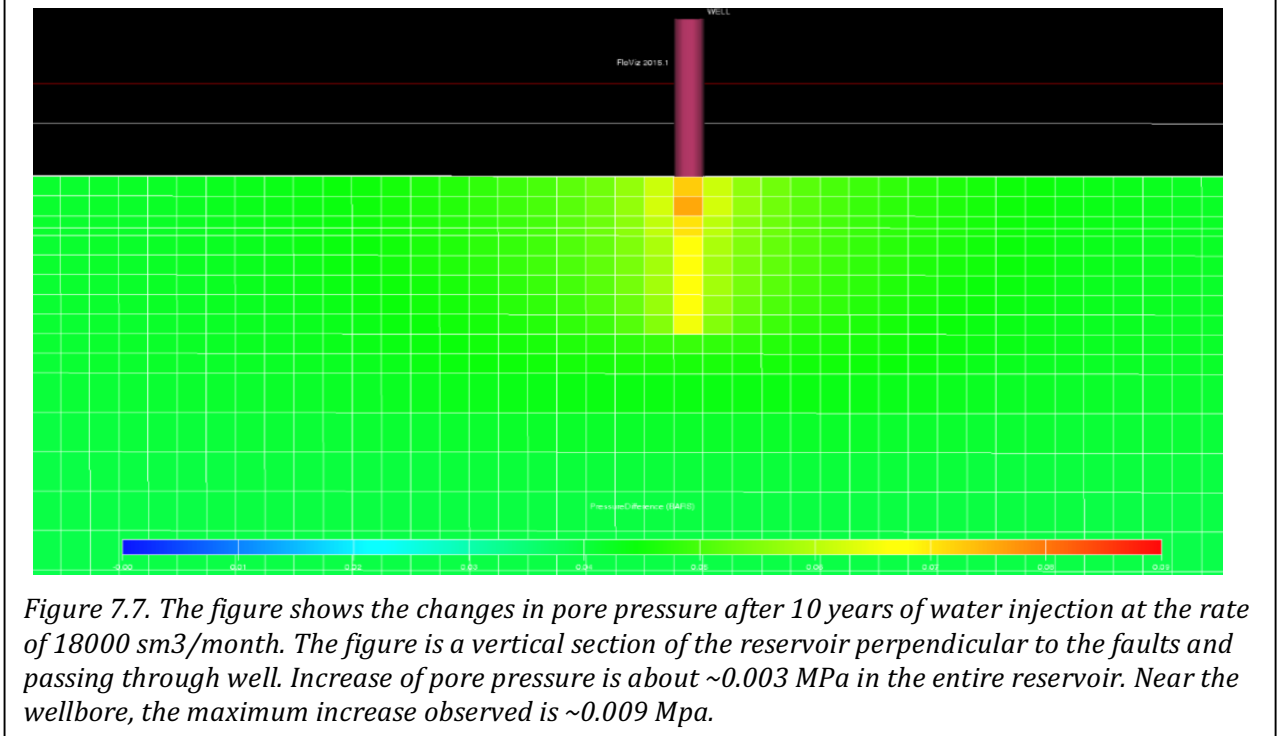
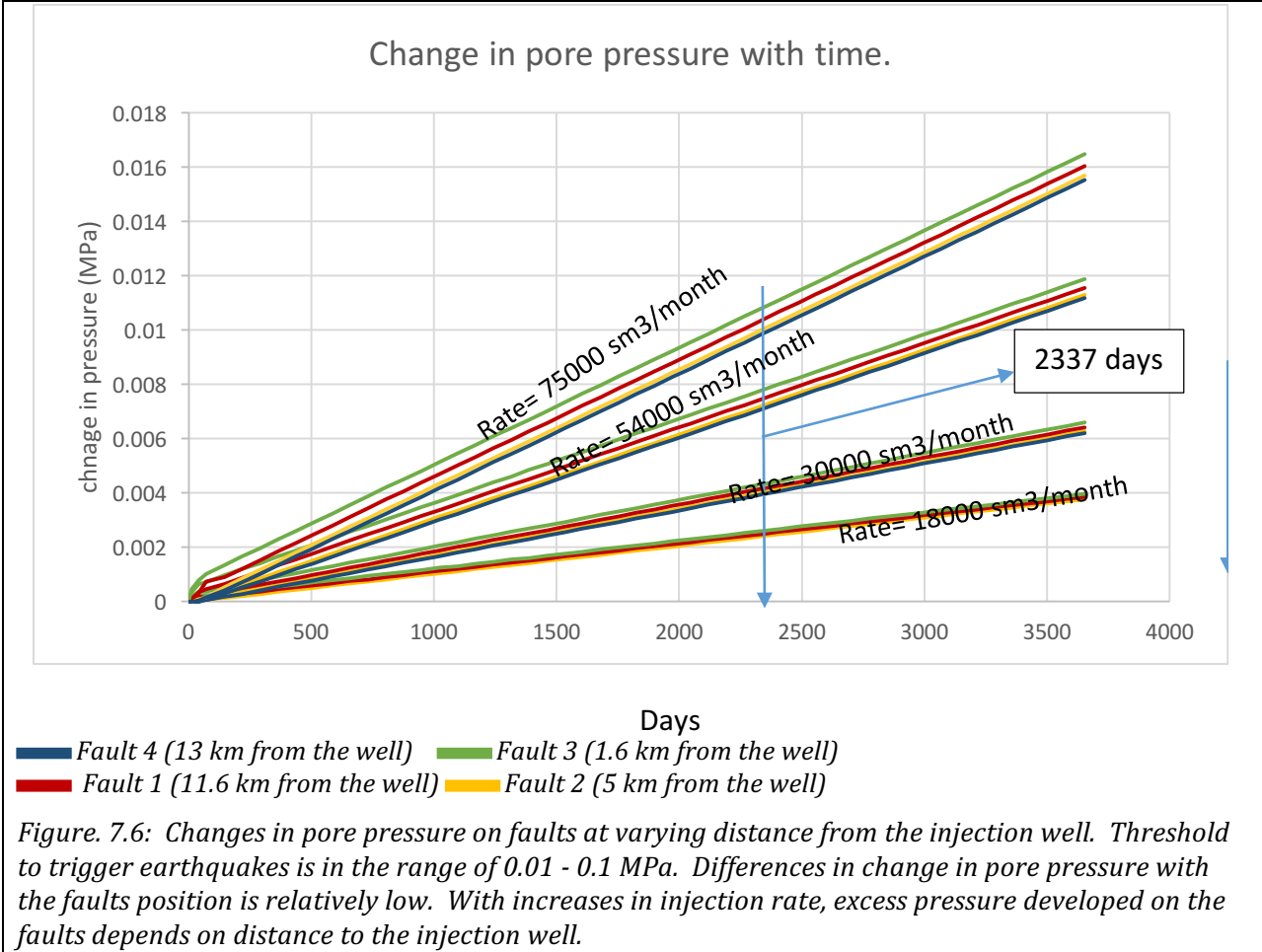


(a)



(b)

Fig. 7.5: a) Schematic diagram of the reservoir boundary showing basement fault impression on the top of the reservoir (Arbuckle) b) Segmentation Fault in the Basement and well position with maximum well depth in the upper Arbuckle Formation. Because we have not considered the effect of stress in this study, fault is not in accordance with the stress (optimum stress direction should be at specific angle to the fault as described in a later section).



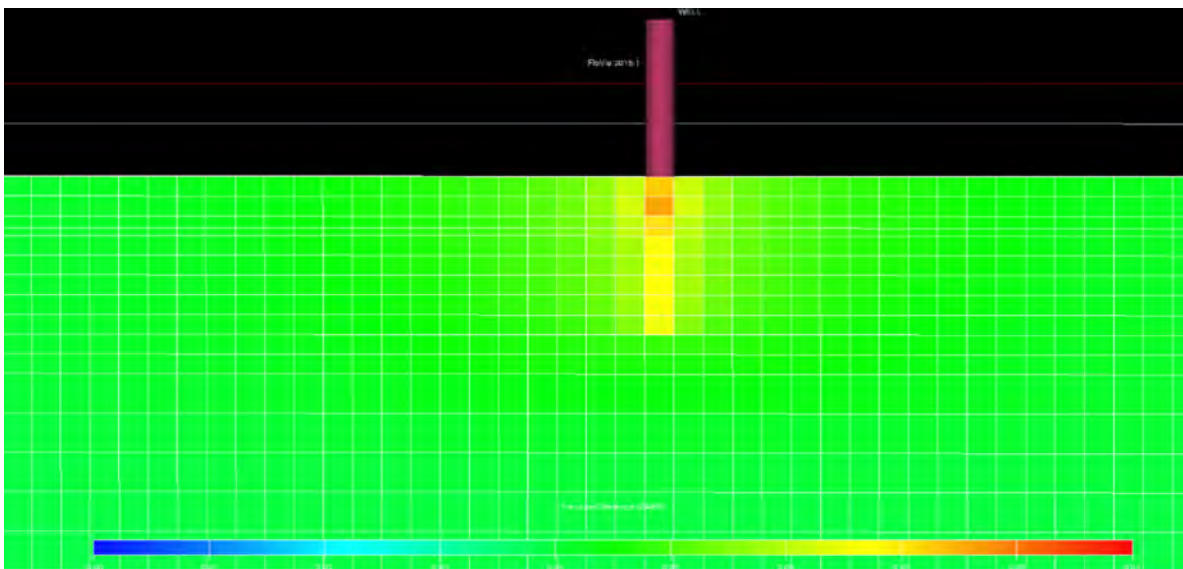
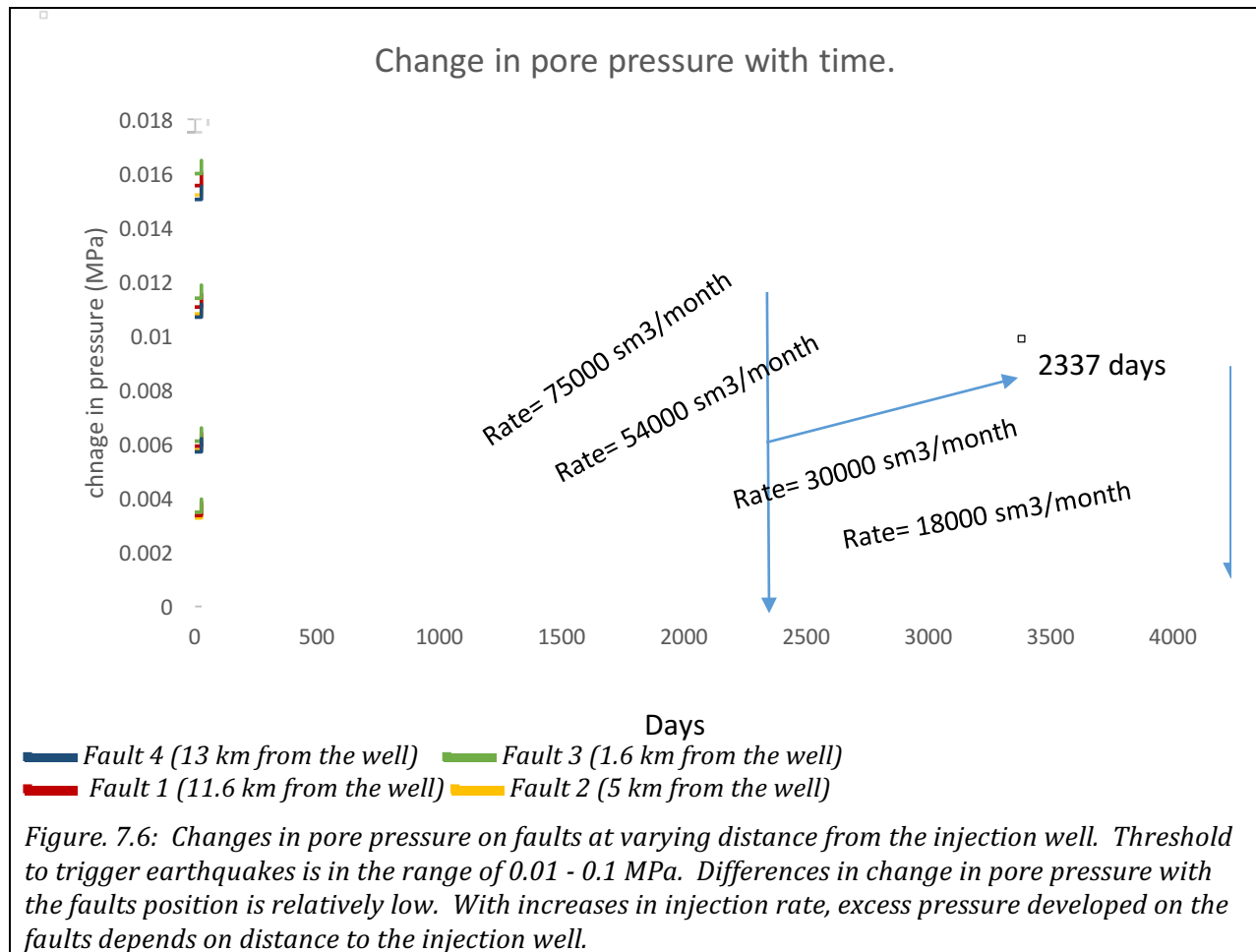


Figure 7.7. The figure shows the changes in pore pressure after 10 years of water injection at the rate of 18000 sm³/month. The figure is a vertical section of the reservoir perpendicular to the faults and passing through well. Increase of pore pressure is about ~0.003 MPa in the entire reservoir. Near the wellbore, the maximum increase observed is ~0.009 Mpa.

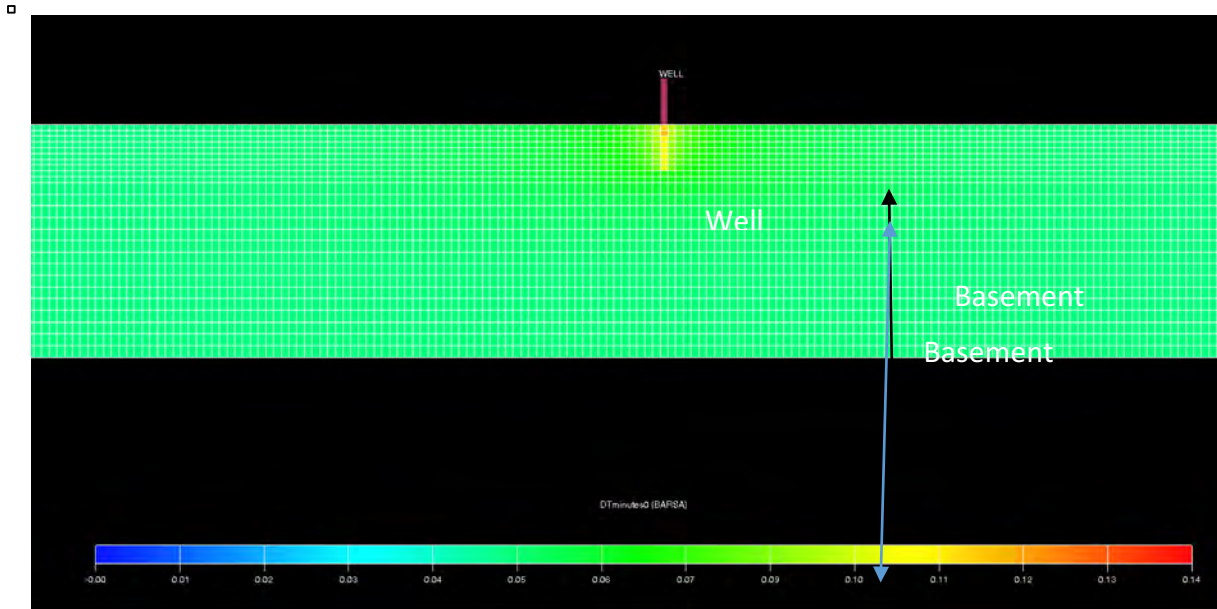


Figure 7.8. The figure shows the changes in pore pressure after 10 years of water injection at the rate of 30,000 sm³/month. The figure is a vertical section of the reservoir perpendicular to the faults and passing through well. Increase of pore pressure is about ~0.004 MPa in the entire reservoir. Near the wellbore, the maximum increase observed is ~0.014 Mpa.

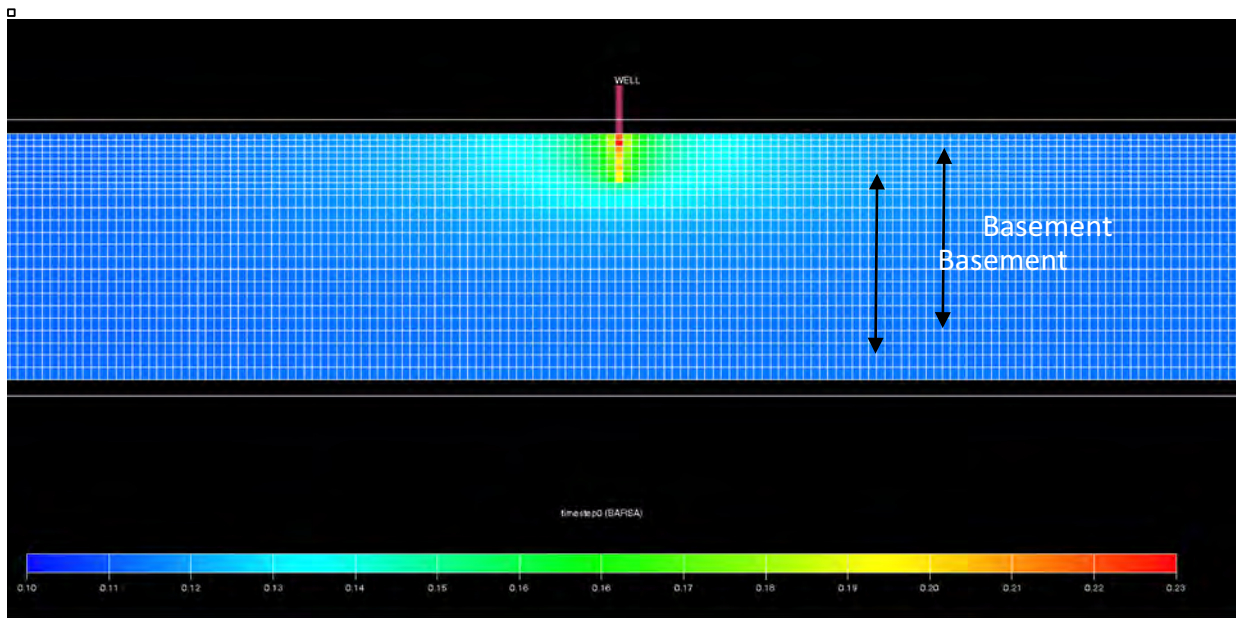


Figure 7.9. The figure shows the changes in pore pressure after 10 years of water injection at the rate of 54000 sm³/month. The figure is a vertical section of the reservoir perpendicular to the faults and passing through well. Increase of pore pressure is about ~0.01 MPa in the entire reservoir. Near the wellbore, the maximum increase observed is ~0.018 Mpa.

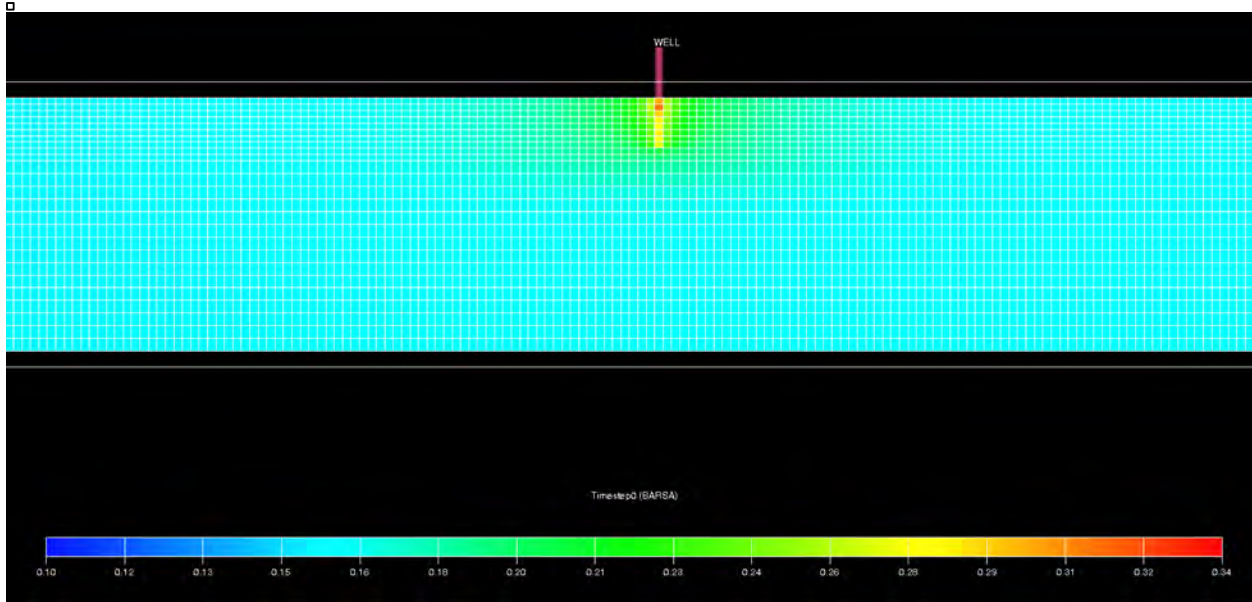


Figure 7.10. The figure shows the changes in pore pressure after 10 years of water injection at the rate of 75000 sm³/month. The figure is a vertical section of the reservoir perpendicular to the faults and passing through well. Increase of pore pressure is about ~0.016 MPa in the entire reservoir. This falls in the threshold range for fault failure. Near the wellbore, the maximum increase observed is ~0.023 Mpa.

For the Arbuckle (Normal faulting zone), minimum horizontal stress is based according to $S_{\text{horizontal, min}} = 0.67 * S_{\text{vertical}}$, giving a value of 4,280 psi for $S_{\text{horizontal, min}}$ (Townend and Zoback, 2000). The difference between the maximum stress and minimum horizontal stress magnitude is low. Therefore, with a lack of published values for the maximum horizontal stress, we assume a value of 5000 psi for $S_{\text{horizontal, min}}$. The magnitude of the stress gradient is obtained from Walsh and Zoback (2015). With this stress gradient, the stress regime changes from normal faulting in the Arbuckle to strike slip faulting in the basement.

The stress gradient for the horizontal maximum stress in the basement is obtained from Townend and Zoback (2000). Additionally, the stress magnitude of the earth's crust is specified to be critically stressed. The relationship between maximum stress and minimum stress during faulting is given by Jaeger and Cook (1971) as $\sigma_3 / \sigma_1 = ((\mu^2 + 1)^{1/2} + \mu)^2$, where, μ = coefficient of friction = 0.6 in the model.

7.4.1. One-way Flow-Geomechanical Coupling Model Description

The model is described on a 96*96*15 Cartesian grid with a total area of 14.5 km*14.5 km. The depth of the Arbuckle group with a thickness of 750 m is between 2.0 km and 5.74 km. The granite basement is specified to be 3000 m thick. The optimal pre-existing fault direction is specified to be 105 degrees to 120 degrees from Darold and Holland (2015). The optimal fault direction represents faults more likely to be associated with an earthquake in the contemporary stress field. The maximum horizontal stress orientation is N 85°E. The fault start from the base of the Arbuckle and extends throughout the basement granite and is specified to be 500 m from the injection well. Water injection rate is specified to be 3000 STB/day. The water saturation within the salt water aquifer is assumed to be 100%.

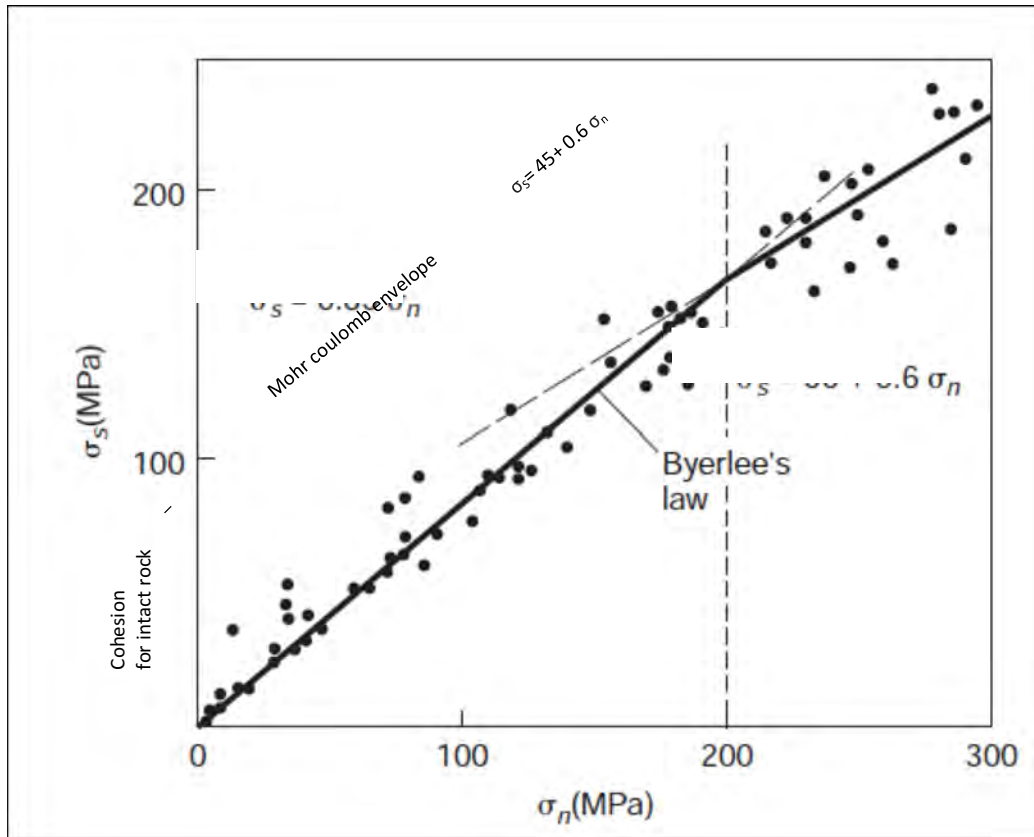


Figure 7.11. Graph of shear stress and normal stress values at the initiation of sliding on preexisting fractures in a variety of rock types. The best-fit line defines Byerlee's law (Ben and Stephan, 2004). From above we can see that shear stress requires for the fault slippage is less than the fault failure of intact rock (Mohr-Coulomb failure envelope).

A model diagram is shown in Figure 7.12.

7.4.2. Simulation Results

The simulation results indicate that a maximum change in the pressure of close to 12 psia is observed at a depth of 5.4 km from the surface adjacent to the fault that is 500m away from the injection well.

7.5. References

1. Walsh, F. R., and Zoback, M. D. (2015) Oklahoma's recent earthquakes and saltwater disposal. Sci. Adv. 2015; 1:e1500195, 18 June 2015
2. Darold A.P., Holland,A., Morris, J.K.,and Gibson, A., R. (2015), Oklahoma Earthquake Summary Report 2014, Okla. Geol. Surv. Open-File Report, OF1-2015.

□

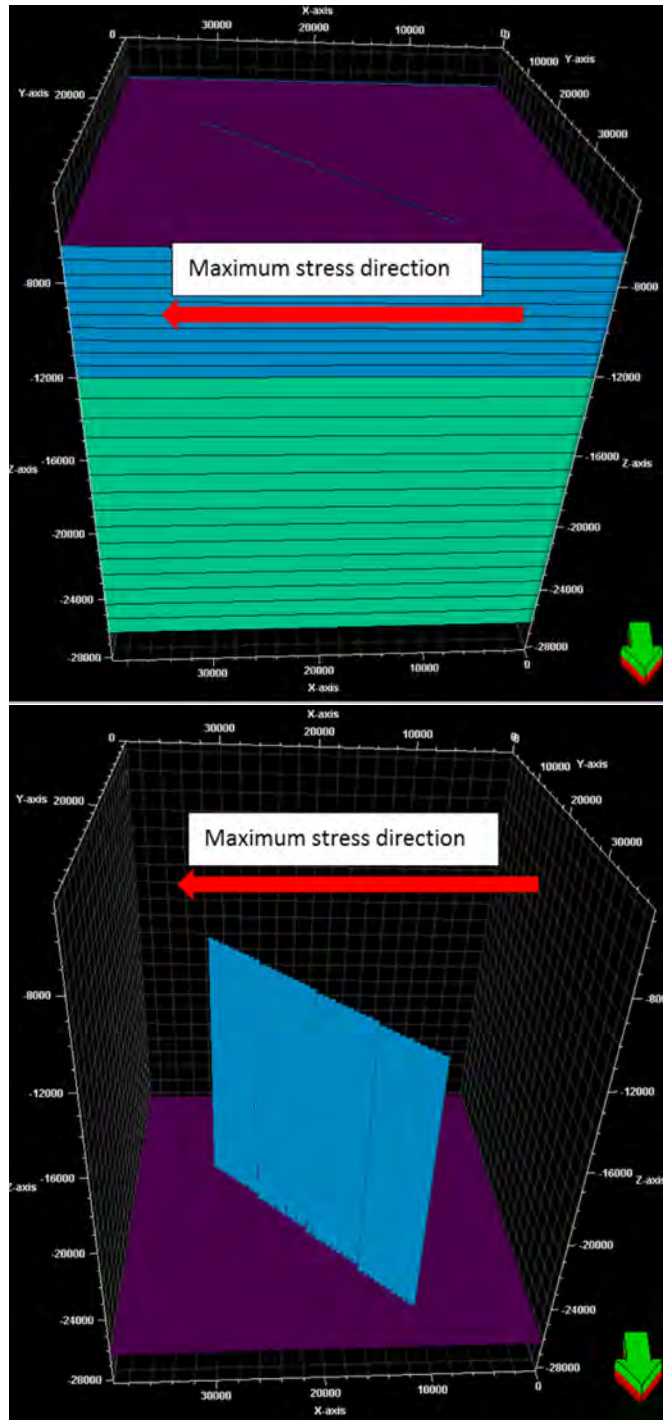
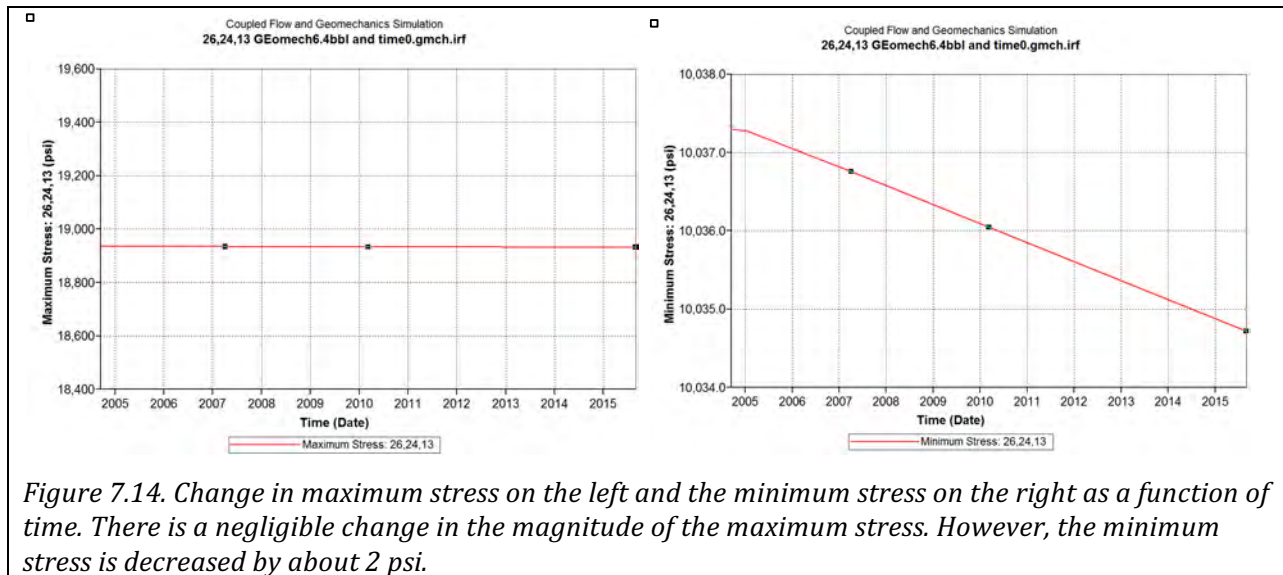
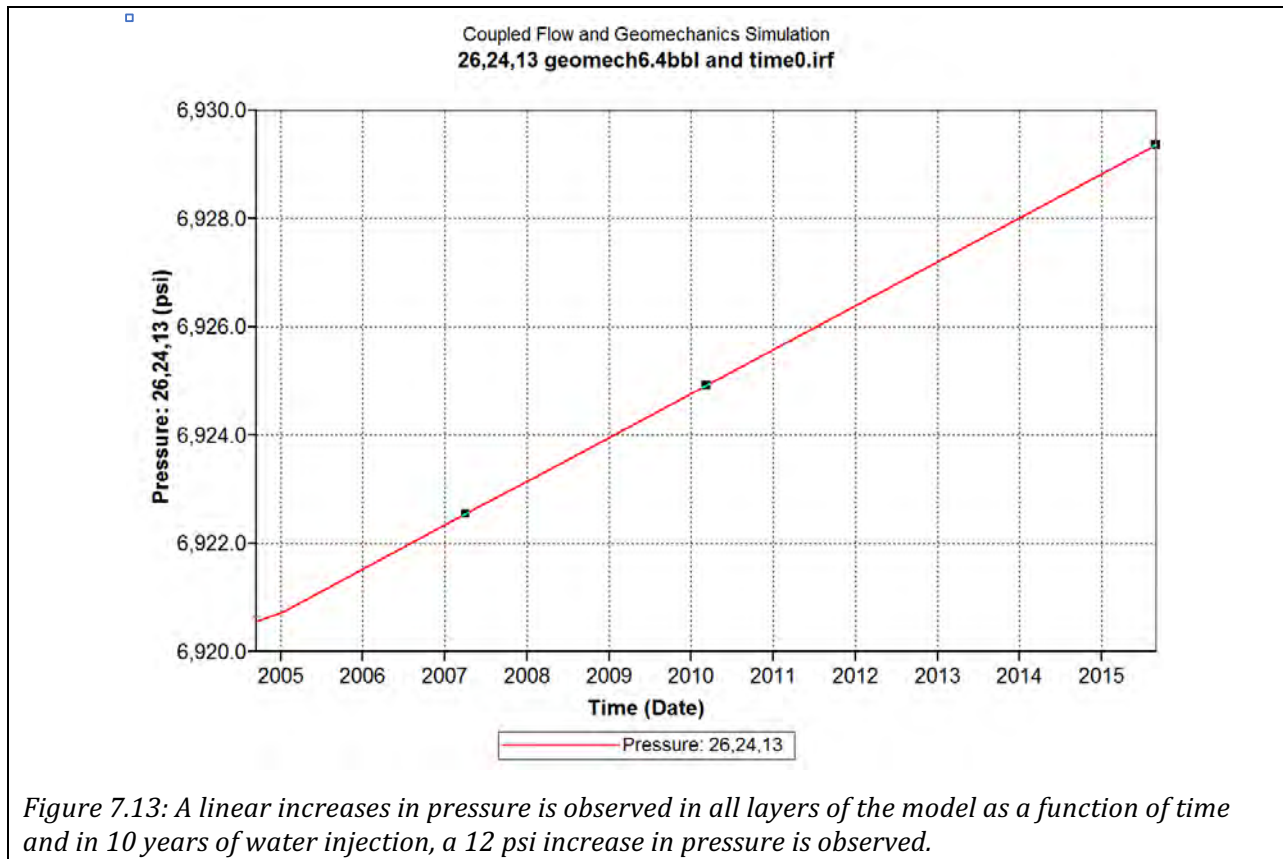
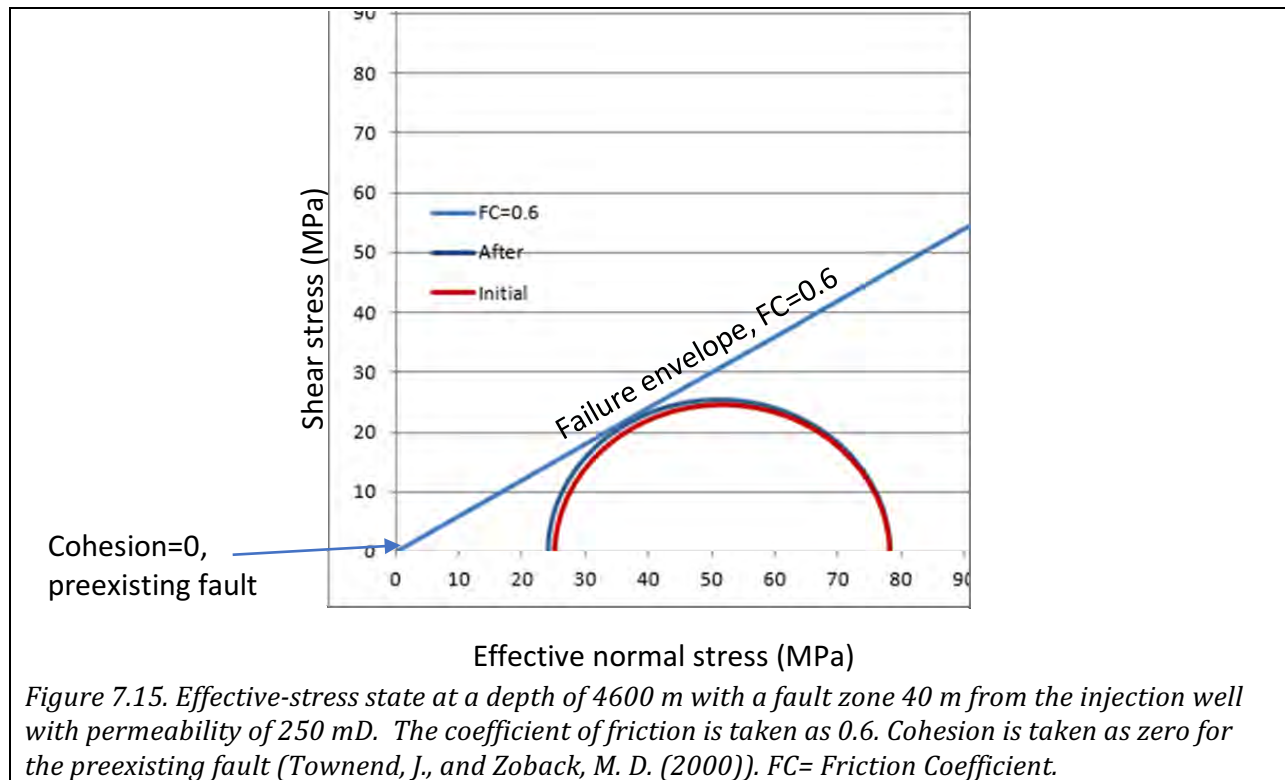


Figure 7.12. Schematic diagram of the reservoir boundary, Basement Fault impression on the top of the reservoir in the figure on top. The figure below shows a representative model of the Arbuckle formation with associated basement layers and the fault in basement in blue and initial stress direction (Red arrow showing maximum horizontal stress condition) (Distance in ft).





8. Darold A.P. , Holland, A., Chen C., A. Youngblood (2014), Preliminary Analysis of Seismicity Near Eagleton 1-29, Carter county, July 2014, Okla. Geol. Surv. Open-File Report, OF2-2014.
9. Jeremy Boak, (2016), Oklahoma Earthquakes and Injection of Produced Water, OGS Survey, 2016.
10. Richard D. Fritz, Patrick Medlock, Michael J. Kuykendall, and J. L. Wilson (2013), Geology of the Arbuckle Group in the Midcontinent: Sequence Stratigraphy, Reservoir Development, and the Potential for Hydrocarbon Exploration, AAPG Annual Convention and Exhibition, 2013.
11. William E Ham, Regional Geology of the Arbuckle Mountains, Oklahoma, The Geological society of America, 1973
12. Morgan, BC, and Murray KE (2015) Characterizing Small-Scale Permeability of the Arbuckle Group, Oklahoma. Oklahoma Geological Survey Open-File Report (OF2-2015). Norman, OK. 12 pages.
13. Murray, K. E. (2015) Class II Saltwater Disposal for 2009-2014 at the Annual-, State-, and County- Scales by Geologic Zones of Completion, Oklahoma. Oklahoma Geological Survey Open File Report (OF5-2015)
14. Darold A.P, A. A. Holland (2015), Preliminary Oklahoma Optimal Fault Orientations, OGS open report, OF1-2015

15. Mark D Zoback, and Mary L Zoback (2002), Stress in the Earth Lithosphere, Encyclopedia of science and technology, 3rd edition, volume 16, 2002
16. Townend, J., and Zoback, M. D. (2000) How faulting keeps the crust strong, *Geology* 28, 399-400
17. Richard C. Alt and Mark D. Zoback (2015), A Detailed Oklahoma Stress Map for Induced Seismicity Mitigation. AAPG Convention and Exhibition, 2015.
18. Talwani P. and Acree Steve (1984), Pore Pressure Diffusion and the Mechanism of Reservoir-Induced Seismicity. *PAGEOPH*, Vol. 122.
19. William L. Ellsworth (2013), Injection-Induced Earthquakes, *Science* 341, 2013
20. Ruth A. Harris, Robert W. Simpson and Paul A. Reasenber (1995). Influence of Static Stress Changes on Earthquake Locations in Southern California. *Nature*. Vol 375.
21. Murray KE (2015) Class II Saltwater Disposal for 2009–2014 at the Annual-, State-, and County- Scales by Geologic Zones of Completion, Oklahoma. Oklahoma Geological Survey Open-File Report (OF5-2015). Norman, OK. pp. 18.
22. Rall Walsh and Mark Zoback, (2015) Probabilistic Geomechanical Assessment of Potentially Active Faults in North Central Oklahoma.
23. Jaeger J. C. and Cook, N.G.W., (1971) *Fundamentals of Rock mechanics*.
24. James M. Gere, Stephen P. Timoshenko, (1997), *Mechanics of Material*.
25. Keranen, K.M et al. (2014). Sharp increase in central Oklahoma seismicity since 2008 induced by massive wastewater injection. *Science*: 448-451.

Description of RPSEA Project Task 11 – Integrated Rock Mechanics Studies

Available rock properties, *in-situ* stress estimates, observed seismic data, and natural fracture distributions, shall be used to compute the pore pressure and the stress conditions needed to bring the rock mass into critical state.

Available seismic data and knowledge of the tectonic framework of the region shall be used to estimate the *in-situ* stresses, and determine discontinuity orientations and their mechanical properties. Results from analysis of seismic waveforms shall provide the distribution and orientations of shear and possible tensile events, the fracture orientations obtained from event clusters, and estimates of the amount of slip from waveform analysis. Then analysis of how the reservoir rock should fail in response to injection shall be done. A 3D conceptual model of the response of the reservoir to the stimulations shall be used.

A 3D model that considers pore pressure and stress effects shall be used to model more details of the microseismic events. The spatio-temporal pressure distributions within the model shall be obtained on the irregularly spaced nodes of the grid and criticality or rock failure criterion (triggering criterion) shall be defined through the reservoir. Once the criticality condition is satisfied, a synthetic cloud of seismic events can be created by comparing it with the threshold value for each cell in the rock and at each time step. The model parameters shall be adjusted by modifying diffusivity, stress, and critically parameters to match the characteristics of the observed microseismicity.

The report appended below summarizes integrated rock mechanical studies, supported by the RPSEA Project.

5. Integrated Rock Mechanics Studies

Ahmad Ghassemi

*Mewbourne College of Petroleum and Geological Engineering, Sarkeys Energy Center
100 East Boyd St., Norman, Oklahoma 73019-0628*

Earthquakes in the continental interior of the United States have historically been rare, but starting in 2009 there was a significant increase in the number of felt events. A prominent example are the four earthquakes with magnitudes of 4.0 or greater, including one M5.7 earthquake, near Prague, Oklahoma in November 2011. These earthquakes led to widespread concern about potential damage from induced seismicity.

The earthquakes occurred close to Class II Underground Injection Control wells for salt water disposal (SWD) from oil and gas operations. The injected water increases pore pressure within the target layer and can pressurize deeper crystalline basement rocks via natural fracture systems and faults. It has been suggested that this has led to pressurization and stress redistribution within the basement, causing fault reactivation and increased seismicity.

Almost all studies on the increased seismicity in central Oklahoma have focused on pore pressure effects without explicit consideration of large-scale rock mass deformation. In this study, we develop a large-scale geomechanical conceptual model for the faults system and assess its response to salt water injection. This portion of the RPSEA Project aims to

understand the effect of water injection on pore pressure increase and its consequences within the Wilzetta fault zone near Prague, Oklahoma, United States. We simulate the hydraulic overpressures and potential for induced seismicity during hydraulic injection.

The study area selected for modeling salt water injection, encompassing approximately 460 square kilometers (approximately 22 × 23 km) is shown by the blue rectangle in Figure 8.1a and b (Fault database from OGS, <http://www.ou.edu/content/ogs/data/fault.html>). Selection of this site was based on the increased number of earthquake events in this area. The location of injection wells (shown in Figure 8.1c) and related information such as rate, volume, and duration of injection are extracted from reported data by OGS and the Oklahoma Corporation Commission (<http://www.occeweb.com/og/ogdatafiles2.htm>). Locations and magnitudes of earthquakes (shown in Figure 8.1d) were found in a similar fashion. Figure 8.2 shows different subsurface geologic units relevant to this work.

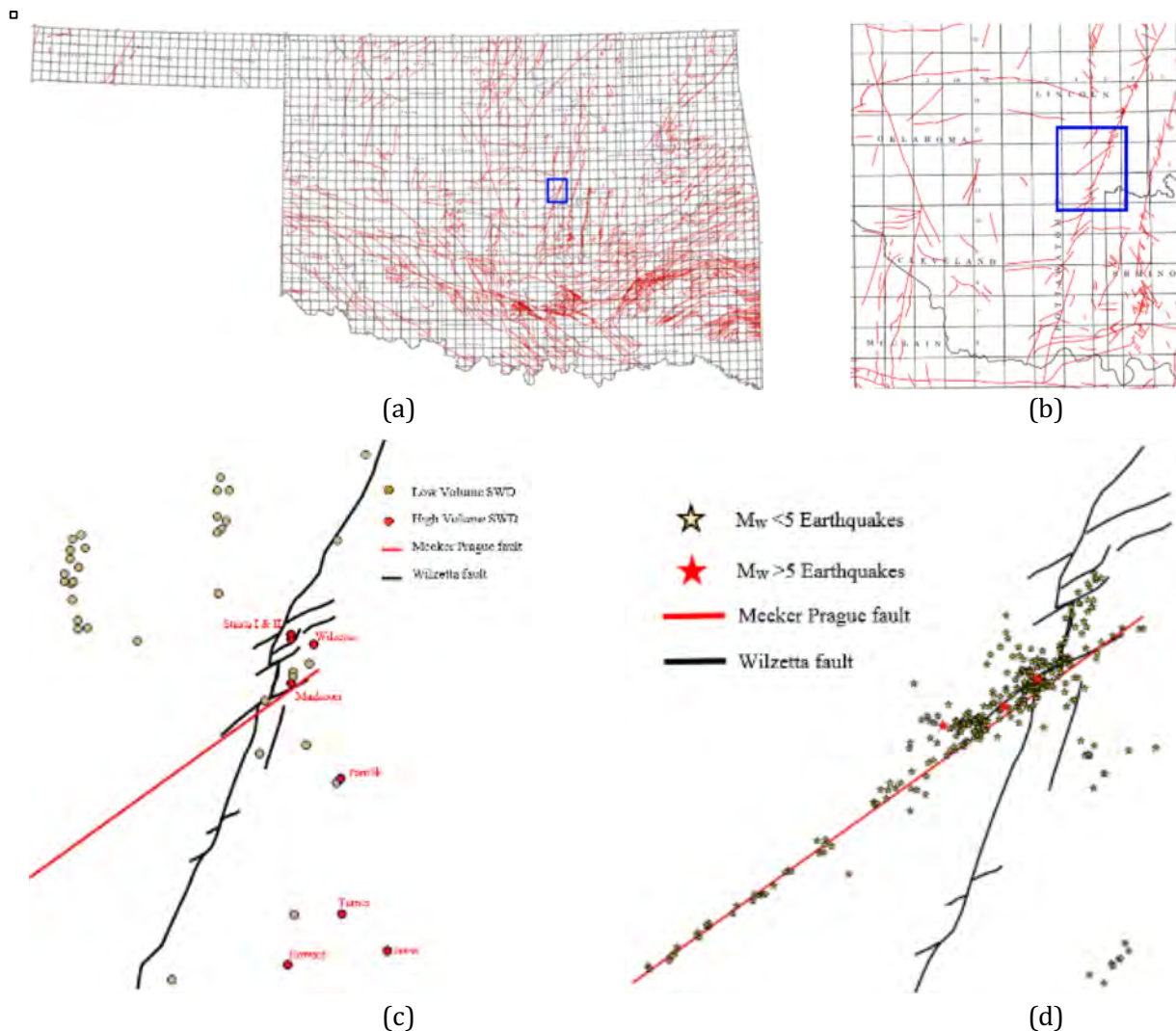


Figure 8.1: (a) and (b) General study area. Focus area extents in blue. Traces of significant faults shown as red lines. (c) Location of injection wells in the area of interest. (d) Seismic events between 2009 and 2011.

Zone	Group	Formation	
Permian		Garber	
	Chase	Brown Dolomite	
	Council Grove	Pontotoc	
	Admire	Belveal	
Virgilian	Wabaunsee	Cisco Lime	
	Shawnee	Pawhuska	
		Endicott	
Missourian	Hoxbar	Tonkawa	
		Lansing	
		Cottage Grove	
		Kansas City	
		Hogshooter	
		Layton	
Desmoinesian	Marmaton	Oswego	
	Cabaniss	Skinner	
	Krebs	Red Fork	
		Burbank	
		Bartlesville	
		Hartshorne	
Atokan-Morrowan	Atoka	Gilcrease	
		Dutcher	
	Morrow	Cromwell	
	Springer	Wamsley	
Mississippian	Chester	Manning	
		Caney	
	Meramec	Miss Lime	
		Miss Chat	
		St. Louis	
		Mayes	
	Osage	Sycamore	
	Kinderhook	Kinderhook	
Woodford	Upper Devonian	Woodford	
Dev to Mid Ord	Middle Devonian	Misener	Key to Symbols
	Lower Dev - Silurian	Hunton	Sandstone
	Cincinnatian	Sylvan	
		Viola	Carbonate
	Simpson	Bromide	
		Wilcox	Shale
		McLish	
Oil Creek			
Arbuckle	Arbuckle Group	West Spring Creek	Coal
		Kindblade	
		Butterly Dolomite	Granite
Basement & Crystalline Rock	Cambrian	Reagan	
	Pre-Cambrian	Granite	

2
Figure 8.2: Stratigraphic correlation chart of groups, sub-groups or formations comprising injection zones (Murray and Holland, 2014).

Our model includes two major faults; the Wilzetta fault (WFZ) and the Meeker-Prague fault (MPF), shown in Figure 8.1c and 8.1d. Tapp and Dycus (2013) show that the ~N25-30E trending WFZ is a relatively long, narrow zone of high-angle normal, strike-slip, and reverse faults. The Meeker-Prague fault strikes ~N55E and obliquely intersects the Wilzetta fault. We used the ubiquitous-joint model to model the faults.

An inventory of fluid injection volumes by Murray and Holland (2014) indicates 4,124 active SWD wells in Oklahoma in 2011. Figure 8.3 shows the volume of fluids that were injected into different zones using Class II UIC wells during 2011. FLAC3D (a coupled flow geomechanical code) is used in this part of the work to simulate pressure buildup and fluid migration, stress analysis, and fault motion. The simulation domain and its dimensions are shown in Figure 8.4. The simulation domain is a 50 km × 50 km area, and consists of three layers; the Simpson group, the Arbuckle group, and the basement, with average thickness of 180 m, 650 m, and 850 m, respectively. These layers are the ones that have been subjected to significant injection (Figure 8.3).

The presence of other layers is considered through their contributions to the vertical stress. According to data compilation by Crain (2015, unpublished data), the deepest earthquake has occurred at a depth of 12 km, but for now our model includes the basement to a depth of 3 km to reduce the computation time.

The important input parameter of in-situ stress is not well known in the study area. To generate a reasonable stress state in the simulation domain, we introduce gravity loading (the density is 2305 kg/m³) for the lithostatic stress, and set the $S_{H,max}$ and $S_{h,min}$ to as 27.1 MPa and 15.3 MPa respectively (Hair, 2012). $S_{H,max}$ orientation is assumed to be in the east-west direction and $S_{h,min}$ is perpendicular to it. We assume that the lateral boundaries

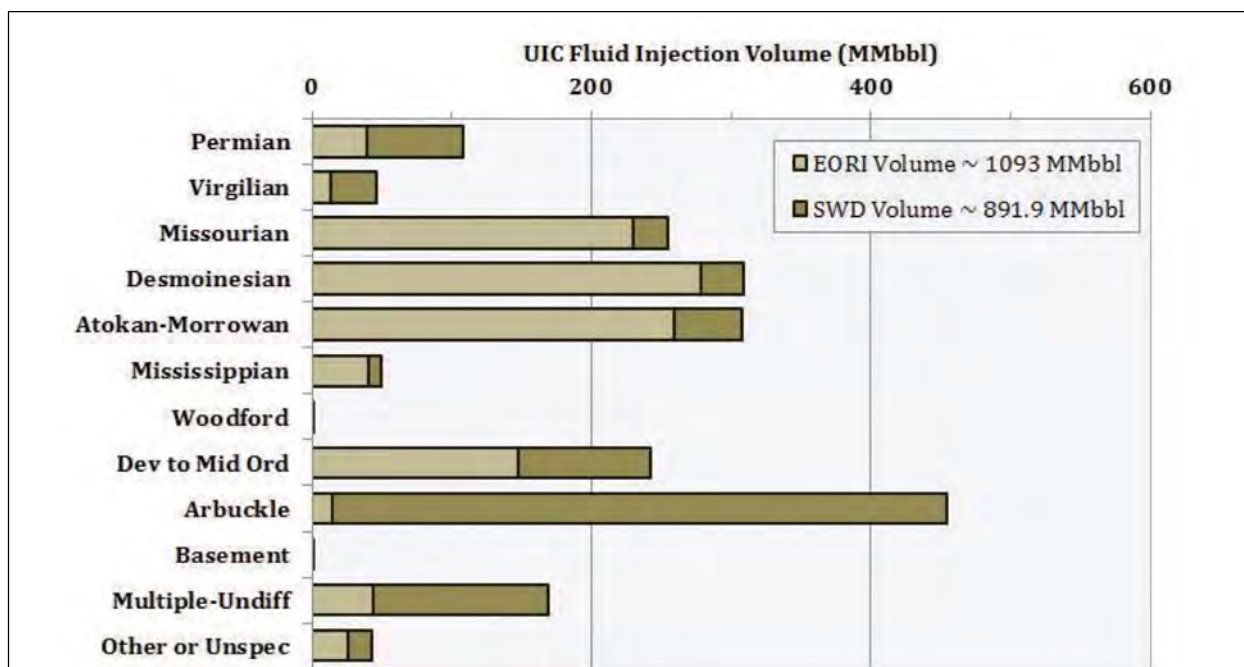


Figure 8.3: Fluid injection volumes injected into stratigraphic zones in Oklahoma, 2011 (Murray and Holland, 2014).

are fixed in the horizontal directions (x and y -direction). Rollers are used at the base so that the vertical displacement is fixed in the z -direction. The upper surface of the simulation domain, which is the boundary with the Viola layer is free to move vertically. Fig. 8.4 shows the initial condition of stress before injection. The initial pore pressure of the model is considered to be 5MPa; this value can be adjusted for greater accuracy in the future.

The Mohr-Coulomb model is used for the rocks, and the elastic properties are as follows: bulk modulus (K) is 13.2 GPa, shear modulus (G) is 11.6 GPa, friction angle (ϕ) is 46.2° and cohesion is 17.6 MPa. Currently, all three layers are assumed to have the same mechanical properties (which is obviously an incorrect assumption). In future simulations each layer will be given its own set of properties based on lab measurements.

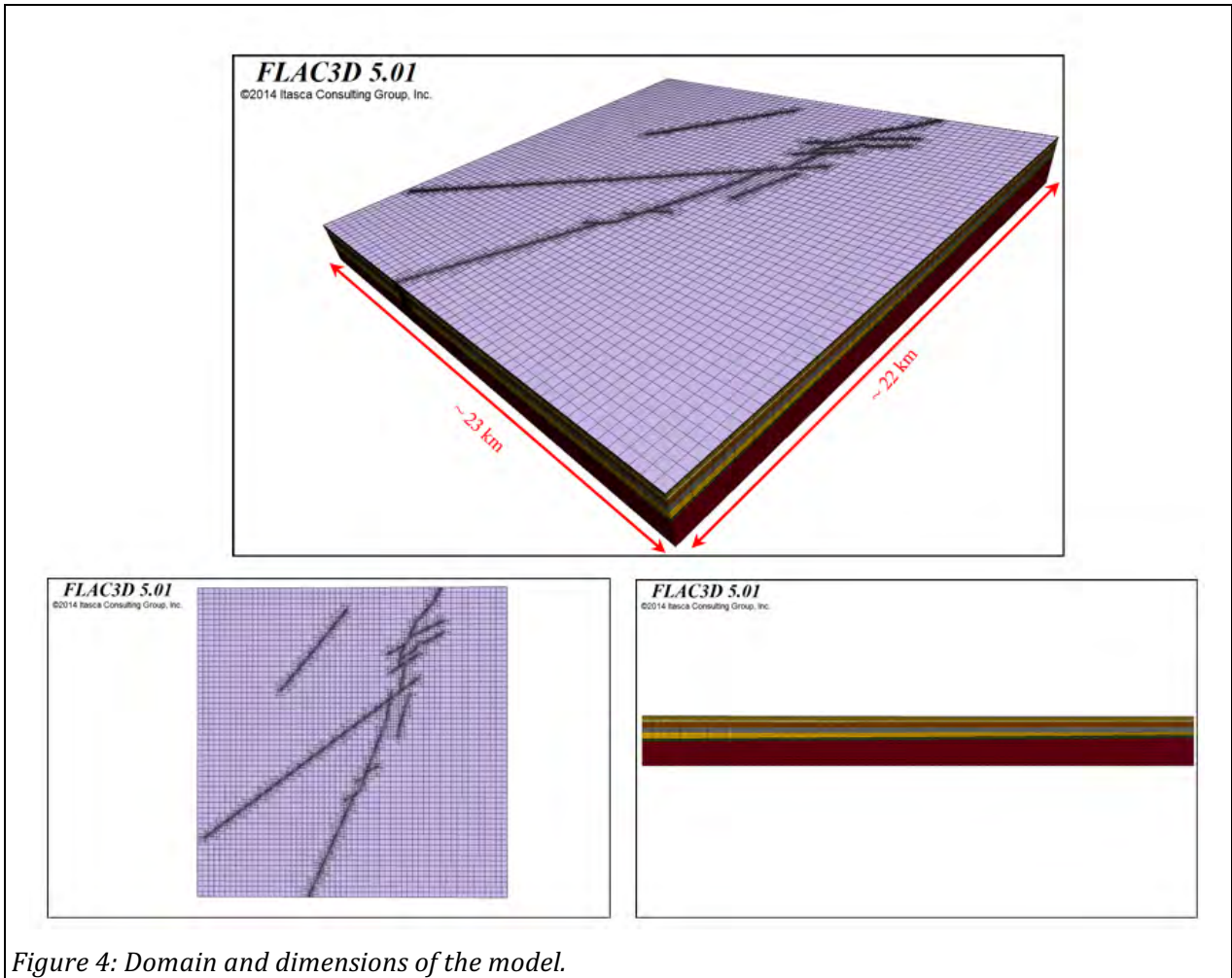


Figure 4: Domain and dimensions of the model.

Table 8.1 shows subsurface layers and their corresponding hydraulic properties. The fluid is considered an incompressible brine and has a density and bulk modulus of about 1110 kg/m^3 and 2.15 GPa, respectively (Potter and Brown (1977)).

This simulation domain is divided into 876,932 grid points and 729,668 elements. The fault zones are meshed by refining the zones along the faults and assigning the ubiquitous

Table 8.1: Subsurface layers and their corresponding hydraulic properties

Rock stratigraphic unit	Top of the unit elevation (meters below sea level)	Permeability(md)	Porosity (%)
Simpson Group	1100-1350	80	20
Arbuckle Group	1250-1550	400	25
Basement	1800-2200	70	20

model to the zones which cross the faults. So the ubiquitous joint directions are parallel to the fault direction to simulate the fault effect.

The diffusivity coefficient, defined as the mobility coefficient, k , divided by storativity, S , for the Arbuckle layer can be obtained by the following equation:

$$c = \frac{k}{S} = \frac{k}{\frac{1}{M} + \frac{\alpha^2}{K + \frac{4G}{3}}} \quad (1)$$

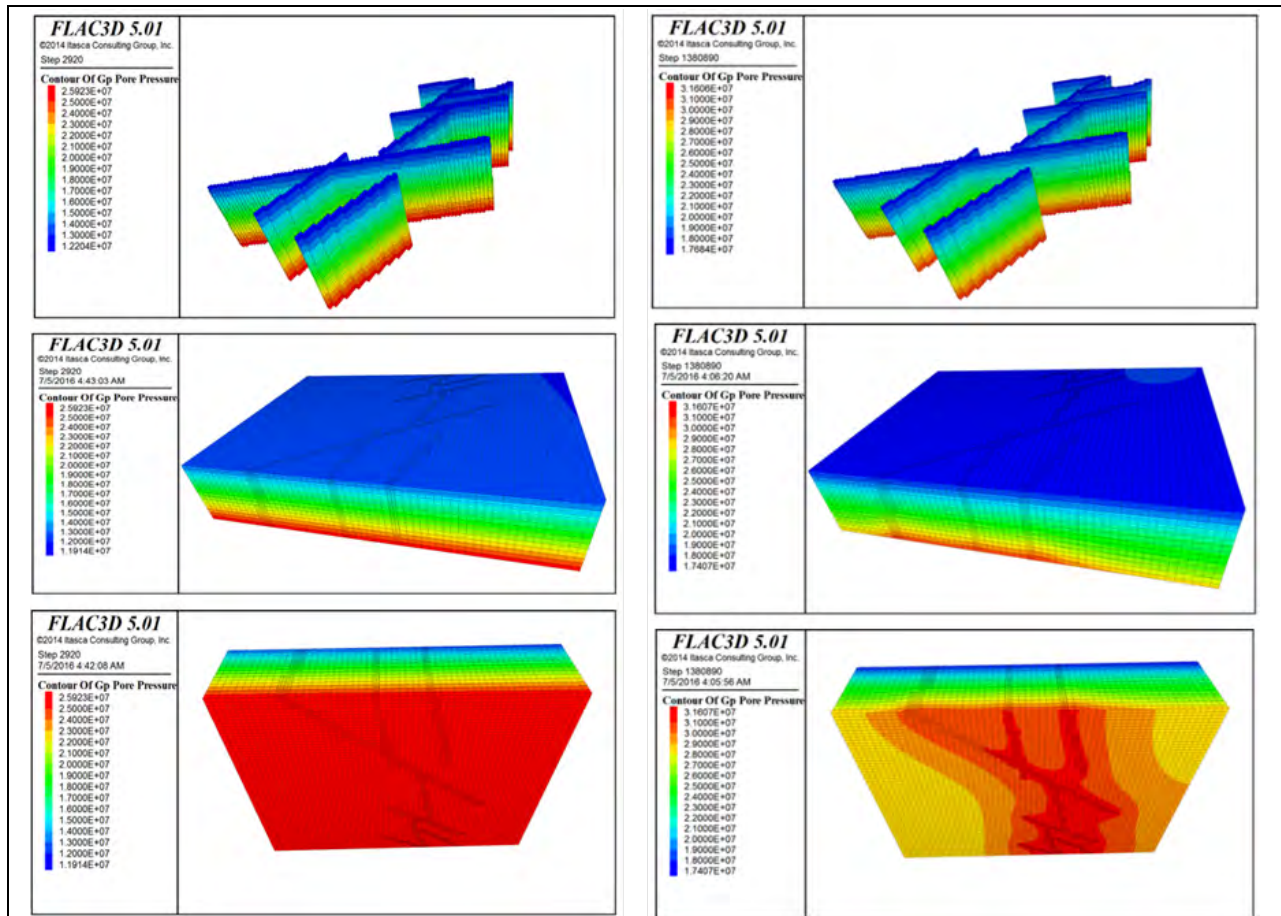
where M is the Biot modulus, α is the Biot effective stress coefficient ($M = K_f/n$ and $\alpha = 1$ for incompressible grains), K is the drained bulk modulus, G is the shear modulus (Cheng, 2014).

From this equation, the diffusivity coefficient for the Arbuckle layer is $1.6 \text{ m}^2/\text{s}$.

The first step of the modeling work in this study was conducted with the FLAC3D code, considering topography, and spatial geometry of faults and different formations. The domain is more than 22 km in the east-west and north-south direction, and varies in depth to about 3000 m (Figure 8.2). The model consists of seven layers; three of them are the target of the injection (the Hunton group, the Simpson group, the Arbuckle group) and the bottom layer (the basement) is the location of most earthquakes. Zones surrounding the faults are refined to more accurately reflect the fault zone. A smaller subdomain has been simulated by excluding the layers which have a minor volume of injection and reducing the domain size to approximately $5 \times 6 \text{ km}$. In this way, we can assess response of the system faster, and if needed modify the model. The rock layers are assigned the built-in Mohr-Coulomb plasticity constitutive model. The presence of natural fractures in the rock mass is also considered.

After applying initial and boundary conditions of the model, and letting the system reach the equilibrium, injection was commenced and continued for 19 years (1993 to 2011) using reported data (injection rate and well pressure). We monitor change of stress condition, redistribution of the pore pressure in the domain, and displacement along the faults to evaluate the possibility of induced seismicity.

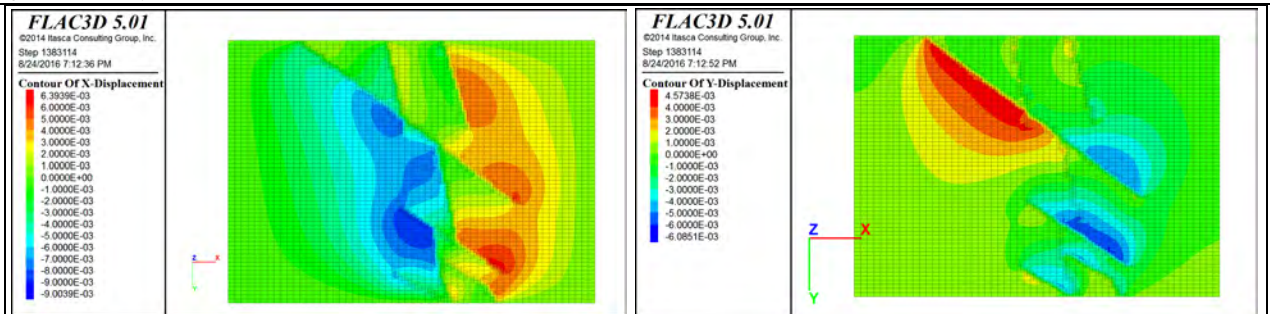
Figure 8.5 shows the pore pressure distribution before injection and after 14 years of injection. It suggests that injection can change the initial pore pressure by a significant amount (6 MPa) along the fault (for the assumed boundary conditions), which reduces the effective stress. Figure 8.6 shows the induced displacement in the X and Y directions after 14 years



(a)

(b)

Figure 8.5: Pore pressure distribution for impermeable boundary a) before injection b) after 14 years of injection.



(a)

(b)

Figure 8.6: a) x-displacement and b) y-displacement of the model after 14 years of injection.

of injection, which gives an indication of the potential for earthquakes. In the absence of sufficient data for hydraulic and mechanical properties of some layers and uncertain boundary conditions, the current results should be used in a qualitative manner to understand the trend.

On the experimental side, multi-stage tests have been carried on one-inch-diameter Fort Sill Limestone plugs and Troy Granite plugs. All the samples are dried and under un-drained test condition. The data were used to construct failure envelopes for these rocks. The results are shown in Figures 8.7 and 8.8 below. Other important test were not carried out due to budget constraints.

References

Cheng, A.H.D. (2014). Fundamentals of poroelasticity. Analysis and Design Methods: Comprehensive Rock Engineering: Principles, Practice and Projects, 113.

Tapp, B., & Dycus, M. (2013). Structural Characterization of the Wilzetta Fault Zone; Lincoln, Pottawatomie, and Creek Counties, Oklahoma. In Mid-Continent Section.

Hair, T. J. (2012). Constructing a geomechanical model of the Woodford Shale, Cherokee Platform, Oklahoma, USA effects of confining stress and rock strength on fluid flow.

Murray, K. E., & Holland, A. A. (2014). Inventory of class II underground injection control volumes in the midcontinent.

Hubbert, M. K., and W. W. Rubey (1959), Role of fluid pressure in mechanics of overthrust faulting: 1. Mechanics of fluid-filled porous solids and its application to overthrust faulting, *Geol. Soc. Am. Bull.*

Itasca Consulting Group (2012): Fast Lagrangian Analysis of Continua in 3 Dimensions (FLAC3D), Minneapolis, MN, USA.

Keranen, K. M., H. M. Savage, G. A. Abers, and E. S. Cochran (2013), Potentially induced earthquakes in Oklahoma, USA: Links between 5.7 earthquake sequence, *Geology*.

Keranen, K. M., M. Weingarten, G. A. Abers, B. A. Bekins, S. Ge (2014), Sharp increase in central Oklahoma seismicity since 2008 induced by massive wastewater injection, *Science*.

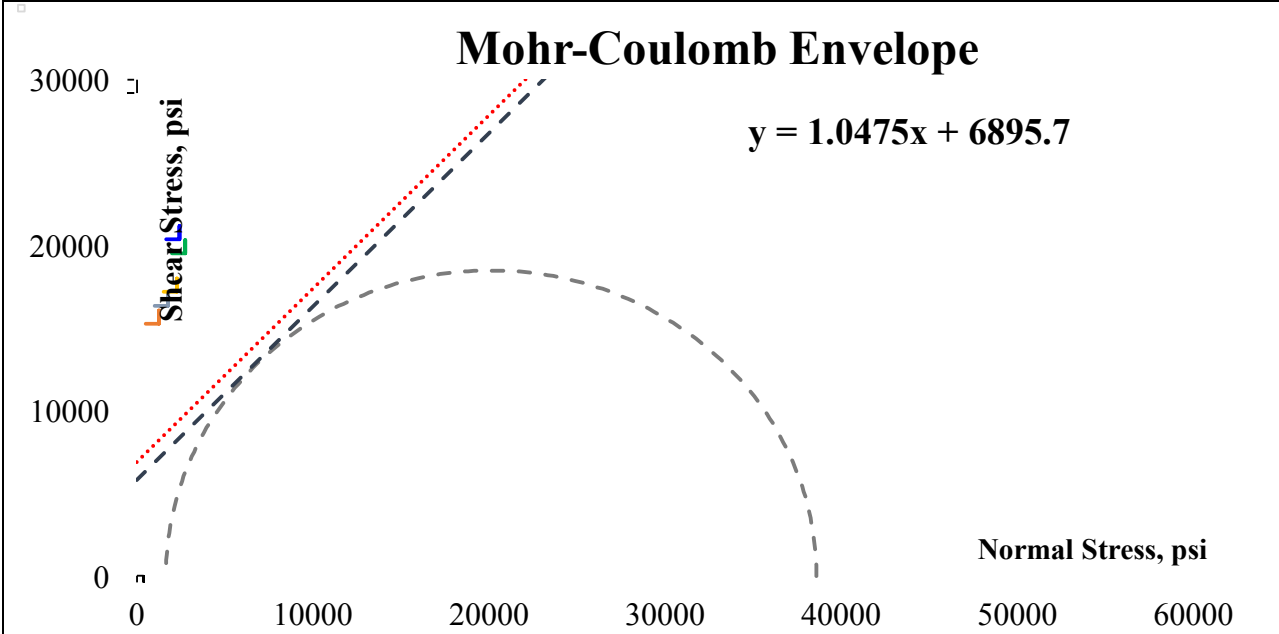


Figure 8.7. Mohr Circles and Mohr-Coulomb Envelope of Arbuckle Sample Ar-4.

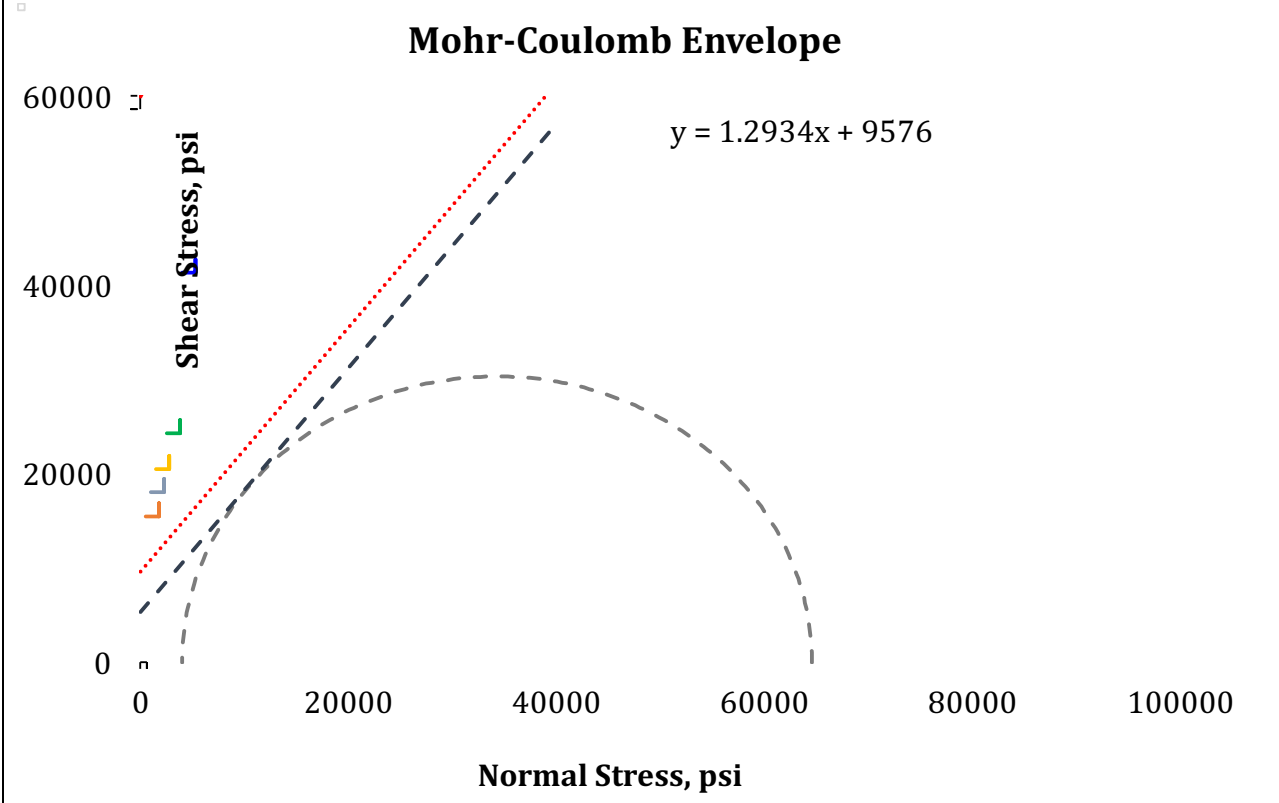


Figure 8.8. Mohr Circles and Mohr-Coulomb Envelope of basement Granite Sample Tr-4.

Description of RPSEA Project Task 3.0 - Technology Transfer: SUBCONTRACTOR shall work with RPSEA throughout the project to develop and implement an effective overall Technology Transfer program. The SUBCONTRACTOR shall participate in all appropriate RPSEA workshops and shall regularly present research results at professional meetings such as the annual meetings of the Society of Exploration Geophysicists and American Association of Petroleum Geologists. The SUBCONTRACTOR has a long history of hosting regional workshops and shall annually host workshops on topics such as its recent one on Fluid Injection Induced Seismicity. Technology transfer activities shall also be detailed in the Project Management Plan. SUBCONTRACTOR shall report the cost associated with project level technology transfer activities on each monthly report and invoice.

The report appended below summarizes technology transfer activities supported by the RPSEA Project.

10. Technology Transfer Activities

Publications

Chen C., and A. A. Holland (2016) PhasePapy: A Robust Pure Python Package for Automatic Identification of Seismic Phases, *Seismological Research Letter*.

The authors provided the program package of version 1.1 to the public through GitHub <https://github.com/austinholland/PhasePapy>. Version 1.0 has been used by Oklahoma Geological Survey (OGS) for near real time earthquake monitoring since 2014.

Darold, A. P., and A. A. Holland (2015) Preliminary Oklahoma Optimal Fault Orientations Oklahoma Geological Survey Open-File Report, OF4-2015. <http://wichita.ogs.ou.edu/documents/OF4-2015/>.

Darold, A., A. A. Holland, C. Chen, and A. Youngblood (2014), Preliminary Analysis of Seismicity Near Eagleton 1-29, Carter County, July 2014, *Okla. Geol. Surv. Open-File Report, OF2-2014*, 17.

Holland, A. A. (2014), Imaging time dependent crustal deformation using GPS geodesy and induced seismicity, stress and optimal fault orientations in the North American mid-continent, University of Arizona, Tucson, Arizona, USA.

Holland, A. A. (2015), Preliminary Fault Map of Oklahoma, Oklahoma Geological Survey Open File Report, OF3-2015. . [OF3-2015](#) | [Shape-file](#) (GIS) | [Supplemental](#)

McNamara, D. E., H. M. Benz, R. B. Herrmann, E.A. Bergman, P. Earle, A. Holland, R. Baldwin, and A. Gassner (2015), Earthquake hypocenters and focal mechanisms in central Oklahoma reveal a complex system of reactivated subsurface strike-slip faulting, *Geophysical Research Letters*,

Murray, K. E. (2014), Class II Underground Injection Control Well Data for 2010-2013 by Geologic Zones of Completion, Oklahoma, *Okla. Geol. Surv. Open-File Report, OF1-2014*, 32.

Murray, K. E., and A. A. Holland (2014), Inventory of Class II Underground Injection Control Volumes in the Midcontinent, *Shale Shaker*, 65(2), 98-106.

Oklahoma Geological Survey, [April 21, 2015 OGS Statement on Oklahoma Earthquakes](#)

Toth, C. R. (2014), Separation of the Earthquake Tomography Inverse Problem to Refine Hypocenter Locations and Tomographic Models: A Case Study from Central Oklahoma, 59 pp, University of Oklahoma, Norman, OK, USA.

U. S. Geological Survey and Oklahoma Geological Survey, 2014, USGS OGS Joint Press Release May 5, 2014 (PDF)

Workshops

In November 2014, The OGS co-hosted a workshop with the USGS. The title was Workshop on Hazard from Induced Seismicity with about 140 people in attendance and another 42 participated via a webinar. The meeting was two days long with one day for the broad scientific community and the public. The second day was a more targeted meeting with the USGS, additional researchers, and the steering committee for the National Seismic Hazard Maps. More information on the workshop is available at <https://sslearnquake.usgs.gov/regional/ceus/workshop/>. The agenda for this meeting is provided on the following page.

The USGS is responsible for regularly updating seismic hazard maps that inform regulatory bodies and impact updates of building codes. The most recent version of the map did not include seismic events that were interpreted as being induced. As a result of this workshop, this stance is being reversed and all seismicity will be considered in the new map. The first version of that map was issued by the USGS in March 2016, and shows the one year likelihood of a damaging earthquake in the United States. Earthquake probabilities for Oklahoma are derived from the catalog of earthquakes interpreted to be mainly induced.

Another outcome of this meeting was technology transfer to regulatory bodies and during this meeting the Oklahoma and Kansas Corporation Commissions had a very productive discussion with our research team. In a broader context, we are regularly exchanging information between our research group, regulatory agencies, and industry.

The Technology Transfer **Workshop: Seismicity in Oklahoma** was held September 7-8, 2016 at the Moore-Norman Technology Center in Norman OK to gather researchers working on various aspects of seismicity in Oklahoma, emphasizing those researchers based in Oklahoma (but including others with significant research programs in Oklahoma and adjoining states (Texas, Arkansas, and Kansas). The workshop was attended by about 140 researchers from Oklahoma and elsewhere, in Government (USGS, OGS, Oklahoma Corporation Commission, Kansas and Arkansas Geological Surveys, Texas Bureau of Economic Geology, DOE, NETL, EPA) Universities (University of Oklahoma, Oklahoma State University, University of Texas, University of Colorado, Stanford University, etc.) and industry (Devon, Chesapeake, ExxonMobil, Pioneer, White Star Petroleum, Newfield, Cimarex, Sand Ridge, XTO, Marathon, Oklahoma Oil and Gas Association, Oklahoma Independent Petroleum Association, GE Global Research, CH2M). The Workshop Agenda is provided following the previous workshop agenda.



National Seismic Hazard Workshop on Induced Seismicity

Tuesday, November 18, 2014

AM

8:00-9:15 Welcome and Background

- Welcome -- Oklahoma Geological Survey – *Keller, Holland (15 min)*
- Welcome USGS – *Rubinstein and Petersen (20 min)*
- Overview of Induced seismicity – *Ellsworth (20 min)*
- A Case Study Of Seismicity In Azle, Texas – *DeShon (20 min)*

15 min Break

9:30-11:00 Part 1: The National Seismic Hazard Model and Potentially Induced Seismicity

- How Is The NSHM Put Together? What Are The Key Factors That Influence Hazard?
–*Mueller (30 min)*
- Is Mmax Different For Induced Seismicity? *(15 min)*
- Ground Motions And Source Properties Of Natural Vs Induced Earthquakes *(15 min)*
- How Does Varying Smoothing Affect Hazard? *Moschetti (15 min)*
- Discussion *(15min)*

15 min break

PM

11:15-12:30 Part 2: The Logic Tree

- Overview Of The Logic Tree To Assess Hazard From Varying Earthquake Rates
–*Rubinstein (20 min)*
- The Potentially Induced Seismicity Model: Sensitivity To Parameters, Future Seismicity, And The Final Model – *Petersen (25 min)*
- Discussion *(30 min)*

12:30-1:45 Lunch

Special Lunch Presentation: **Can Stress Measurements Help Determine Whether Induced Seismicity Is likely?** *(30 min)*

1:45-3:45 Part 3: Other Methods & Government Panel

- One Application Of A Traffic Light System – *Holland (20 min)*
- Another Option – Operational Earthquake Forecasting – *Field (20 min)*
- Discussion *(20 min)*
- Government Agency Panel And Discussion – *(1 hour)*

15 min break

4:00-5:30 Industry Panel and Wrap-up

- Industry panel *(1 hour)*
- Wrap-up, Next Steps, & Comments *(30 min)*





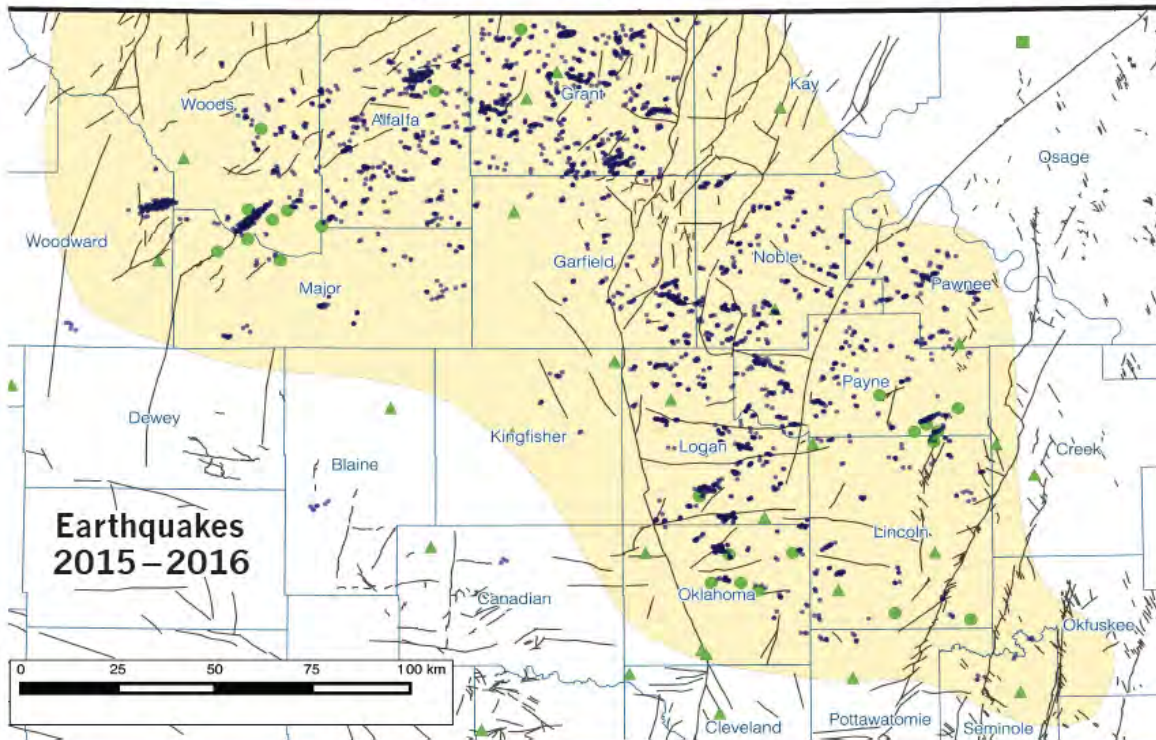
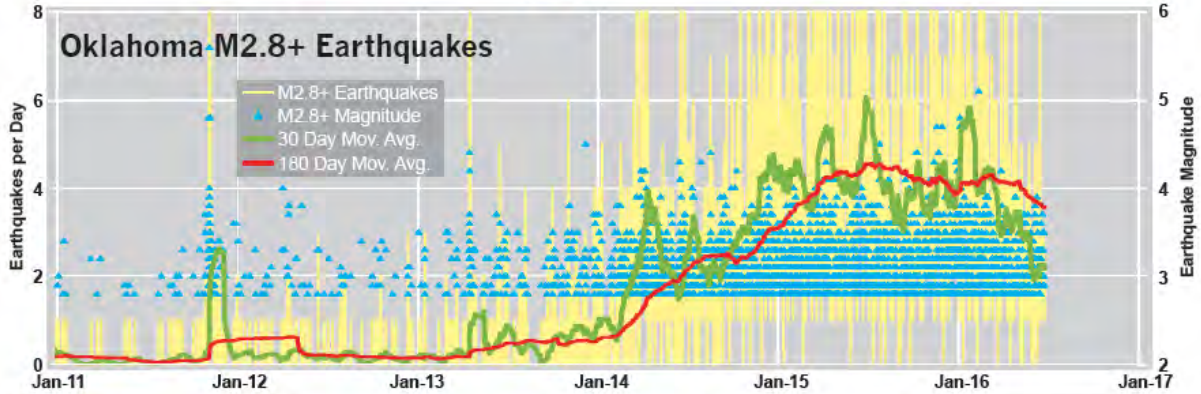
U.S. DEPARTMENT OF
ENERGY



NATIONAL
ENERGY
TECHNOLOGY
LABORATORY



Office of the
**Secretary of
Energy &
Environment**



Sponsored
by the
Oklahoma
Geological
Survey

The University of Oklahoma
MEWBOURNE COLLEGE OF EARTH AND ENERGY

WORKSHOP:
SEISMICITY IN OKLAHOMA
September 7 & 8, 2016
Moore Norman Technology Center

WORKSHOP AGENDA: DAY 1

<u>Date/Time</u>			<u>Title</u>
SEPT. 7, 8:00-8:30 am	Welcome:		
	Mike Stice - Dean of MCEE		• Welcome to Oklahoma, OU, Norman
	Mike Teague - Oklahoma Secretary of Energy & Environment		• Briefing on the Coordinating Council
	Jeremy Boak - Director of OGS		• Welcome and Introduction to the Workshop
	Kyle Murray - OGS		• Format and Design of Panel and Discussion Sessions
SEPT. 7, 8:30-10:00 am Session 1: Networks and Monitoring, Moderated by Todd Halihan from Oklahoma State University			
	Jefferson Chang - OGS	Oral	• State of the Network
	Scott Ausbrooks - AR GS	Oral	• Developing Criteria to Characterize and Classify Discreet Clusters of Earthquakes from 2009-2015
	Alexandros Savvaidis - TX BEG	Oral	• TexNet-Texas Seismological Network: A Contemporary Approach for Monitoring the Earthquake Activity in Texas
	Sara Dougherty - USGS	Oral	• LArge-n Seismic Survey in Oklahoma (LASSO): Probing Injection-Induced Seismicity with a Dense Array
COFFEE BREAK & POSTERS 10:00-10:30 am			
SEPT. 7, 10:30-12:00 pm Session 2: Data Acquisition and Management, Moderated by Steve Tipton from ALL Consulting			
	Chen Chen - OU	Oral	• 3D Velocity Model and Earthquake Relocations in Central Oklahoma
	Rex Buchanan - KS GS	Oral	• Induced Seismicity in Kansas: Events and Responses
	Tim Baker - OCC	Oral	• OGCD Presentation of Dashboard Software of Seismicity/Disposal Volumes
	Jackson Haffener - OU	Oral	• Spatio-Temporal Correlations between Wastewater Disposal and Seismicity in Oklahoma
	David Brown - OGS	Poster	• Methodology for 3D Spatial Analysis of Okla. Earthquakes
LUNCH BREAK & POSTERS 12:00-1:00 pm			
SEPT. 7, 1:00-2:30 pm Session 3: Fluids and Pressure, Moderated by Hal Macartney from Pioneer Natural Resources			
	Caitlin Barnes - OSU	Oral	• Pressure Migration Predictions in USGS Areas of Potentially Induced Seismicity
	Matthew Weingarten - Stanford	Oral	• Are We Past Peak Pressure in Oklahoma? A Hydrogeologic Evaluation of Reduced Saltwater Injection Rates on Induced Seismicity
	Kayla Kroll - LLNL	Oral	• Mitigating Induced Seismicity Through Active Pressure Management in Simulation-Based Studies
	Kyle Murray - OGS	Oral	• Monitoring of Fluid Levels and Pressures in the Arbuckle Group
COFFEE BREAK & POSTERS 2:30-3:00 pm			
SEPT. 7, 3:00-4:30 pm Session 4: Seismological Data Analysis, Moderated by Rex Buchanan from the Kansas Geological Survey			
	Tim Sickbert - OSU	Oral	• Progress, Status & Plans: Oklahoma Earthquake Research at OSU
	Xiaowei Chen - OU	Oral	• Seismogenic Processes of Induced Sequence in Central Oklahoma
	Colin Pennington - OU	Oral	• Seismological Analysis of the Prague Earthquake Sequence
	Jacob Walter - TX BEG	Oral	• A Myriad of Mechanisms for Inducing Texas (and Oklahoma) Earthquakes in the Last Century
	Noor Ghouse - OGS	Poster	• B-Values in Oklahoma
	Rob Skoumal - USGS	Poster	• Seismicity Induced by Hydraulic Fracturing in Oklahoma

WORKSHOP AGENDA: DAY 2

<u>Date/Time</u>			<u>Title</u>
SEPT. 8, 8:30-10:00 am	Session 5: Geological and Reservoir Characterization, Moderated by		<i>Kyle Murray from the Oklahoma Geological Survey</i>
	Jordan Williams - OGS	Oral	• Defining Formation Level Details in the Arbuckle Group
	Stacey Evans - OGS	Oral	• Characterization of Fluid Migration and Alteration in Basement Rocks of Northern Oklahoma
	Anjana Shah - USGS	Oral	• Influence of Subsurface Geology on Induced Seismicity in Oklahoma
	Gabriel Machado - OU	Oral	• Multidisciplinary Characterization of Geomechanical Properties and Flow Behavior of the Coupled Arbuckle-Basement System, Payne County, Northern Oklahoma
	Shane Matson - BlueJacket Energy	Oral	• Structural Fabric of Northeast Oklahoma from Aeromagnetic Data, Seismic Data, and Surface Geology

COFFEE BREAK & POSTERS 10:00-10:30 am

SEPT. 8, 10:30-12:00 pm	Session 6: Structure and Stress, Moderated by		<i>Meg Coleman from the U. S. Department of Energy</i>
	Will Levandowski - USGS	Oral	• Imaging Complex Crustal Structure and Stress in Oklahoma and Southern Kansas
	Ze'ev Reches - OU	Oral	• Intraplate Seismicity in Oklahoma: Interplay of Tectonic and Anthropogenic Effects
	Rall Walsh - Stanford	Oral	• Probabilistic Assessment of Potentially Active Oklahoma Faults
	Kevin Crain - OGS	Poster	• Gravity Effect of the Upper Basement

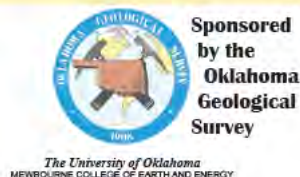
LUNCH BREAK & POSTERS 12:00-1:00 pm

SEPT. 8, 1:00-2:30 pm	Session 7: Hazards and Ground Motion, Moderated by		<i>Tom Robins from the Oklahoma Secretary of Energy and Environment's Office</i>
	Morgan Moschetti - USGS	Oral	• Ground Motions from Induced Earthquakes in Oklahoma and Kansas
	Charles Mueller - USGS	Oral	• Modeling Seismic Hazard from Induced Earthquakes
	Dan McNamara - USGS	Oral	• USGS Efforts to Monitor and Characterize Seismicity in Central Oklahoma
	Stephen Holloway - OGS	Poster	• Industry Contributed Fault Map of Oklahoma
	Nicole McMahan - CSU	Poster	• The November 6, 2011 M5.6 Prague, Oklahoma Aftershock Sequence Studied Using Subspace Detection

COFFEE BREAK & POSTERS 2:30-3:00 pm

SEPT. 8, 3:00-4:00 pm	Session 8: Engineering and Built Environment, Moderated by		<i>Kris Nygaard from Exxon-Mobil</i>
	Scott Harvey - OU	Oral	• Post-Earthquake Bridge Inspection Protocol for the Oklahoma Department of Transportation
	Abbie Liel - CU	Oral	• Risks of Damage to the Built Environment from Induced Seismicity

SEPT. 8, 4:00-4:30 pm	Wrap-Up Session: What Have We Learned? Where Do We Go From Here?		<i>Moderated by Kris Nygaard from Exxon-Mobile and Kyle Murray from the Oklahoma Geological Survey</i>
-----------------------	---	--	--



WORKSHOP:
SEISMICITY IN OKLAHOMA
September 7 & 8, 2016
Moore Norman Technology Center

Professional Presentations with Abstracts

Chang, J. (2015) Semi-Infinite Geology Modeling Algorithm (SIGMA): A Modular Approach to 3D Gravity [Abstract 86140], American Geophysical Union Fall Meeting, December 17, 2015.

Darold, A. P., Holland, A., Gibson, A. (2014), Analysis of Seismicity Coincident with Hydraulic Fracturing of a Well in Southern Oklahoma , in *Amer. Geophys. Union Fall Meeting*, Poster, San Francisco, CA.

Darold, A.P. and A.A. Holland (2015), Analysis of Seismicity Coincident with Hydraulic Fracturing of a Well in Southwest Oklahoma, Seismological Society of America Meeting, Pasadena CA, April 20-23, 2015.

Darold, A.P. and A.A. Holland (2015), Analysis of Seismicity Coincident with Hydraulic Fracturing of a Well in Southwest Oklahoma, Geological Society of America South-Central Section Meeting, Stillwater OK, March 19-20, 2015. [PDF Download](#)

Holland, A. A. (2014, Potential Case of Induced Seismicity from a Water Disposal Well in South-Central Oklahoma, *Seismol. Res. Lett.*, 85(2), 452.

Holland, A. A. (2014), Induced Seismicity from Fluid Injection and Draft Best Practices, Ground Water Protection Council UIC Conference, New Orleans, LA, Jan. 21-23, 2014.

Holland, A. A. (2014), Recent Earthquakes in Oklahoma and the Mid- continent: Significance and Potential for Induced Seismicity, 21st Integrated Petroleum Environmental Consortium Conference, Houston, TX, Oct. 13-14, 2014.

Holland, A.A. (2014), Induced seismicity “Unknown Knowns”: the role of stress and other difficult to measure parameters of the subsurface, National Research Council Joint Meeting of the Committee on Earth Resources and Committee on Geological and Geotechnical Engineering, Oct. 23, 2014.

Holland, A. A., and A. P. Darold (2014), Potential Case of Induced Seismicity from a Water Disposal Well in South-Central Oklahoma, in *GSA South Central Section*, edited, Geol. Soc. Amer., Fayetteville, AR.

Holland, A. A, and A. P. Darold (2014), Considerations in disposal well siting and operations: relative hazard and identification of injection-induced seismicity using regional or local seismic monitoring, SPE/SEG/ARMA Injection Induced Seismicity Workshop, Banff, Canada, Sep. 15-18, 2014.

Holland, A.A. and A.P. Darold (2015), Are earthquakes triggered by hydraulic fracturing more common than previously recognized?, Geological Society of America South Central Section Meeting, Stillwater OK, March 19-20, 2015. [PDF Download](#)

Holland, A.A. and A.P. Darold (2015), Are earthquakes triggered by hydraulic fracturing more common than previously recognized?, Seismological Society of America Meeting, Pasadena CA, April 20-23, 2015.

Holland A. A., and G. R. Keller (2015) Industry Contributions to the Oklahoma Fault Database AAPG Mid-Continent Section Meeting, Tulsa OK Oct. 6-8, 2015

Holland, A., G. R. Keller, A. Darold, K. Murray, and S. Holloway (2014), Multidisciplinary Approach to Identify and Mitigate the Hazard from Induced Seismicity in Oklahoma, in *Amer. Geophys. Union Fall Meeting*, San Francisco, CA.

Keller, G.R., (2015) The Role of Rifting in the Tectonic Evolution of the Oklahoma Region (2015), Geological Society of America South-Central Section Meeting, Stillwater OK, March 19-20, 2015.

S. Marsh and A. A. Holland, (2015) Comprehensive Fault Database and Interpreted Fault Map for Oklahoma, AAPG Mid-Continent Section Meeting, Tulsa OK Oct. 6-8, 2015

Kevin Crain and **Jefferson Chang** presented Project work on Crustal Scale Tomography (Task 8) at an AGU potential fields workshop in Keystone, Colorado in August 2015. Links to abstracts for the presentations are listed below.

J.C.Chang and K.D.Crain:

<https://agu.confex.com/agu/seg15/webprogram/Paper38018.html>

K.D.Crain: <https://agu.confex.com/agu/seg15/webprogram/Paper38020.html>

<https://agu.confex.com/agu/seg15/webprogram/Paper38027.html>

On October 19, 2016, **Jeremy Boak** presented a talk on Induced Seismicity and Oklahoma Earthquakes to the Society for Exploration Geophysicists Annual Meeting in Dallas TX.

Other Presentations and Invited Talks

Austin Holland was an invited speaker at a National Research Council joint standing committee meeting on October 23, 2014 on the topic of "Critical Issues in the Subsurface: Using Field Observatories and Data to Advance Understanding of Rock Behavior".

Austin Holland was an invited speaker at a briefing about induced seismicity convened by the U.S. Department of Energy in October 2014.

The project team had a significant presence at the December 2014 American Geophysical Union Fall Meeting in San Francisco, California. Four related abstracts included investigators on the project (Darold *et al.*, 2014, Holland *et al.*, 2014, Llenos *et al.*, 2014, Majer *et al.*, 2014). The presentation by Holland *et al.* (2014) was an introduction to both this RPSEA project and other related efforts underway in Oklahoma.

Randy Keller gave a talk on Oklahoma earthquakes and their possible relationships to oil and gas activity to a professional engineering group who earned Continuing Education Credits (CEUs) for their attendance in September 2015

Austin Holland presented the Oklahoma fault data database to the Stanford Consortium on Induced and Triggered Seismicity (SCITS) in February 2015, including lessons learned from the industry contribution of fault data for the database as similar efforts are being considered elsewhere.

Austin Holland presented at the IEAGHG Monitoring Network Meeting in Berkeley, CA in June 2015 with a talk titled "Strategy for Monitoring Large Regions of Fluid Injection and Induced Seismicity: Oklahoma's Experience".

Kyle Murray made the following presentations in August 2015:

Aug 14, 2015 Chicago, IL: National Association of Insurance Commissioners (NAIC) Center for Insurance and Policy Research (CIPR) Event – Oral Presentation titled *State of the Science: Triggered Seismicity in Oklahoma*.

Aug 15, 2015 Chicago, IL: National Association of Insurance Commissioners (NAIC) Earthquake Study Group Meeting – Oral Presentation titled *Overview of Earthquake Activity in the Contiguous States*.

Aug 27, 2015 Woodward, OK: Water Transfer, Treatment and Reuse Workshop with Sustaining Oklahoma's Energy Resources (SOER) – Oral Presentation titled *Water Use and Permitting in Oklahoma Produced Water, UIC and SWD*.

On September 10, 2015, **Jeremy Boak** presented a discussion of the current seismic activity to the Harvard Club of Oklahoma City

On September 16, 2015, **Jeremy Boak** presented a discussion of Induced Seismicity and Oklahoma Earthquakes to the Oklahoma City Geological Society.

On October 7, 2015, **Jeremy Boak** presented a discussion of Induced Seismicity and Oklahoma Earthquakes to the Society of Independent Petroleum Earth Scientists.

On October 15, 2015, **Jeremy Boak** presented a discussion of Induced Seismicity and Oklahoma Earthquakes to a conference of Noble County Assessors.

On January 20, 2016, **Jeremy Boak** presented a discussion of induced seismicity in Oklahoma to the Consumer Energy Alliance State of the Energy Industry Roundtable in Oklahoma City,

On January 27, 2016, **Jeremy Boak** presented a discussion of induced seismicity in Oklahoma to the Oklahoma Aggregates Association annual meeting in Norman.

On February 11, 2016, **Jeremy Boak** presented discussions of induced seismicity in Oklahoma to the Oklahoma City Rotary Club, The Tulsa Geophysical Society, and the Ardmore Geological Society.

On February 16, 2016, **Jeremy Boak** presented a discussion of induced seismicity in Oklahoma to the Oklahoma Structural Engineering Association and to the Sac & Fox Nation.

On March 3, 2016, **Jeremy Boak** presented a talk on Induced Oklahoma Seismicity to the Rocky Mountain Association of Geologists/Denver Geophysical Society 3-D Seismic Symposium in Denver.

On March 7, 2016, **Jeremy Boak** presented a talk on Induced Seismicity in Oklahoma to the Kiwanis Club of Oklahoma City.

On March 23, 2016, **Jeremy Boak** presented a talk on Induced Seismicity in Oklahoma to the Norman Board of Realtors.

On March 29, 2016, **Jeremy Boak** presented a talk on Induced Seismicity in Oklahoma to the SEG/SPE (Society of Exploration Geophysicists/Society of Petroleum Engineers) Workshop on Induced Seismicity in Fort Worth (March 28-30)

On April 5, 2016, **Jeremy Boak** presented a talk on Oklahoma Seismicity to the Association

of Energy Service Companies in Oklahoma City and to the Spring Conference of the Oklahoma Structural Engineering Association.

On April 13, 2016, **Jeremy Boak** presented a talk on Oklahoma Seismicity to the Tulsa Association of Lease and Title Analysts of Tulsa, Oklahoma.

On May 2, 2016, **Jeremy Boak** presented a talk on Induced Seismicity and Oklahoma Earthquakes to the Norman Lions Club, Norman, Oklahoma.

On May 6, 2016, **Jeremy Boak** presented a talk on Induced Seismicity and Oklahoma Earthquakes to the Geographic Information Council of Oklahoma, in Oklahoma City.

On May 9, 2016, **Jeremy Boak** presented a talk on Induced Seismicity and Oklahoma Earthquakes to the Geophysical Society of Oklahoma City, in Oklahoma City.

On May 10, 2016, **Jeremy Boak** presented a talk on Induced Seismicity and Oklahoma Earthquakes to the Fortune Club, in Oklahoma City.

On May 19, 2016, **Jeremy Boak** presented a talk on Induced Seismicity and Oklahoma Earthquakes to the North Texas Geological Society in Wichita Falls TX.

On June 21, 2016, **Jeremy Boak** presented a talk on Induced Seismicity and Oklahoma Earthquakes to the Unconventional Resources Group of the Energy Minerals Division, American Association of Petroleum Geologists in Calgary, Alberta.

On August 26, 2016, **Jeremy Boak** participated in a panel discussion on Induced Seismicity and Oklahoma Earthquakes at the Oklahoma School Boards Association conference in Oklahoma City.

On September 2, 2016, **Jeremy Boak** presented a talk on Induced Seismicity and Oklahoma Earthquakes to the Department of Geological Sciences at Oklahoma State University in Stillwater, OK.

On September 7, 2016, **Jeremy Boak** presented a talk on Induced Seismicity and Oklahoma Earthquakes at an American Chemical Society Chemistry Café in Tulsa Oklahoma as part of a panel discussion.

On September 14, 2016, **Jeremy Boak** participated in a panel discussion on Induced Seismicity and Oklahoma Earthquakes to the Oklahoma Municipal League Annual Conference in Oklahoma City, OK.

On September 15, 2016, **Jeremy Boak** presented a talk on Induced Seismicity and Oklahoma Earthquakes to the Council of Petroleum Accountants Societies of Oklahoma in Oklahoma City.

On September 20, 2016, **Kyle Murray** presented a talk on Induced Seismicity and Oklahoma Earthquakes to the Tulsa Geological Society in Tulsa OK.

On September 21, 2016, **Jeremy Boak** presented a talk on Induced Seismicity and Oklahoma Earthquakes to the Oklahoma Commercial Real Estate Forum on Earthquakes in Oklahoma City.

On October 11, 2016, **Jeremy Boak** presented a talk on Induced Seismicity and Oklahoma Earthquakes to the Oklahoma Independent Petroleum Association Wildcatter Wednesday

in Oklahoma City.

On October 26, 2016, **Jeremy Boak** presented a talk on Induced Seismicity and Oklahoma Earthquakes to the Oklahoma Corporation Commission Oil and Gas Institute in Tulsa OK.

On October 26, 2016, **Jeremy Boak** presented a talk on Induced Seismicity and Oklahoma Earthquakes to the U. S. Association of Energy Economists Annual Meeting Workshop on Induced Seismicity in Tulsa.

On October 27, 2016, **Jeremy Boak** presented a talk on Induced Seismicity and Oklahoma Earthquakes to the 5th Annual Produced Water Quality Recycling and Reuse Congress in Denver CO.

On November 1, 2016, **Jeremy Boak** presented a talk on Induced Seismicity and Oklahoma Earthquakes to the Norman Lions Club in Norman.

Industry Interactions

During Fall 2014, Project staff interacted with New Dominion, which provided a significant cost share for our project. They are sharing ideas about the causes of Oklahoma seismicity, and we discussed the data that they plan to provide as part of their cost share commitment.

On August 27, 2015, and December 2, 2015, **Jeremy Boak** attended the Seismicity Working Group Meeting of the Oklahoma Independent Petroleum Association, and discussed data needs from the industry for evaluation of induced seismicity.

On November 20, 2015, **Jeremy Boak** sat on a panel discussing seismicity and wastewater injection at the annual conference of the Oklahoma Oil and Gas Association

Jeremy Boak met with Julie Shemeta of MEQ Geo, an industry consultant during the week before Christmas 2015.

On February 5, 2016, **Jeremy Boak** and **Kevin Crain** met with Chesapeake Energy to review seismic data.

On March 2, 2016, RPSEA team members participated in a meeting with ExxonMobil and XTO personnel regarding their assessment of potentially induced seismicity in Texas, and on a risk assessment tool being developed for injection wells.

Government Interactions

Jeremy Boak attended meetings of the Governor's Coordinating Council on Seismicity in Oklahoma City on September 8, 2015, October 7, 2015, May 23, 2016, July 18, 2016, August 23, 2016, and November 2, 2016.

Jeremy Boak, and **Jefferson Chang** attended a meeting of the Governor's Coordinating Council on Seismicity on April 19, 2016, August 23, 2016.

On January 19, 2016, **Jeremy Boak** and **Kyle Murray** attended the January meeting of the Governor's Coordinating Council on Seismicity in Oklahoma City.

On February 16, 2016, **OGS staff members** attended the February meeting of the Governor's Coordinating Council on Seismicity in Oklahoma City

On March 21, 2016, **Jeremy Boak, Jefferson Chang, and Kyle Murray** also attended the March meeting of the Governor's Coordinating Council on Seismicity. Both Murray and Boak were invited speakers.

On March 25, 2016, **OGS staff members** discussed the upcoming release of the U. S. Geological Survey's one-year seismic hazard assessment of the United States, which showed both natural and induced seismic hazard for the first time, and highlighted north central Oklahoma as an area with significant risk of damage.

Jeremy Boak attended the Secretary of Energy and Environment's monthly Director's meeting On September 14, 2015, October 19, 2015, November 30, 2015, February 22, 2016, March 21, 2016, April 25, 2016, May 31, 2016, July 25, 2016, October 10, 2016.

The **OGS seismology team** met with the Oklahoma Corporation Commission's Oil and Gas Division in Norman on Tuesday, October 15, 2015, on December 15, 2015, February 1, 2016, April 18, 2016, June 10, 2016, September 27, 2016, October 11, 2016.

On October 30, 2015, **Jeremy Boak** presented a talk discussing seismicity and wastewater injection to an Interim Study Group of the Oklahoma legislature.

On November 10, 2015, **Jeremy Boak** joined a panel discussing seismicity and wastewater injection at the Oklahoma Governor's Energy Conference

Jeremy Boak attended meetings on seismic hazard evaluation at the Oklahoma Department of Transportation on December 8, 2015, April 4, 2016, May 16, 2016.

Jeremy Boak attended the fall liaison meeting of the Association of American State Geologists in Washington, DC, September 27-30, 2015, and met with personnel from USGS, Geological Society of America, National Mining Association, The National Academies, and a DOE undersecretary, as well as staff of several Congressional Committees.

USGS

Jeremy Boak met with a group at the USGS National Earthquake Information Center during the week before Christmas.

Jeremy Boak met with Robert Williams of the USGS National Earthquake Information Center June 7, 2016.

The **OGS seismology team** met with a group of U.S. Geological Survey and Congressional staff on June 28, 2016.

Jeremy Boak, Jefferson Chang, and Kyle Murray met with USGS and Oklahoma Corporation Commission staff to discuss seismicity in Oklahoma on June 30, 2016.

Jeremy Boak, Noorulan Ghose, and Jefferson Chang visited the USGS National Earthquake Information Center on July 22, 2106 to discuss analysis of seismologic data.

RPSEA Meetings

On September 17, 2015 and March 9, 2016, **Jeremy Boak** gave a Webex update on the RPSEA Project to RPSEA, NETL and DOE personnel.

On November 4, 2015, **Jeremy Boak** presented a discussion of the current seismic activity to a RPSEA Technology Transfer workshop in Houston, Texas, along with Randy Keller, who discussed the larger tectonic picture of Oklahoma seismicity.

Jeremy Boak presented a talk on the RPSEA Project and Induced Seismicity in Oklahoma at the Best of RPSEA conference in Galveston TX, August 31, 2016.